CHAPTER 4 RESULTS AND DISCUSSION

4.1 Introduction

The main objectives of this research project were to synthesise and characterize thermally stable, low-temperature, and multinuclear ionic copper(II) mixed carboxylates as potential hybrid heat-light solar-cell materials. The general formula of these complexes are $K_n[Cu_2(p\text{-}OC_6H_4COO)_n(RCOO)_{4-n}]$, where n = 1-3, and R = saturated or unsaturated alkyl chain.

The ionicity and arylcarboxylate ligand is to increase the thermal stability, while the alkylcarboxylate ligand is to favour the formation of low-temperature complexes. The latter concept is based on metallomesogenic $[Cu_2(RCOO)_4]$, where R is a long linear or branched alkyl group. Examples are $[Cu_2(CH_3(CH_2)_{14}COO)_4]$ and $[Cu_2(CH_3(CH_2)_7)_2CHCOO)_4]$ (**Figure 4.1**), reported to melt at 112^oC and below -20^oC respectively [1].

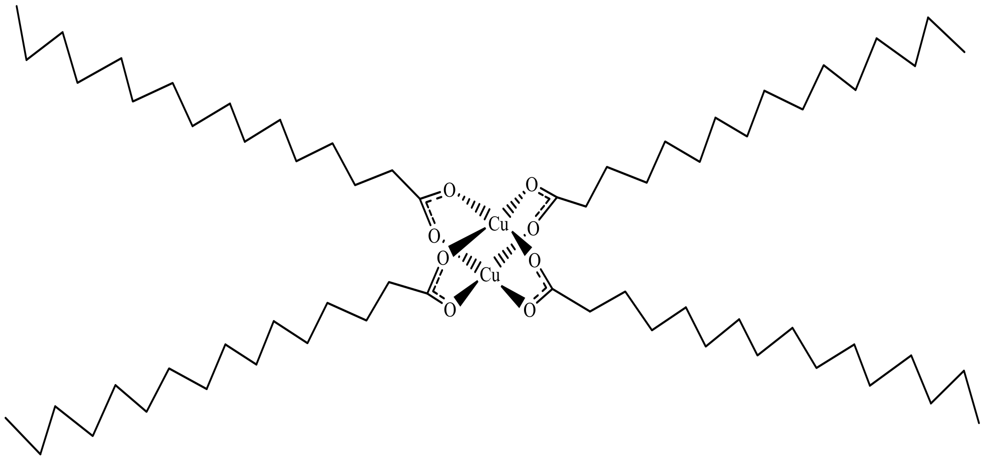

(a)

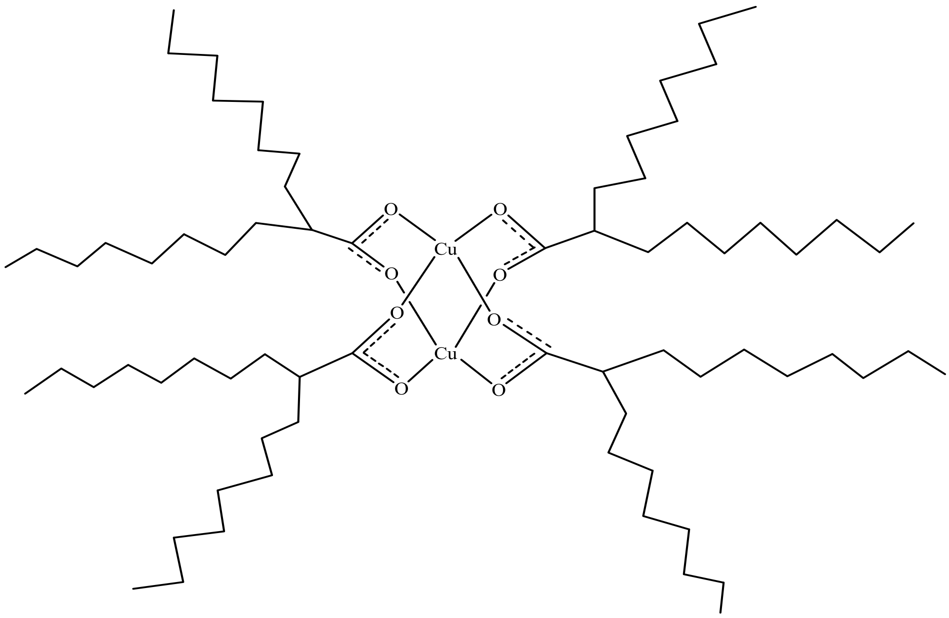

(b)

Figure 4.1 Structural formula of (a) $[Cu_2(CH_3(CH_2)_{14}COO)_4]$; and (b) $[Cu_2(CH_3(CH_2)_7)_2CHCOO)_4]$

The current research objective was also partially based on the knowledge that oligonuclear complexes play key roles in the development for multicomponent (supramolecular) artificial systems for photochemical energy conversion and other related photonic devices. It was reported that in designing such systems, the bridging ligands are crucial because they allow the assembly of the metal ions in a topologically controlled fashion, and can afford electronic coupling between the metal ions to allow

for the intercomponent energy and/or electron-transfer processes.

Another emerging class of inorganic materials with rich photophysics, photochemistry and structural diversity are the polynuclear copper(I) chalcogenides. For example, Xu and Yip [2] reported the synthesis, structures and spectroscopy of two novel luminescent polynuclear copper(I) complexes with 1,8-naphthalenedithiolate ligand (**Figure 4.2**), while Miller, Gantzel and Karpishin [3] studied the photophysical and electrochemical properties of copper(I) bis(2,9-phenylethynyl-1,10-phenanthroline) complexes (**Figure 4.3**).

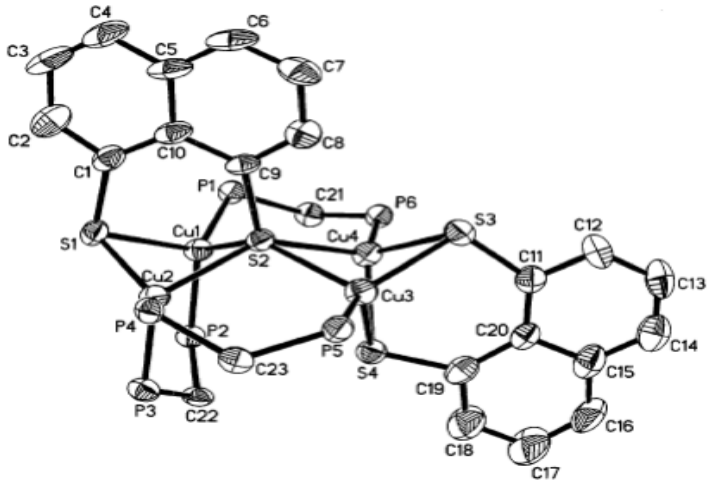

Figure 4.2 Structural formula of a copper(I) complex with 1,8-naphthalenedithiolate

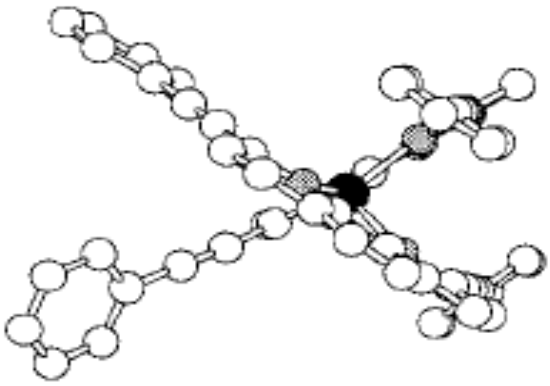

Figure 4.3 Structural formula of a copper(I) with (2,9-phenylethynyl-1,10-phenantroline)

The initial challenge of this work was to find the correct synthetic method for the intended mixed carboxylates. Two methods were employed: one-pot [4] and ligand-exchange [5] reactions. The total number of complexes obtained was seventeen (17). These complexes were characterized by elemental analyses, Fourier transform infrared spectroscopy (FTIR), UV-visible spectroscopy (UV-vis), thermogravimetry (TGA), differential scanning calorimetry (DSC), magnetic susceptibility, cyclic voltammetry (CV), and for suitable complexes, single crystal X-ray crystallography and photoluminescence spectroscopy.

4.2 One-Pot Reaction

The one-pot reaction [4] was used to synthesize five (5) ionic dimeric complexes and two ionic monomeric complexes of general formula $K_n[Cu_2(p\text{-}OC_6H_4COO)_n(RCOO)_{4-n}]$, where R is $CH_3CH{=}CH$ or $CH_2{=}C(CH_3)$; n = 1-3, $K[Cu(OH)_2(CH_3CH{=}CHCOO)(H_2O)]$ and $\{K[Cu(OH)(CH_2{=}C(CH_3)COO)]\}_3$ respectively.

The reaction involved reacting p-HOC_6H_4COOH, $CH_3CH{=}CHCOOH$ or $CH_2{=}C(CH_3)COOH$, KOH and $CuCl_2$ in hot aqueous ethanol for 30 minutes. The general equation for the expected reaction is shown below.

$$n\ p\text{-}HOC_6H_4COOH + (4\text{-}n)\ RCOOH$$

$$\downarrow \quad \begin{matrix} 1.\ 3n\ KOH/CH_3CH_2OH \\ 2.\ \ 2\ CuCl_2 \end{matrix}$$

$$K_n[Cu_2(p\text{-}OC_6H_4COO)_n(RCOO)_{4-n}]$$

4.2.1 $K_n[Cu_2(p\text{-}OC_6H_4COO)_n(CH_3CH{=}CHCOO)_{4-n}]$

A total of four (4) complexes were obtained by this method. These are discussed below, starting with the more symmetrical complexes (n =2), followed by the less symmetrical complexes (n = 1 and then n = 3).

(a) $K_2[Cu_2(p\text{-}OC_6H_4COO)_2(CH_3CH{=}CHCOO)_2]$

Two complexes were obtained from the one-pot reaction involving p-HOC_6H_4COOH and $CH_3CH{=}CHCOOH$ (mol ratio = 1:1): a pale green powder and pale blue small needles.

(i) Pale green powder

The pale green powder (**Complex 1**) was the formed as the residue from the hot reaction mixture. It was sparingly soluble in methanol, ethanol and chloroform, and insoluble in most other common organic solvents.

The results from the **elemental analyses** give the C:H ratio equals 3.9:1.0. This is in good agreement with the chemical formula $KCuC_4H_{11}O_6$ (formula weight = 257.8 g mol^{-1}; calculated C:H ratio = 4.3:1.0).

Its **FTIR** spectrum (**Figure 4.4**), recorded as a KBr disc in the range of 4000 cm^{-1} to 600 cm^{-1}, is different from those of the starting materials (**Figure 4.5** and **Figure 4.6**). From this, it may be stated that *p*-HOC_6H_4COOH has participated with $CH_3CH{=}CHCOOH$ in the above reaction.

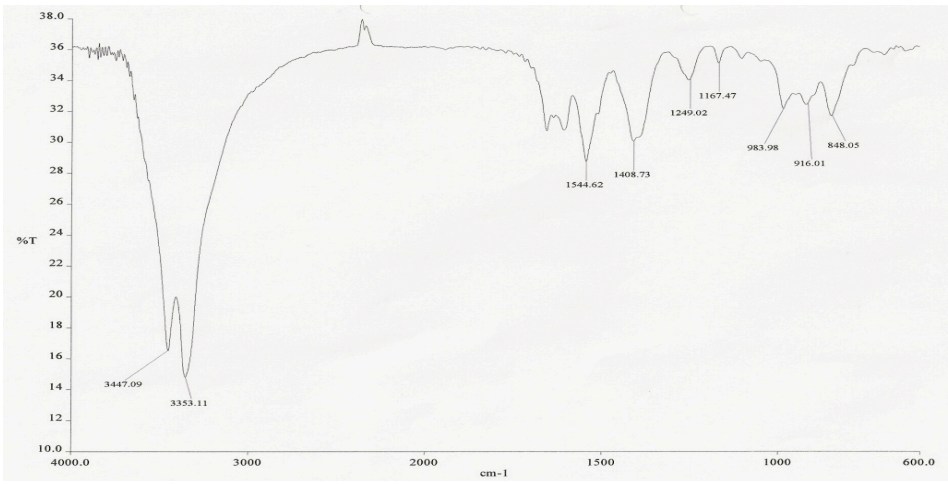

Figure 4.4 FTIR spectrum of **Complex 1**

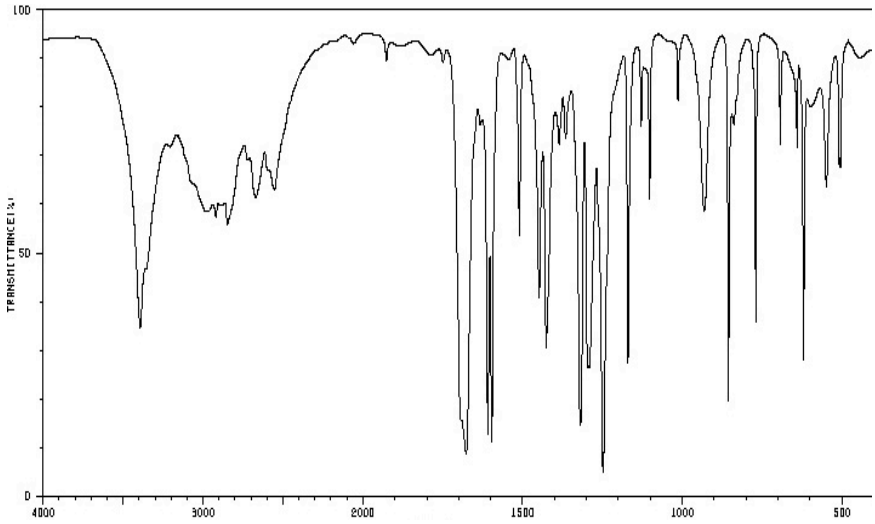

Figure 4.5 FTIR spectrum of *p*-HOC_6H_4COOH

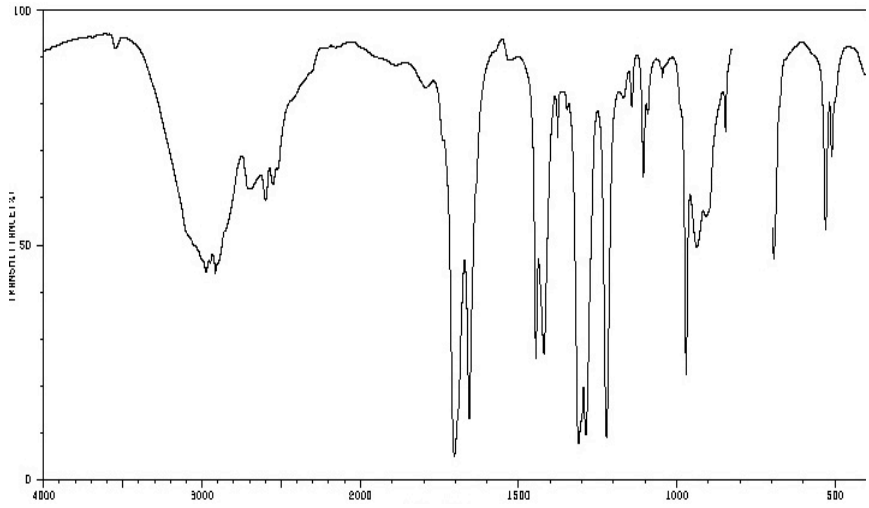

Figure 4.6 FTIR spectrum of $CH_3CH=CHCOOH$

The spectrum also shows two very strong overlapping peaks at 3447 cm^{-1} and 3353 cm^{-1}, assigned to –OH group. The asymmetrical (υ_{asym}) and symmetrical (υ_{sym}) COO vibrations appear at 1545 cm^{-1} and 1409 cm^{-1}. Thus, the difference (ΔCOO) between υ_{asym}COO and υ_{sym}COO is 136 cm^{-1}, suggesting chelating carboxylate ligand [6].

Its **UV-vis** spectrum in the solid state (**Figure 4.7 (a)**) and as a solution in 9:1 CH_3OH-CH_3CH_2COOH (**Figure 4.7(b)**) show a broad *d-d* band at 725 nm and 703 nm (ε_{max}= 302 $M^{-1}cm^{-1}$) respectively. These suggest that the geometry at Cu(II) is square pyramidal in the solid state, and was retained in solution [7].

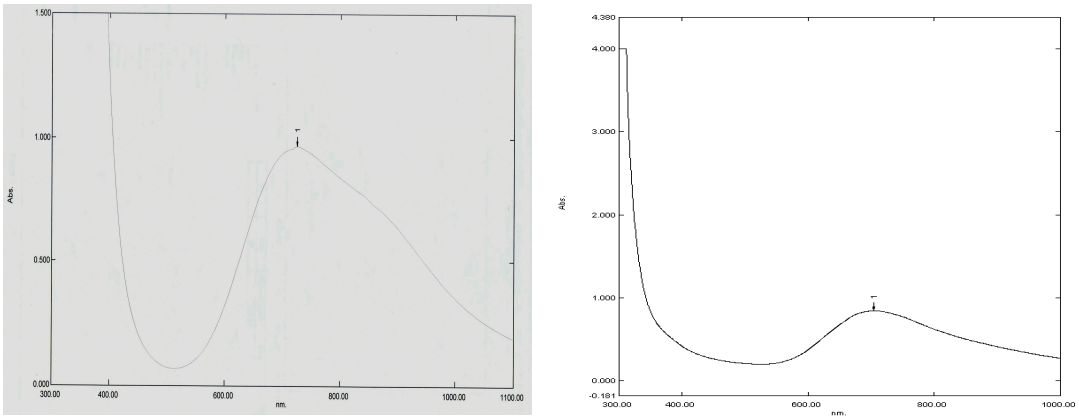

(a) (b)

Figure 4.7 UV of **Complex 1** in (a) solid; and (b) solution

The assignments of the electronic transitions corresponding to these bands are based on the crystal field theory, as shown in **Figure 4.8**.

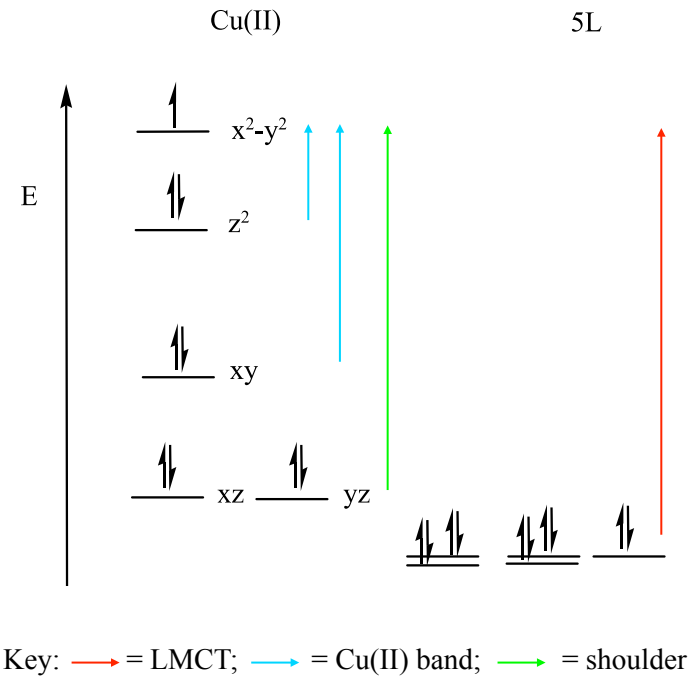

Figure 4.8 Assignment of electronic transitions for a square pyramidal **Complex 1** (not to scale)

Combining the above results, **Complex 1** is proposed to have the structural formula of $K[Cu(CH_3CH{=}CHCOO)(OH)_2(H_2O)].H_2O$ (**Figure 4.9)**. The structure shows a mononuclear square pyramidal copper(II) complex with chelating carboxylate ligand as inferred from FTIR and UV-vis spectra. Thus, its yield was 37.1%, and it is not the expected ionic mixed-carboxylate complex from this reaction.

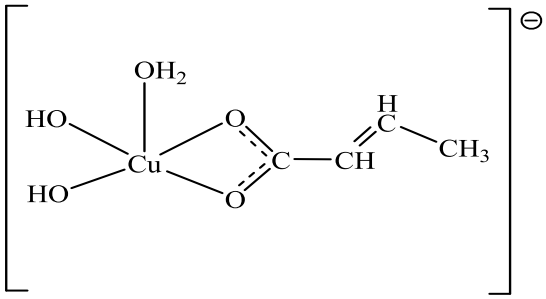

Figure 4.9 Proposed structural formula of **Complex 1** (K^+ ion and H_2O solvate are not shown)

The **TGA** thermogram (**Figure 4.10**) shows that **Complex 1** is thermally stable up to 635^{o}C. It also shows that the complex underwent three weight losses of 8.5% at 170^{o}C, 3.0% at 407^{o}C, and 55.5% at 635^{o}C. The first and second weight losses are probably due to the evaporation of solvated and axially coordinated H_2O molecules (expected, 14.3%). The third weight loss is assigned to the decomposition of the ligands (expected, 46.2%) to CO_2 and other volatiles [8].

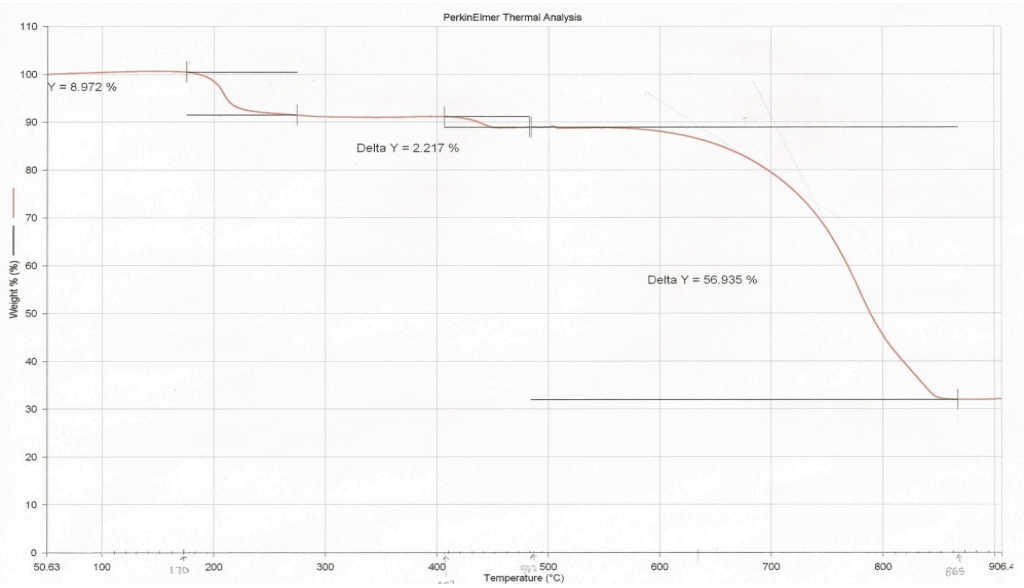

Figure 4.10 TGA of **Complex 1**

The amount of residue at temperatures above 865^{o}C is 34.6%. The expected value, assuming that the residue is a mixture of CuO and K_2O, is 49.1%. The lower amount obtained may either mean that the assumption is not valid, or that volatile inorganic residues were formed. The thermal degradation of the complex is shown in the following equation.

$$2\ K[Cu(CH_3CH{=}CHCOO)(OH)_2(H_2O)].H_2O \longrightarrow 2CuO + K_2O + \text{volatiles}$$

The **DSC** trace (**Figure 4.11**) shows three endothermic peaks at 40^{o}C (ΔH = +5.6 kJ mol^{-1}), 190^{o}C (ΔH = +17.9 kJ mol^{-1}), and 220^{o}C (ΔH = +12.7 kJ mol^{-1}), and two

exothermic peaks at 226°C and 247°C ($\Delta H_{combined}$ = -20.2 kJ mol^{-1}). It is noted that these processes occur below its decomposition temperature (635°C). The three endothermic processes may correspond to crystal-to-crystal transition, evaporation of H_2O and dissociation of all of the ligands, respectively. The exothermic processes may correspond to the polymerization of the dissociated $CH_3CH{=}CHCOO$ to form saturated organic polymer.

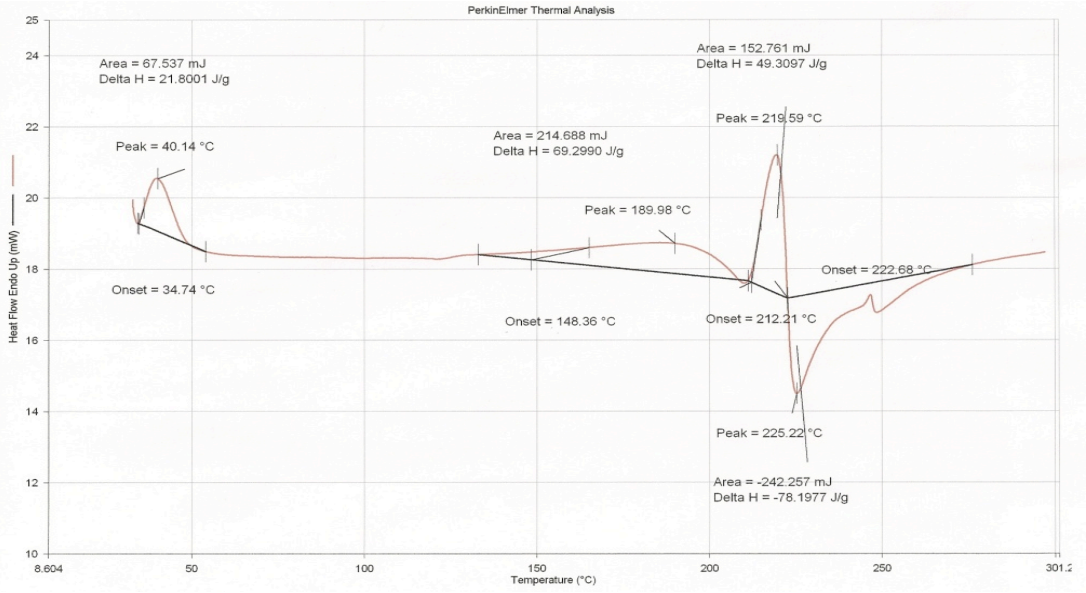

Figure 4.11 DSC of **Complex 1**

The value of effective **magnetic moment** ($\mu_{eff,}$), calculated from the values of χ_g (0.373 x 10^{-5} c.g.s.), χ_m (9.615 x 10^{-4} c.g.s.), χ_{dia} (-6.580 x 10^{-5} c.g.s) and thus χ_m^{corr} (1.027 x 10^{-3} c.g.s), is 1.57 B.M. at 298 K. The value is in good agreement with the expected spin-only value of 1.73 B.M. for a mononuclear copper(II) complex (one unpaired electron).

The **CV** voltammogram (**Figure 4.12**), scanned cathodically in the potential range of -1.6 V to +1.6 V, shows one cathodic peak at -0.70 V and one anodic peak at +0.41 V. It must be pointed out that the weak cathodic peak at +0.04 V was not due to the complex as it was also observed in the blank solution.

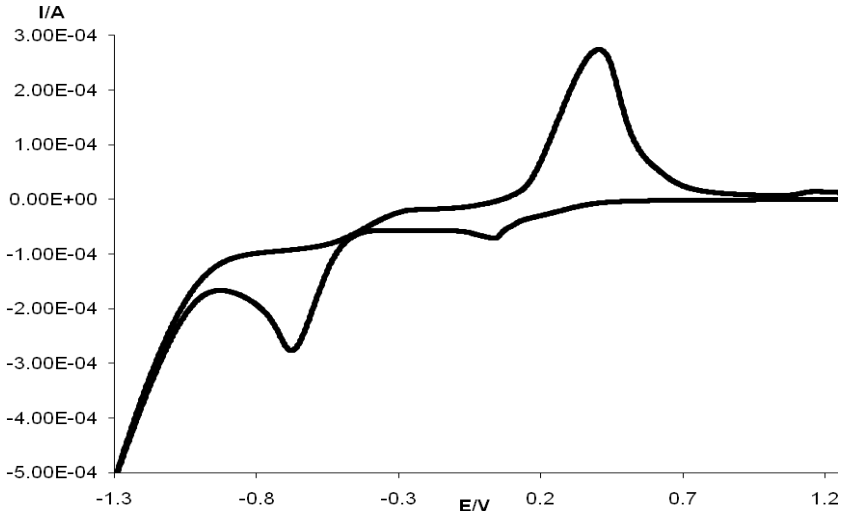

Figure 4.12 CV of **Complex 1**

The peaks are assigned to the reduction of [Cu(II)] complex to the [Cu(I)] complex, which was then reoxidized to [Cu(II)] complex, as shown below.

$$[\text{Cu(II)}] \underset{+0.41\ \text{V}}{\overset{-0.70\text{V}}{\rightleftharpoons}} [\text{Cu(I)}]$$

From the above assignment, the values of ΔE and I_{pa}/I_{pc} ratio are 1110 mV and 0.8 respectively. The expected value of ΔE for a reversible redox reaction is 59 mV at 298 K, and the expected I_{pa}/I_{pc} ratio for a chemically stable reduced complex is 1 [9]. Thus, the results suggest that **Complex 1** underwent a quasireversible redox reaction, possibly due to extensive geometrical change, and that the Cu(I) complex formed was chemically unstable.

The cathodic and anodic peaks obtained are compared to the mononuclear $[Cu(CH_3COO)_2(2,2'\text{-bipy})]$ (**Figure 4.13**) reported by Koo [10] ($E_{cathodic}$ = -0.54 V and E_{anodic} = -0.2 V ($E_{½}$ = -0.37 V). Thus, the reduction of Cu(II) to Cu(I) in **Complex 1** is more difficult, and it is likely due to the reduced positive charge on Cu(II) centre as it is bonded to five ligands, as well as due to the presence of conjugated π electrons from $CH_3CH{=}CHCOO$ ligand.

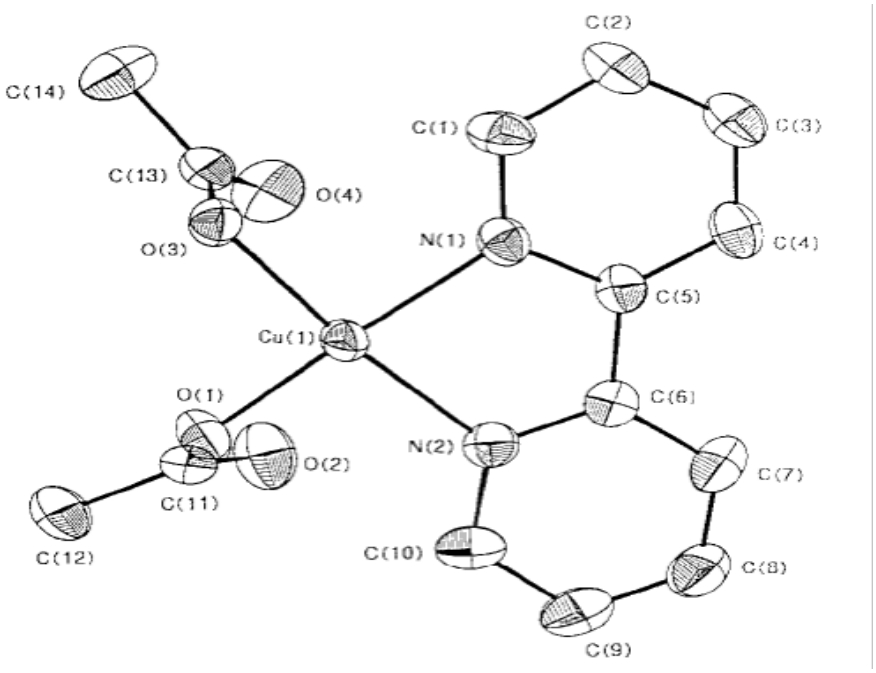

Figure 4.13 Structural formula of $[Cu(CH_3COO)_2(2,2'\text{-bipy})]$ [10]

(ii) Pale blue small needles

The pale blue small needles (**Complex 2**) deposited out of the filtrate on standing at room temperature for a week. It was soluble in methanol and ethanol, but insoluble in most other common organic solvents.

The **elemental analyses** give the C:H ratio of 13.3:1.0, which agrees with chemical formula $K_2Cu_2C_{22}H_{22}O_{12}$ (formula weight = 683.7 g mol^{-1}, calculated C:H ratio = 11.9:1.0).

The **FTIR** spectrum of **Complex 2** (**Figure 4.14)** is different from those of the starting materials (**Figure 4.5** and **Figure 4.6**) and from that of **Complex 1 (Figure 4.4)**.

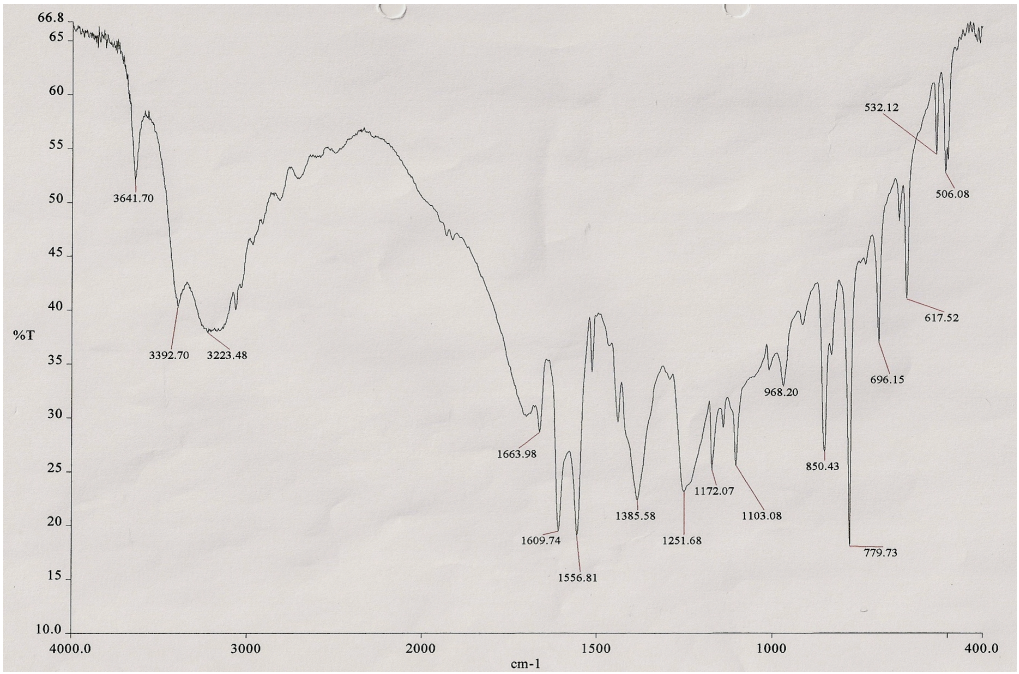

Figure 4.14 IR of **Complex 2**

The FTIR data and assignment for **Complex 2** is given in **Table 4.1.**

Table 4.1 FTIR data and assignment for **Complex 2**

Wavenumber (cm^{-1})	**Intensity**	**Assignment**
3396	Broad	OH
3223	Broad	OH
1610	Medium	C=C aromatic
1557	Medium	$\upsilon_{asymCOO}$
1386	Medium	υ_{symCOO}

The ΔCOO value (171 cm^{-1}) suggests bridging carboxylate ligands, and thus the complex may be dinuclear with the dimeric paddle-wheel structure as was reported for most metal(II) carboxylates [11-12].

The **UV-vis** spectrum for **Complex 2** in the solid state (**Figure 4.15 (a)**) and as a solution in 9:1 CH_3OH-CH_3CO_2H (**Figure 4.15 (b)**) show a broad *d-d* band at 659 nm and 697 nm (ε_{max}= 48.7 $M^{-1}cm^{-1}$) respectively. These suggest that the geometry at Cu(II) is square pyramidal in the solid state, and remained unchanged in the solution. The UV-

vis spectrum of the solution also shows a shoulder at about 380-400 nm. This supports a binuclear complex, as suggested from FTIR. The unexpectedly low ε_{max} for a dinuclear complex (normally about 200 – 400 $M^{-1}cm^{-1}$ [13] indicates a forbidden transition, and suggests a *trans*- geometry with a centre of inversion, *i*.

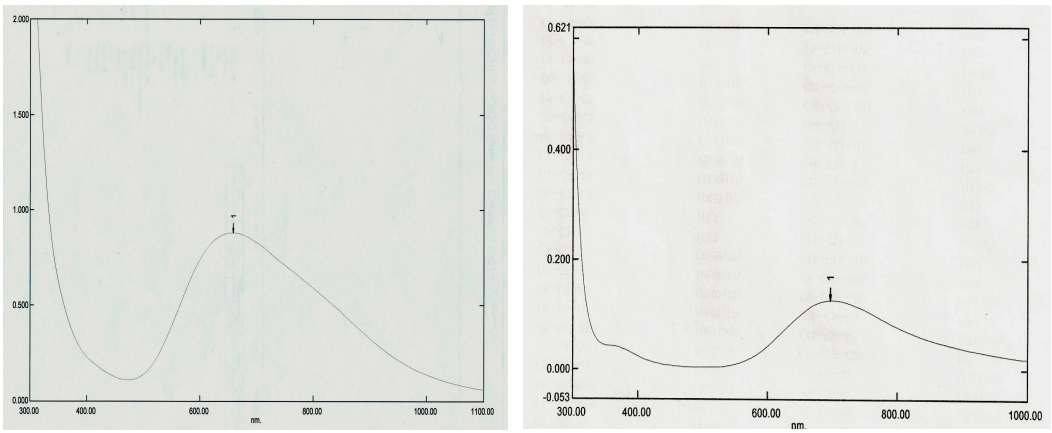

(a) (b)

Figure 4.15 UV of **Complex 2** in (a) solid; and (b) solution

It is noted that the λ_{max} value for **Complex 2** (659 nm) in the solid sample is lower than for **Complex 1** (703 nm). This indicates that the geometry at Cu(II) in **Complex 2** is more planar. The higher energy for the *d-d* electronic transitions for **Complex 2** suggests weaker axial interactions and thus stronger equatorial interactions between Cu(II) and the ligands. As a result, the magnetic $d_{x^2-y^2}$ orbital (SOMO) has more antibonding character (higher energy).

Combining the above results, **Complex 2** is proposed to have the structural formula of $K_2[Cu_2(p\text{-}OC_6H_4COO)_2(CH_3CH{=}CHCOO)_2(H_2O)_2]$ (**Figure 4.16)**. The formula shows bridging carboxylates as inferred from FTIR, and a binuclear complex with square pyramidal geometry at Cu(II) centres as suggested from UV-vis. Thus, it is the intended complex from the reaction, and its yield was 43.4%.

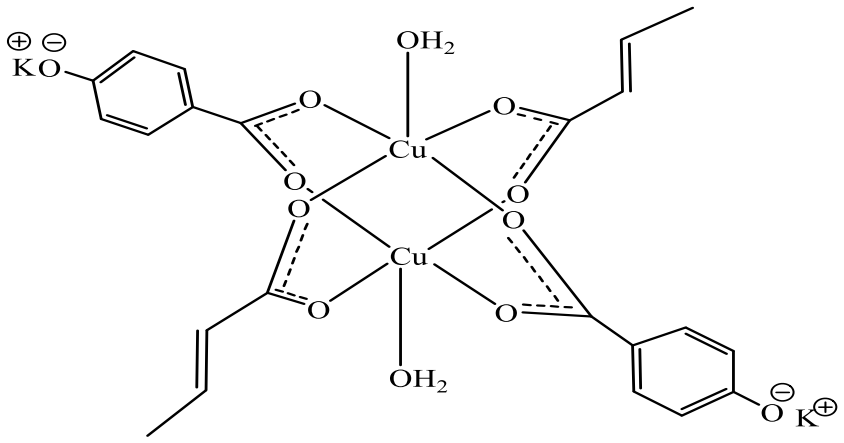

Figure 4.16 Proposed structural formula of **Complex 2,** showing the *trans*- isomer)

The optical **band gap** energy (E_g) is calculated using the formula $E_g = hc/(\lambda \times 1.6\text{x}10^{-19})$, where *h* is Planck constant (6.626 x 10^{-34} J s), *c* is the speed of light (3.0 x 10^8 m s^{-1}), and λ is the onset wavelength for the CT band from the UV-vis spectrum.

For **Complex 2**, the onset λ value is 400 nm, and hence E_g is 3.11 eV. This is higher than copper(I) sulfides (2 eV) [14] and CuO (1.2 eV) [15] but similar to TiO_2 (~3.30-3.87 eV) [16-17].

The **TGA** thermogram (**Figure 4.17**) indicates that **Complex 2** is thermally stable up to 190°C. It underwent four weight losses. The initial slow weight loss of 8.0% from 51°C to about 190°C is assigned the evaporation of weakly coordinated H_2O at the axial positions (expected, 5.3%).

The second weight loss of 41.9% is assigned to the decomposition of *p*-OC_6H_4COO (expected, 40.1%). The next total weight loss of 31.0% from 260°C to 906°C is assigned to the decomposition of $CH_3CH{=}CHCOO$ (expected, 24.9%). The results seem to suggest incomplete decomposition of $CH_3CH{=}CHCOO$, possibly due to the formation of thermally stable polymer(s). The amount of residue cannot be accurately determined from the thermogram as there was no distinct plateau at temperatures below 906°C.

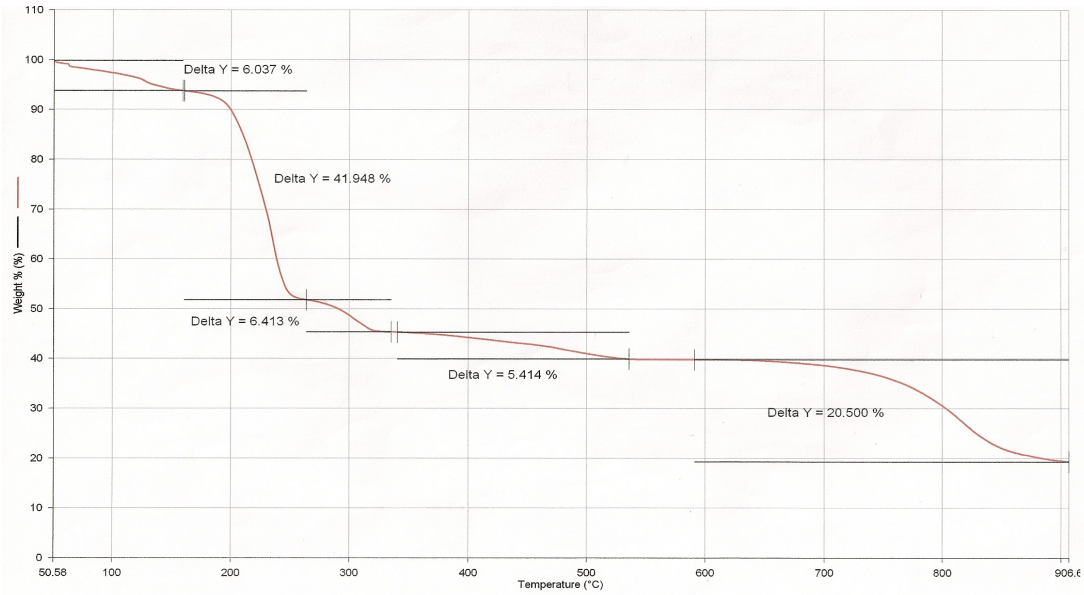

Figure 4.17 TGA of **Complex 2**

The **DSC** scan of **Complex 2** (**Figure 4.18**) shows three sets of two overlapping endotherms. The first set at 64°C ($\Delta H_{combined}$ = +43.5 kJ mol^{-1}) may correspond to the breaking of Cu(II)--OH_2 bond at the axial positions. The second and third sets at 133°C and 150°C ($\Delta H_{combined}$ = +25.7 kJ mol^{-1}), and at 206°C and 242°C ($\Delta H_{combined}$ = +42.2 kJ mol^{-1}), which occurred above its decomposition temperature (125°C from TGA), may correspond to the decomposition of the carboxylates to CO_2 and other volatiles. Beyond this temperature, there is a very strong exotherm at peak temperature 298°C. This is assigned to the polymerization of CH_3CH=CHCOO ligand, in agreement with the suggestion from TGA to account for its incomplete decomposition.

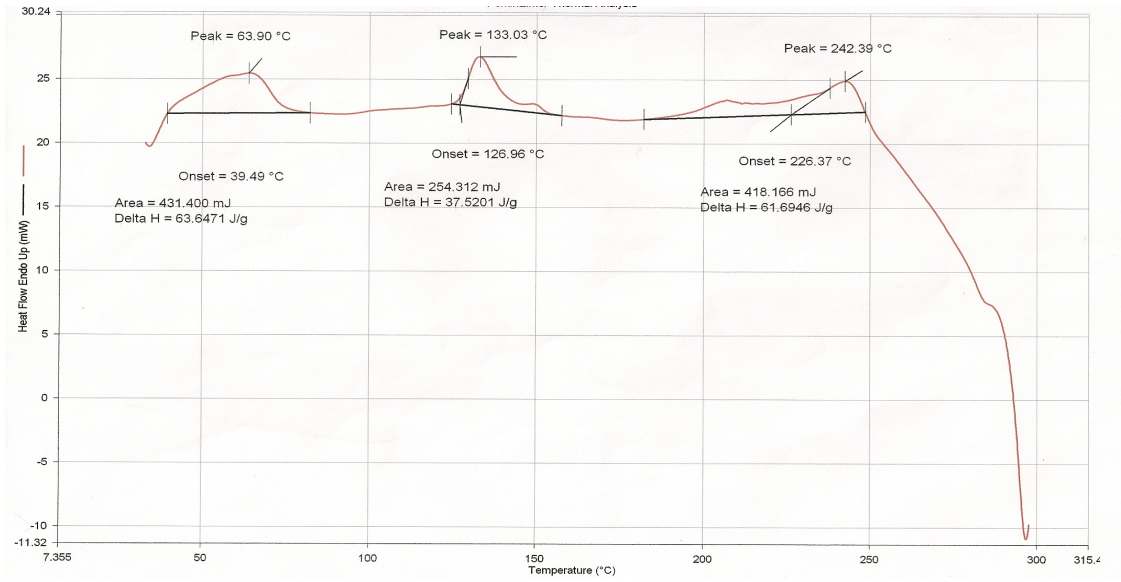

Figure 4.18 DSC of **Complex 2**

The value of μ_{eff}, calculated as before from the values of χ_g (0.04 x 10^{-5} c.g.s.), χ_m (2.74 x 10^{-4} c.g.s.), χ_{dia}, (-2.12 x 10^{-5} c.g.s.) and χ_m^{corr} (2.95 x 10^{-4} c.g.s.), is 0.84 B.M. at 298 K. The expected value for a dicopper(II) complex (two unpaired electrons) is 2.83 B.M.

The singlet and triplet energy level separation (or exchange integral), as a result of the electron spin interaction between the Cu(II) centres, or normally denoted as -2J, calculated using the Bleaney-Bower equation [18, 19], is -870 cm^{-1}.

The above results suggest a strong antiferromagnetic interaction between the two copper(II) centres in **Complex 2**. The interaction is postulated to occur through the carboxylate ligands, and is consistent with the proposed structure (**Figure 4.16)**.

It is interesting to note that the antiferromagnetic interaction in **Complex 2** is very strong compared to most paddle-wheel copper(II) carboxylates reported in the literature. For example, the -2J value for $[Cu_2(HCOO)_4(dmf)_2]$ is -470 cm^{-1} [20]. Possible explanations are: (a) the two unsaturated carboxylate ligands (*p*-OC_6H_4COO and $CH_3CH{=}CHCOO$), located *trans* to each other, provide effective communication routes, and (b) the strong electron donation of these ligands effectively reduced the positive

charge on each Cu(II), thus minimizing the repulsion and allowing for a more planar geometry (more effective orbital overlap), and/or (c) "direct" Cu-Cu δ bond through the magnetic $d_{x^2-y^2}$ orbitals or σ bond through the d_{z^2} orbitals.

The **CV** voltammogram (**Figure 4.19**) shows one cathodic peak at -0.84 V and one anodic peak at +0.32 V. However based on its proposed dinuclear structure, two cathodic and two anodic peaks are expected. A possible explanation is that the second reduction process may occur above -1.5 V (more difficult reduction).

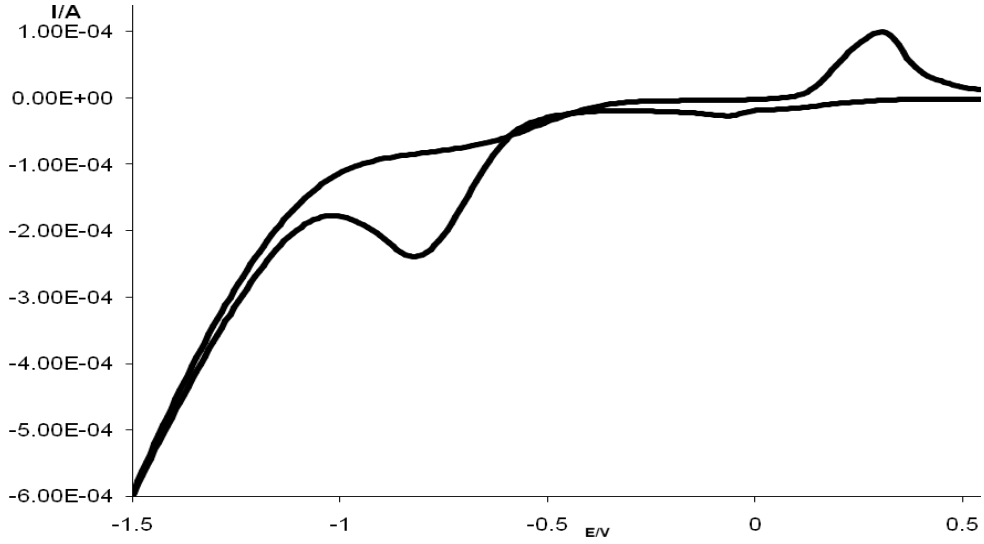

Figure 4.19 CV of **Complex 2**

The cathodic peak is assigned to reduction of dinuclear [Cu(II)Cu(II)] complex to the mixed-valence [Cu(II)Cu(I)] complex, and the anodic peak is assigned to the oxidation of the mixed-valence complex formed to the dinuclear [Cu(II)Cu(II)] complex. The redox process is shown below.

$$[\text{Cu(II)Cu(II)}] \underset{+0.32\ \text{V}}{\overset{-0.84\text{V}}{\rightleftharpoons}} [\text{Cu(II)Cu(I)}]$$

It is noted from the literature that the normally observed values for the reduction of [Cu(II)Cu(II)] to [Cu(II)Cu(I)] is about -0.5 V, reduction of [Cu(II)Cu(I)] to

[Cu(I)Cu(I)] is about -1 V [9], oxidation of [Cu(I)Cu(I)] to [Cu(II)Cu(I)] is about +0.31 V and oxidation of [Cu(II)Cu(I)] to [Cu(II)Cu(II)] is about +0.46V [8].

The current results may be similarly explained as for **Complex 1**. However, it is noted that Cu(II) in **Complex 2** is more difficult to be reduced, but are actually consistent with a more planar geometry at Cu(II) from the UV-vis.

The ΔE value is 1160 mV and I_{pa}/I_{pc} ratio is 1.5. These suggest that the complex undergoes quasireversible redox reaction, and that the mixed-valence [Cu(II)Cu(I)] complex is chemically unstable.

(b) K[Cu_2(p-OC_6H_4COO)(CH_3CH=$CHCOO)_3$]

The one-pot reaction involving *p*-HOC_6H_4COOH and CH_3CH=CHCOOH (mol ratio = 1:3) formed two complexes: a green powder and blue powder.

(i) Green powder

The green powder (**Complex 3**) was formed as the residue from the hot reaction mixture. It was sparingly soluble in methanol, ethanol and chloroform, and insoluble in most other common organic solvents.

The results from the **elemental analyses** give the C:H ratio of 8.3:1.0, which agrees with chemical formula $KCu_2C_{23}H_{31}O_{11}$ (formula weight = 649.7 g mol^{-1}, C:H ratio = 8.8:1.0).

The **FTIR** spectrum of the complex (**Figure 4.20**), is different from those of the starting materials (**Figure 4.5** and **Figure 4.6**). It shows the presence of all of the expected functional groups as previously discussed (**Table 4.1**). The ΔCOO value (167 cm^{-1}) suggests bridging carboxylate ligands.

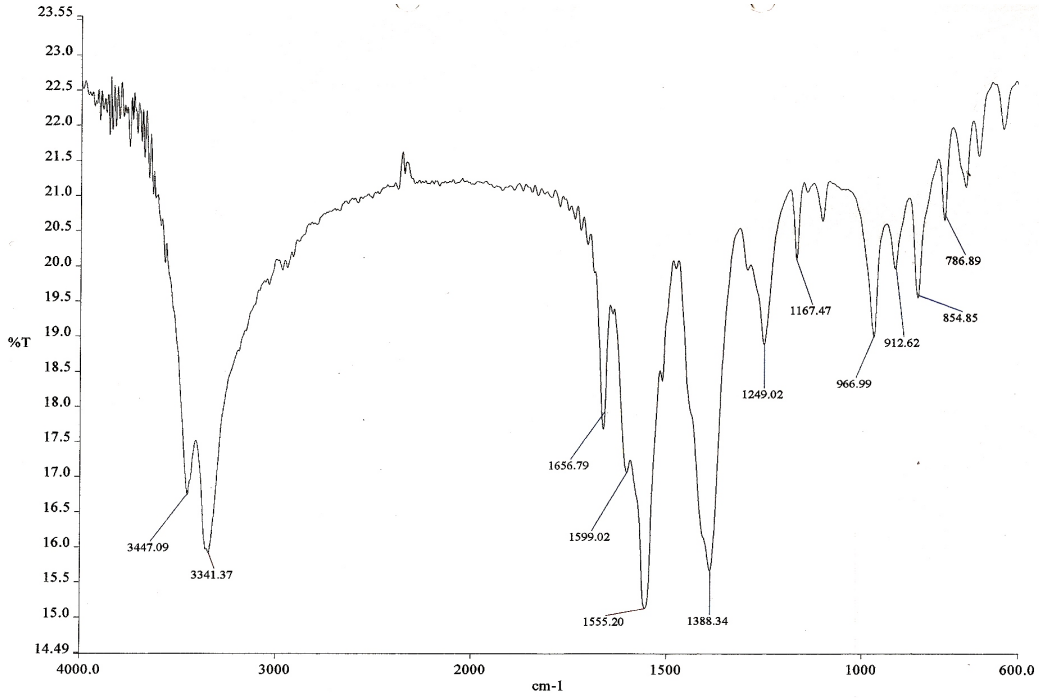

Figure 4.20 FTIR of **Complex 3**

The **UV-vis** spectra of the complex in the solid state (**Figure 4.21(a)**) and as a solution in 9:1 CH_3OH-CH_3COOH (**Figure 4.21(b)**), show a broad *d-d* band at 694 nm and 703 nm (ε_{max}= 197 $M^{-1}cm^{-1}$) respectively. The UV-vis spectrum of the solution also shows a shoulder at 380 nm. From these, it may be inferred that the complex is dimeric with square pyramidal Cu(II) centres in the solid state, and that the structure remained intact in solution.

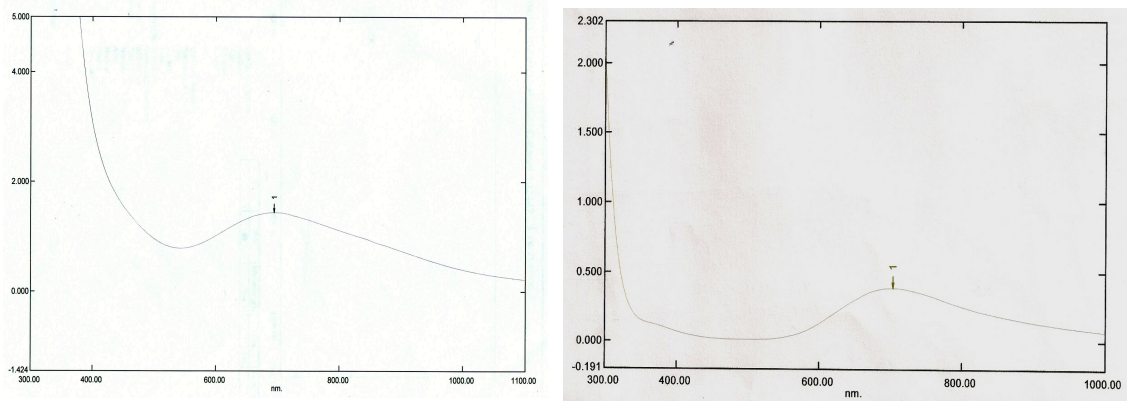

(a) (b)

Figure 4.21 UV of **Complex 3** in (a) solid; and (b) solution

Combining the above results, **Complex 3** is proposed to have the structural formula of $K[Cu_2(p\text{-}OC_6H_4COO)(CH_3CH{=}CHCOO)_3(CH_3CH_2OH)_2]$ as shown in **Figure 4.22**. The structure shows bridging carboxylates as inferred from FTIR, and binuclear complex with square-pyramidal Cu(II) centres as suggested from UV-vis spectra. Thus, it is the expected product from the reaction, and its yield was 55.8%.

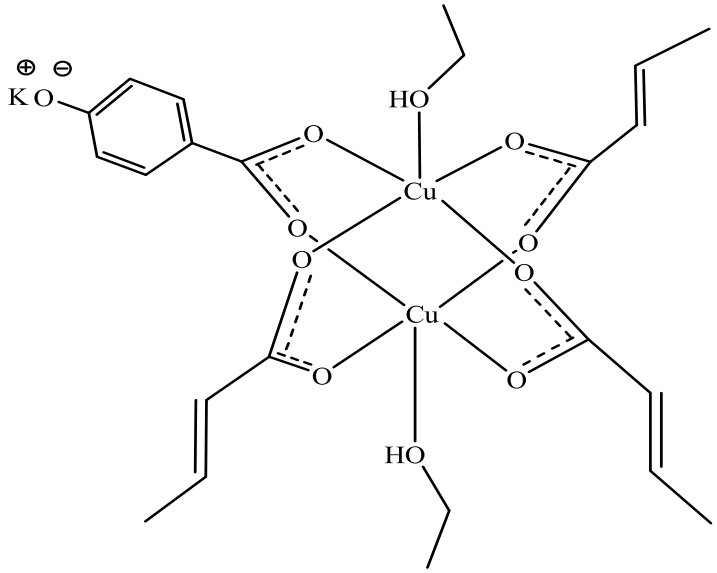

Figure 4.22 Proposed structural formula of **Complex 3**

The optical **band gap** energy for **Complex 3,** calculated as before from the onset λ value of 415 nm, is 2.99 eV. It is comparable to the **Complex 2** (3.10 eV). This suggests that the difference in the ratio of the arylcarboxylate to the alkylcarboxylate ligands has small effect on the photonic properties of these complexes.

The **TGA** thermogram (**Figure 4.23**) shows that **Complex 3** is thermally stable up to 817°C. Thus, the complex is significantly more thermally stable than the more symmetrical **Complex 2** ($K_2[Cu_2(p\text{-}OC_6H_4COO)_2(CH_3CH{=}CHCOO)_2(H_2O)_2]$; T_{dec} = 190°C). The result seems to suggest that $CH_3CH{=}CHCOO^-$ played an important role in increasing the thermal stability of a complex, possibly as a result of more extensive electronic delocalization and/or polymerization.

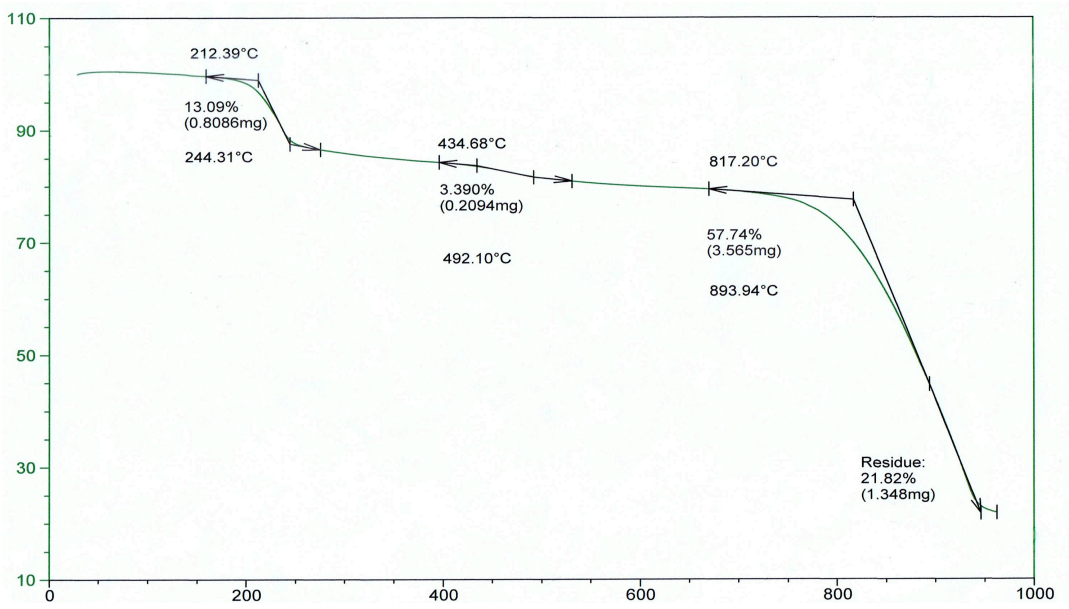

Figure 4.23 TGA of **Complex 3**

The thermogram also shows an initial weight loss of 13.1% at 212°C, assigned to the evaporation of CH_3CH_2OH (expected, 14.2%). Above this temperature, the combined weight loss of 61.1% is accounted for by the decomposition of all of the carboxylato ligands (expected, 60.4%). The small difference, if significant, suggests incomplete decomposition of the ligands, possibly due to the polymerization of $CH_3CH{=}CHCOO$. However, the amount of residue formed cannot be determined as there was no plateau at 900°C.

The **DSC** scan (**Figure 4.24**) shows a broad overlapping endothermic peaks from about 39°C to 121°C ($\Delta H_{combined}$ = +35 kJ mol^{-1}), which may be due to structural changes in the solid state. This is followed by a broad endothermic peak at 170°C (ΔH= +13 kJ mol^{-1}) which may be due to the breaking of H-bond between two CH_3CH_2OH molecules of neighbouring dimers. Finally, a strong exothermic peak at 222°C (ΔH = -82 kJ mol^{-1}), may be due to the polymerization of the $CH_3CH{=}CHCOO$ ligand, in agreement with the suggestion from TGA.

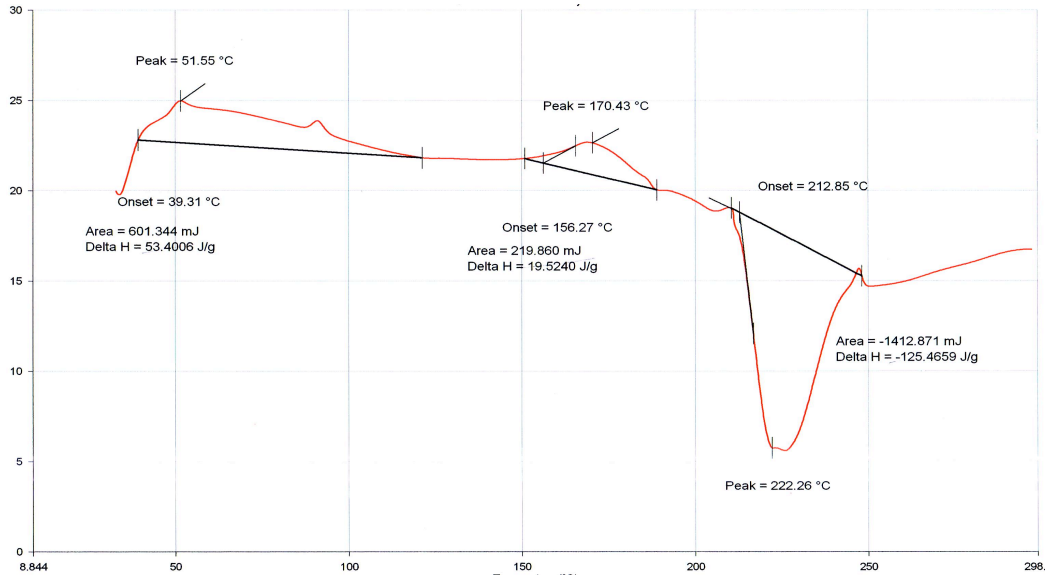

Figure 4.24 DSC of **Complex 3**

The value of μ_{eff}, calculated as before from the values of χ_g (0.013 x 10^{-5} c.g.s.), χ_m (8.45 x 10^{-5} c.g.s.), χ_{dia} (-1.14 x 10^{-4} c.g.s.) and χ_m^{corr} (1.98 x 10^{-4} c.g.s.), is 0.69 B.M. at 298 K. The 2J value is –1041 cm^{-1}. These indicate a strong antiferromagnetic interaction, as was observed for **Complex 2** ($K_2[Cu_2(p\text{-}OC_6H_4COO)_2(CH_3CH{=}CHCOO)_2(H_2O)_2]$, and may be similarly explained.

However, the values for **Complex 3** is significantly lower than that of the more symmetrical **Complex 2** (μ_{eff} = 0.84 B.M.; 2J = -870 cm^{-1}) suggesting a much stronger electronic communication between the two Cu(II) centres in the former complex. The results seem to suggest that $CH_3CH{=}CHCOO$ ligand is a more effective superexchange pathway for electrons and/or electron donor compared to *p*-OC_6H_4COO ligand.

The **CV** voltammogram for **Complex 3** (**Figure 4.25**), recorded cathodically from 1.0 V to -1.5 V, shows one cathodic peak at -0.72 V and one anodic peak at +0.38 V. The value for ΔE is 1100 mV. The results are similar to the more symmetrical **Complex 2** (E_c = -0.84 V; E_a = +0.32 V; ΔE = 1160 mV), and may be similarly explained.

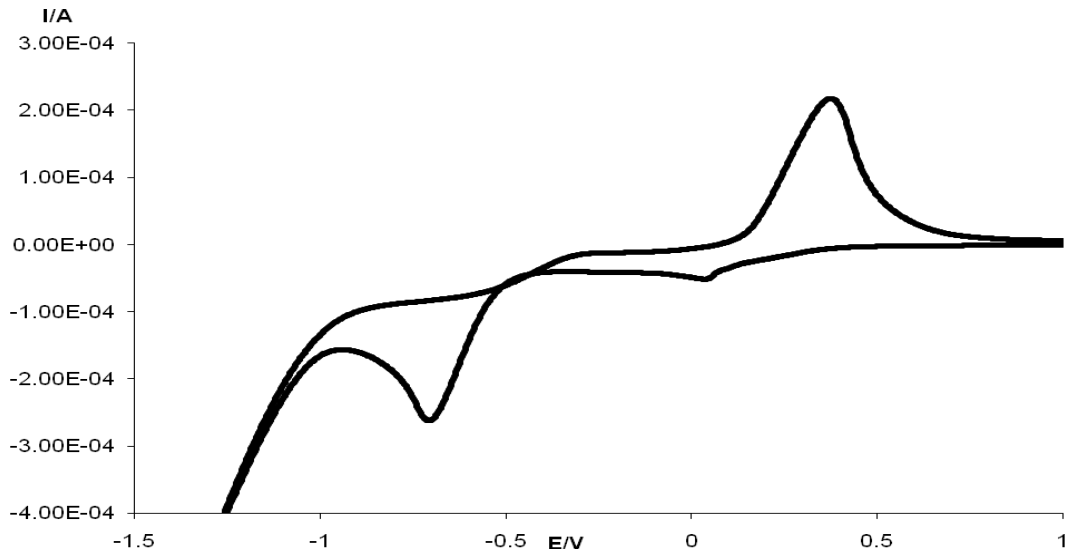

Figure 4.25 CV of **Complex 3**

However, the I_{pa}/I_{pc} ratio for **Complex 3** (1.0) is lower than that of **Complex 2**. (1.5), suggesting that the mixed-valence complex formed from **Complex 3** is chemically more stable. The redox process is shown below.

$$[\text{Cu(II)Cu(II)}] \underset{+0.38\ \text{V}}{\overset{-0.72\text{V}}{\rightleftharpoons}} [\text{Cu(II)Cu(I)}]$$

The results seems to suggest that the difference in the arylcarboxylate:alkylcarboxylate ratios does not significantly affect the redox properties of these mixed-carboxylate complexes.

(ii) Blue powder

The blue powder (**Complex 4**) was deposited out of the filtrate on standing at room temperature for a week. It was sparingly soluble in methanol, ethanol and chloroform, and insoluble in most other common organic solvents.

The results of the **elemental analyses** give the C:H ratio of 9.5:1. This agrees with the chemical formula $KCu_2C_{19}H_{23}O_{11}$ (formula weight = 595.6 g mol^{-1}, C:H ratio = 9.1:1.0).

Its **FTIR** spectrum (**Figure 4.26**) is different from that of **Complex 3**. It shows the presence of all of the expected functional groups as previously discussed. The ΔCOO values are 140 cm^{-1} and 185 cm^{-1}, suggesting chelating and *syn-anti* bridging carboxylate ligands, respectively [21].

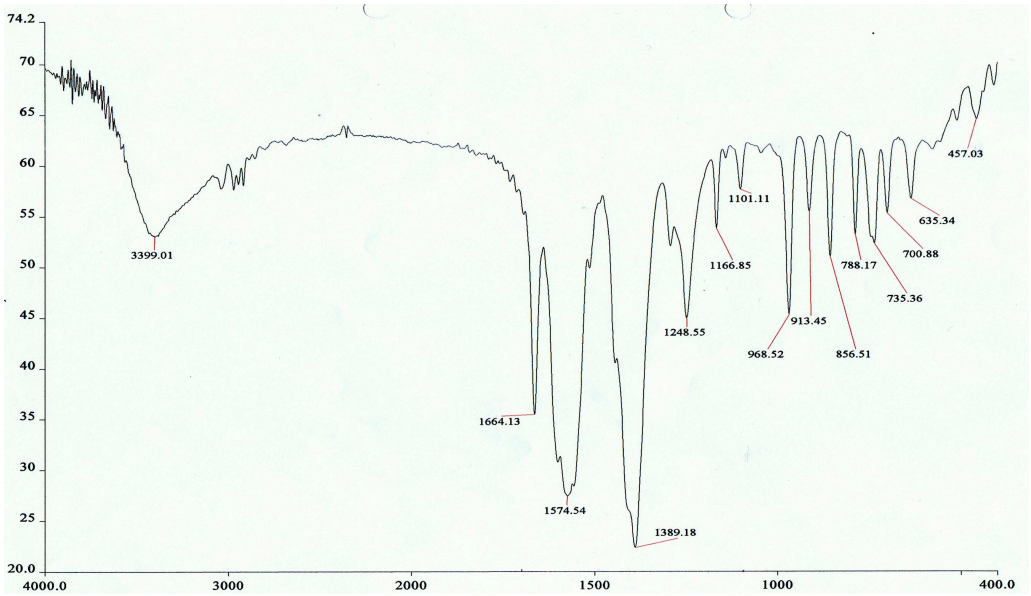

Figure 4.26 FTIR of **Complex 4**

Its **UV-vis** spectra in the solid state (**Figure 4.27(a)**) and as a solution in 9:1 CH_3OH-CH_3COOH (**Figure 4.27(b)**) show a broad *d-d* band at 653 nm and 696 nm (ε_{max}= 150 $M^{-1}cm^{-1}$) respectively. The UV-vis spectrum of the solution also shows a shoulder at 365 nm. From these, it may be inferred that **Complex 4** is dimeric with square pyramidal Cu(II) centres in the solid state, and the structure remained intact in solution. It is noted that the *d-d* band for **Complex 4** is at a higher energy compared to **Complex 3** (694 nm), suggesting a stronger Cu(II)-OOCR interaction in the former complex.

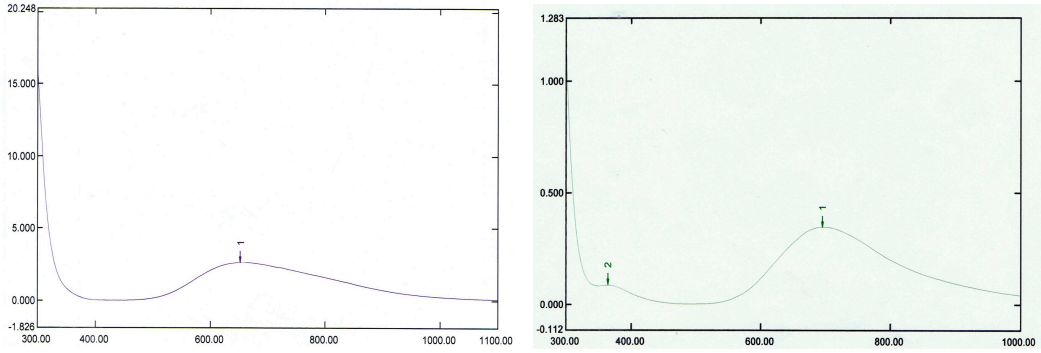

(a) (b)

Figure 4.27 The UV of **Complex 4** in (a) solid; and (b) solution

Combining the above results, **Complex 4** is proposed to have the structural formula of $K[Cu_2(p\text{-}OC_6H_4COO)(CH_3CH{=}CHCOO)_3].2H_2O$ **(Figure 4.28)**. The structure shows *syn-anti* and chelating carboxylates as inferred from FTIR, and binuclear square-pyramidal Cu(II) as suggested from UV-vis spectra. Hence, it is also the expected product from the reaction, and its yield was 49.2%. However, it is to be noted that **Complex 4** differs from **Complex 3** in the binding modes of both carboxylate ligands, and on the presence of different neutral molecules.

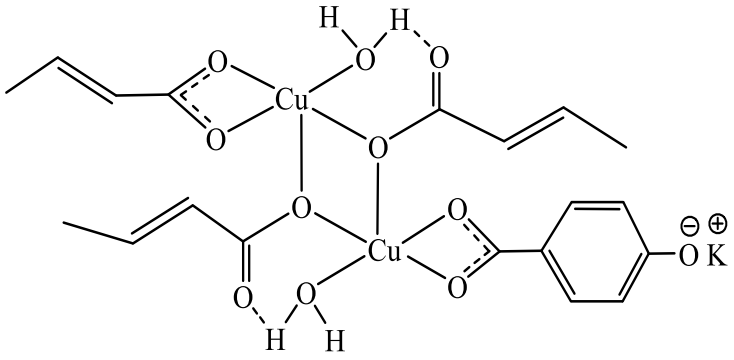

Figure 4.28 Proposed structural formula of **Complex 4**

The optical **band gap** energy for **Complex 4,** calculated as before from the onset λ value of 400 nm, is 3.11 eV. The value is comparable to the **Complex 3** (2.99 eV). This suggest that the geometrical differences do not greatly affect the photonic properties of these complexes.

The **TGA** thermogram (**Figure 4.29**) indicates that **Complex 4** is thermally stable up to 175°C. Thus, it is significantly less stable than **Complex 3** (T_{dec} = 817°C). This may be due to the weaker *syn-anti* bridging mode of $CH_3CH{=}CHCOO$ in the former complex compared to the stronger *syn-syn* bridging mode of the same ligand in the latter complex.

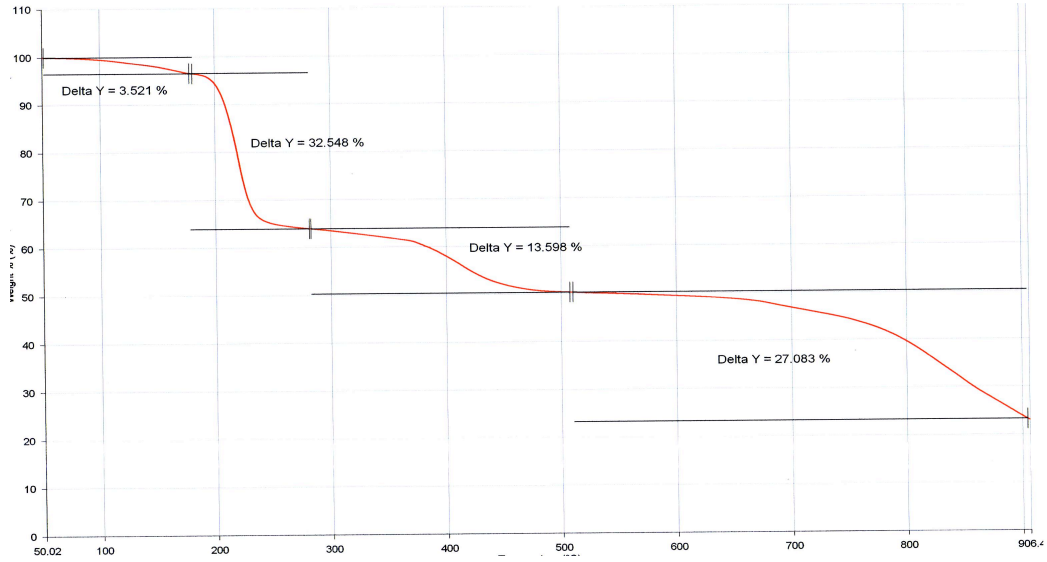

Figure 4.29 TGA of **Complex 4**

The thermogram also shows an initial weight loss of 5% at about 100°C, assigned to evaporation of H_2O molecules (expected, 6%). The complex then suffered three weight losses of 31%, 14% and 27% at 175°C, 280°C, and 622°C, respectively. These are assigned to loss of two *syn-anti* bridging $CH_3CH{=}CHCOO$ ligands (expected, 29%), chelating $CH_3CH{=}CHCOO$ ligand (expected, 14%) and chelating *p*-OC_6H_4COO ligand (expected, 23%) respectively. The results are in agreement with the proposed structural formula (**Figure 4.28**).

However, the amount of residue, which may be a mixture of CuO and K_2O, cannot be determined accurately from the thermogram as there was no distinct plateau at temperatures below 900°C. Thus, its formula weight could not be estimated.

The **DSC** scan (**Figure 4.30**) shows a broad endothermic peak at 170°C (ΔH = +34.8 kJ mol^{-1}) and a less broad endothermic peak at 214°C (ΔH = +22.9 kJ mol^{-1}). This is followed immediately by a strong exothermic peak at 227°C (ΔH = -99.9 kJ mol^{-1}). The first endothermic peak occurs just below its decomposition temperature (T_{dec} = 175°C), and thus is assigned to the dissociation of *syn-anti* bridging $CH_3CH{=}CHCOO$ and chelating *p*-OC_6H_4COO ligands. The second endotherm is assigned to the decomposition of the chelating $CH_3CH{=}CHCOO$ ligand, while the exothermic peak is assigned to the polymerization of unsaturated $CH_3CH{=}CH$ radical formed from the decarboxylation of $CH_3CH{=}CHCOO$ ligand. These results are in good agreement with TGA.

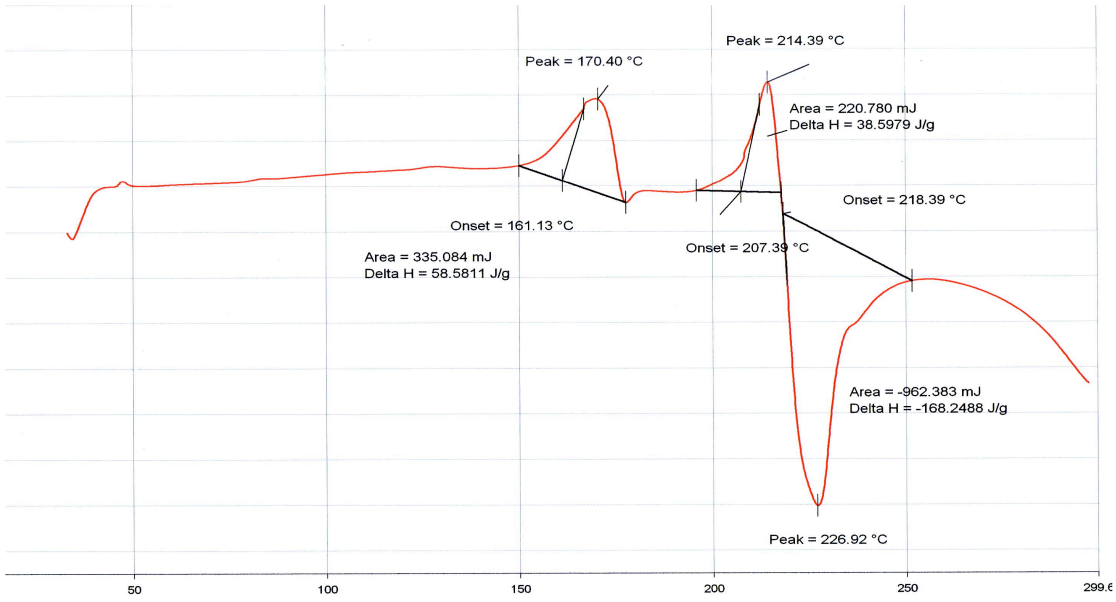

Figure 4.30 DSC of **Complex 4**

The value of μ_{eff}, calculated as before from the values of χ_g (0.387 x 10^{-5} c.g.s.), χ_m (2.30 x 10^{-3} c.g.s.), χ_{dia} (-8.75 x 10^{-5} c.g.s.) and χ_m^{corr} (2.38 x 10^{-3} c.g.s.), is 2.39 B.M. at 298 K. The 2J value is –180 cm^{-1}. These values are significantly higher than those of **Complex 3** (0.63 B.M.; -1041 cm^{-1}), suggesting a weaker antiferromagnetic interaction between the two Cu(II) centres.

However, the result is actually in good agreement with the proposed structural formula, and with that reported by Konar et al. [22], in which the two Cu(II) were also *syn-anti* bridged by the carboxylate ligand [21]. These authors suggested that the almost negligible coupling between the Cu(II) centres in their complex was because of the reduction of the magnetic pathway as the basal ligand was well directed ($d_{x^2-y^2}$ magnetic orbital) but the axial ligand was unfavourably located (d_{z^2} orbital).

The **CV** voltammogram (**Figure 4.31**) shows a cathodic peak at -0.77 V and an anodic peak at +0.38 V.

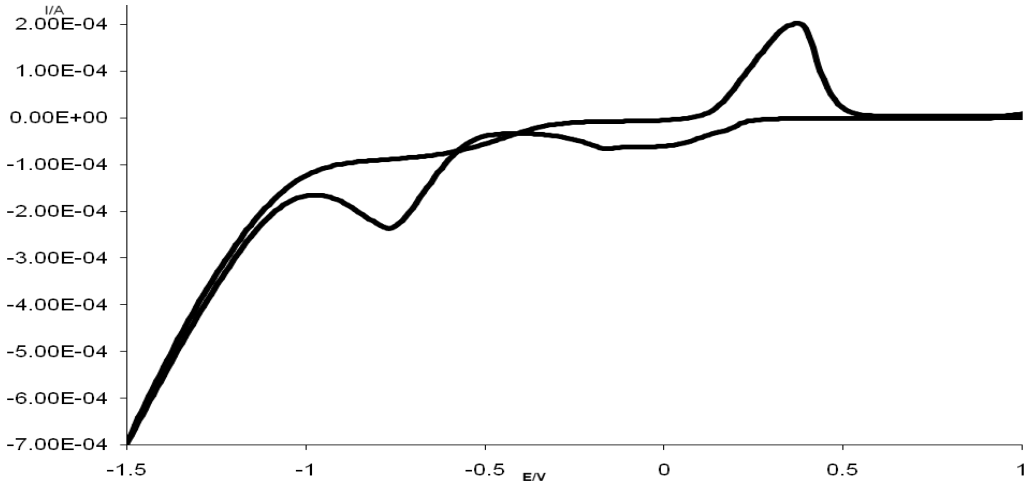

Figure 4.31 CV of **Complex 4**

The value for ΔE is 1150 mV and for I_{pa}/I_{pc} ratio is 1.0. The redox process is shown below.

$$[\text{Cu(II)Cu(II)}] \underset{+0.38\ \text{V}}{\overset{-0.77\text{V}}{\rightleftharpoons}} [\text{Cu(II)Cu(I)}]$$

It can be seen that the results are similar to those of **Complex 3** (-0.72 V; +0.38 V; ΔE = 1100 mV; I_{pa}/I_{pc} = 1.0), and thus may be similarly explained.

From this, it may be concluded that the difference in the structure does not significantly affect the redox properties of these complexes.

(c) $K_3[Cu_2(p\text{-}OC_6H_4COO)_3(CH_3CH{=}CHCOO)]$

The one-pot reaction involving *p*-HOC_6H_4COOH and $CH_3CH{=}CHCOOH$ (mol ratio = 3:1) formed a dark brown powder. Based on the following analytical results, the product is actually **Complex 1** ($K[Cu(CH_3CH{=}CHCO_2)(OH)_2(H_2O)].H_2O$) (**Figure 4.9**). Hence, its yield was 19.5%.

The results from the elemental analyses give the C:H ratio of 3.9:1.0, which agrees with chemical formula $KCuC_4H_{11}O_6$ (formula weight = 257.8 g mol^{-1}; calculated C:H ratio = 4.3:1.0). Its FTIR spectrum (**Figure 4.32**) is similar to that of **Complex 1** (**Figure 4.4**).

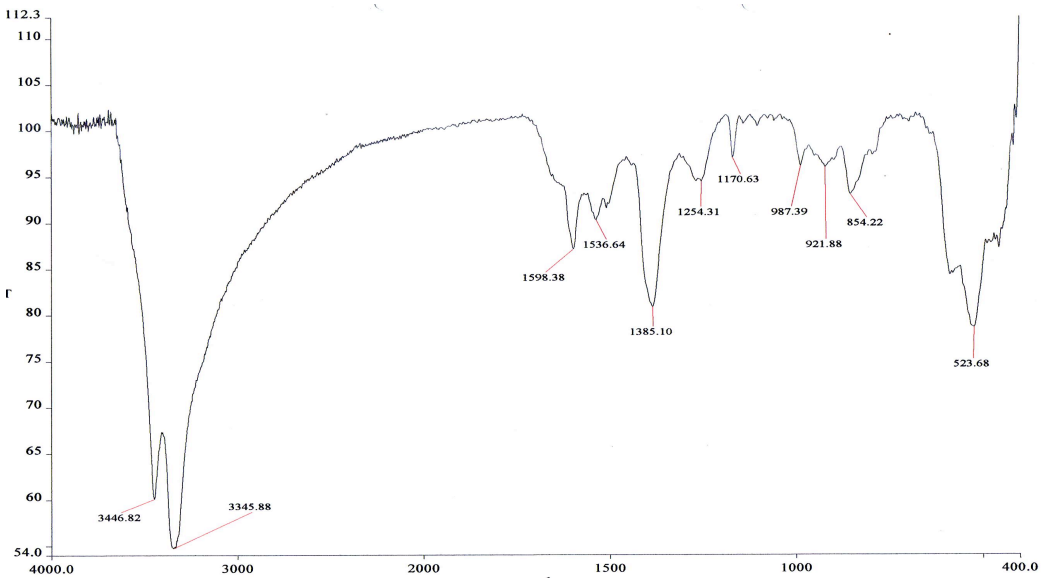

Figure 4.32 FTIR of dark brown powder

From this, it may be conclude that the one-pot method is unsuitable for the preparation of $K_3[Cu_2(p\text{-}OC_6H_4COO)_3(CH_3CH{=}CHCOO)]$.

(d) *Summary*

The one-pot reaction involving different ratios of *p*-OC_6H_4COO and $CH_3CH{=}CHCOO$ ligands was successfully used to prepare the intended ionic complex for n = 1 and 2, but not for n = 3. Except for **Complex 1**, which was mononuclear, the other complexes

were dinuclear with square pyramidal geometry at the two Cu(II) centres. The thermal stability of these complexes cannot be correlated with nuclearity, geometry, and ratio of aromatic to unsaturated aliphatic carboxylates. As expected, complexes with *syn,syn* bridging carboxylate ligand have a stronger antiferromagnetic interaction compared to *syn,anti* bridging carboxylate ligand; the strongest interaction was exhibited by **Complex 3** (higher ratio of unsaturated aliphatic carboxylate ligand). All complexes showed quasi-reversible redox properties. The mixed–valence [Cu(II)Cu(I)] complexes formed from the complexes with a higher ratio of unsaturated aliphatic carboxylate ligands were chemically stable. The analytical results are summarized in **Table 4.2**.

Table 4.2 Analytical results for complexes from the one-pot reaction

	Complex 1	**Complex 2**	**Complex 3**	**Complex 4**
Structural formula*	$K[Cu(OH)_2L'(H_2O)]$	$K_2[Cu_2L_2L'_2(H_2O)_2]$	$K[Cu_2LL'_3(EtOH)_2]$	$K[Cu_2LL'_3]$
ΔCOO/ cm^{-1}	136 (chelating)	171 (bridging)	167 (bridging)	140 (chelating) 185 (*syn,anti*-bridging)
λ_{max}/nm solid	725	659	694	653
solution (ε_{max}/ $M^{-1}cm^{-1}$)	703 (302)	697 (48.7)	703 (197)	696 (150)
$T_{decomposition}$ /^oC	635	190	817	175
μ_{eff} (2J)	1.57 #	0.84 (-870) antiferromagnetic	0.69 (-1041) antiferromagnetic	2.39 (-180) antiferromagnetic
E_{pc}/V E_{pa}/V (I_{pc}/I_{pa})	-0.70 +0.41 (0.8)	-0.84 +0.32 (1.5)	-0.72 +0.38 (1.0)	-0.77 +0.38 (1.0)

* solvates are not shown; L = *p*-OC_6H_4COO; L' = $CH_3CH{=}CHCOO$; # Not applicable

4.2.2 $K_n[Cu_2(p\text{-}OC_6H_4COO)_n(CH_2=C(CH_3)COO)_{4-n}]$

The second part of this work was to study the effect of branched unsaturated alkylcarboxylate ligand, namely $CH_2=C(CH_3)COO$, on the geometry, thermal, magnetic and redox properties of the ionic mixed-carboxylate complexes. A total of three (3) complexes were obtained by the one-pot synthesis. These are again discussed, starting with more symmetrical complexes (n =2), and then less symmetrical complexes (n=1 followed by n =3).

(a) $K_2[Cu_2(p\text{-}OC_6H_4COO)_2(CH_2=C(CH_3)COO)_2]$

The one-pot reaction involving p-HOC_6H_4COOH and $CH_2=C(CH_3)COOH$ (mol ratio = 1:1) formed a green powder (**Complex 5**), obtained as the residue from the hot reaction mixture. It was sparingly soluble in methanol, ethanol and chloroform, and insoluble in most other common organic solvents.

The results from the **elemental analyses** give the C:H ratio of 12.2:1.0, which agrees with chemical formula $(KCuC_{15}H_{15}O_7)_3$ (formula weight = 1229.8 g mol^{-1}; calculated C:H ratio = 11.9:1.0).

Its **FTIR spectrum** (**Figure 4.33**) is different from those of the starting materials (**Figure 4.34** and **Figure 4.5**). It shows the presence of all of the expected functional groups as previously discussed. The ΔCOO value is 130 cm^{-1}, suggesting chelating carboxylate ligands.

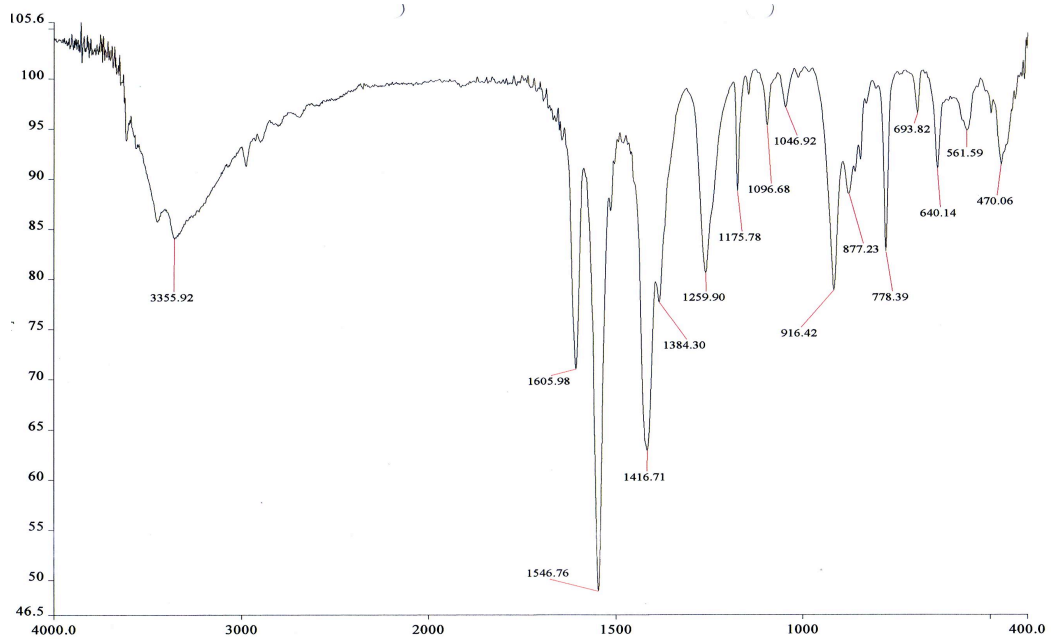

Figure 4.33 FTIR of **Complex 5**

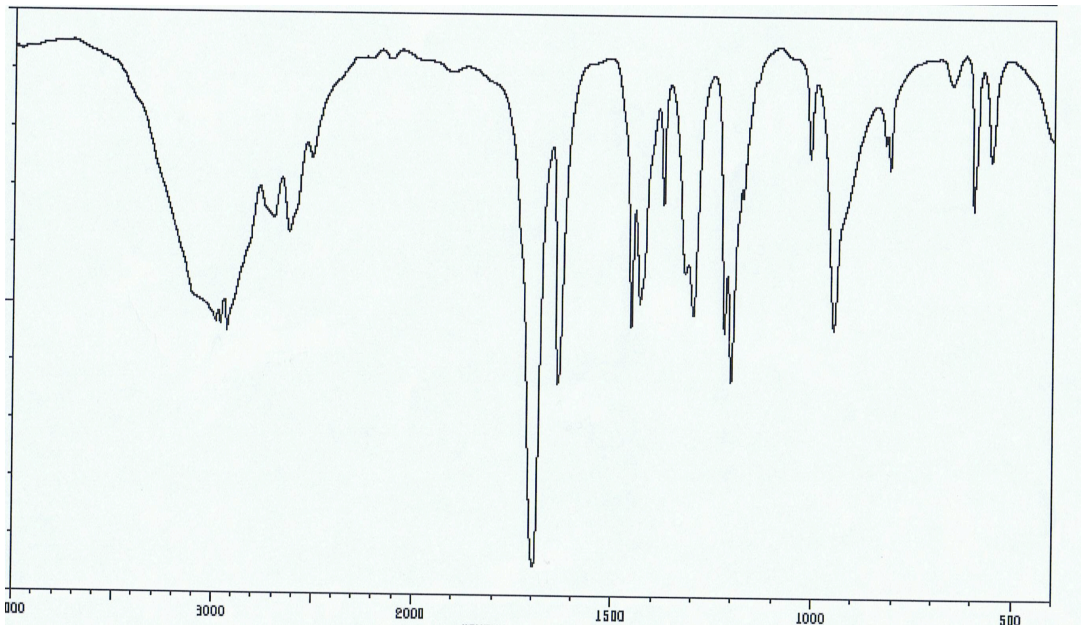

Figure 4.34 FTIR of CH_2=C(CH_3)COOH

The **UV-vis spectra** of the complex in the solid state (**Figure 4.35 (a)**) and as a solution in 9:1 CH_3OH-CH_3COOH (**Figure 4.35 (b)**), show a broad *d-d* band at 730 nm and 699 nm (ε_{max}= 207 $M^{-1}cm^{-1}$) respectively. From these, it may be inferred that the complex has octahedral Cu(II) centre in the solid state, and square pyramidal in solution.

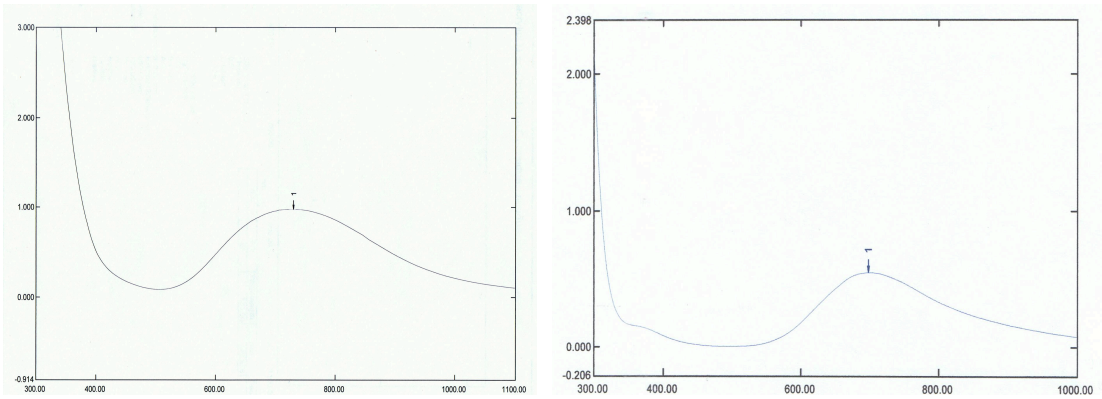

(a) (b)

Figure 4.35 UV-vis of **Complex 5** in (a) solid; and (b) solution

Combining the above results, **Complex 5** is proposed to be a trimer with the structural formula $\{K[Cu(p\text{-}OC_6H_4COO)(CH_2{=}C(CH_3)COO)(CH_2{=}C(CH_3)COOH)]\}_3$ (**Figure 4.36)**. The structure agrees with the empirical formula of $KCuC_{15}H_{15}O_7$ from the elemental analyses, chelating carboxylates as inferred from FTIR, and octahedral Cu(II) as suggested from UV-vis spectra. Hence, its yield was 59.2%, and it is not the expected product from the reaction.

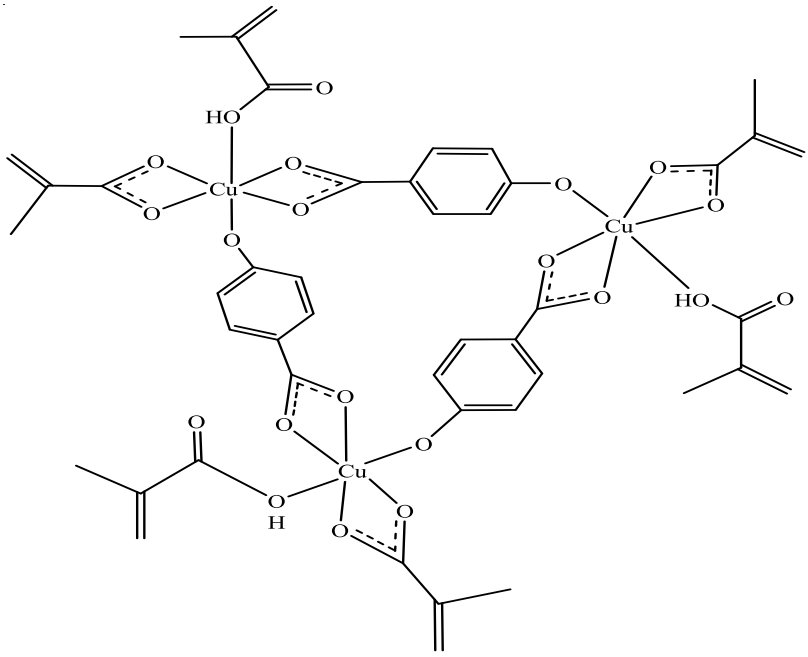

Figure 4.36 Proposed structural formula of [**Complex 5**]$^-$ (K^+ ions are not shown)

The **TGA** thermogram (**Figure 4.37**) shows that **Complex 5** decomposed at 720°C. Thus it is significantly more thermally stable than **Complex 2** ($K_2[Cu_2(p\text{-}OC_6H_4COO)_2(CH_3CH{=}CHCOO)_2(H_2O)_2]$; T_{dec} = 190°C), consistent with the proposed trimeric structure.

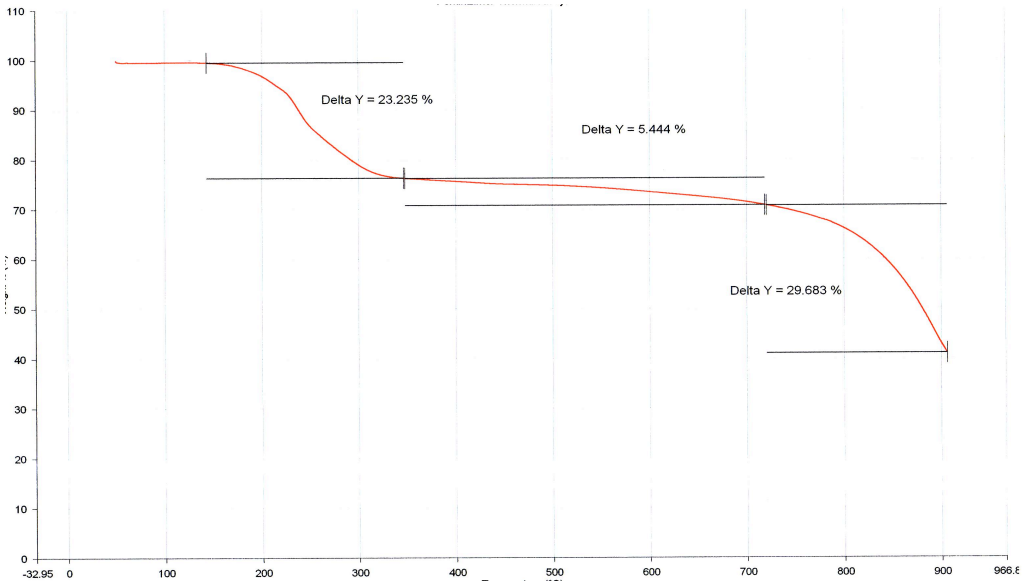

Figure 4.37 TGA of **Complex 5**

The thermogram also shows that the complex underwent the first weight loss of 23.2% at 160°C assigned to the evaporation of $CH_3CH_2{=}CCOOH$ (expected, 21.0%; boiling point, 161°C). There is no residue above 905°C, which is as expected from its proposed trimeric structure.

The **DSC** scan (**Figure 4.38**) shows a weak endothermic peak at 93°C (ΔH = +10 kJ mol^{-1}), assigned to the energy needed to overcome the weak axial bonds formed between the monomers. This is followed by a broad and very exothermic peak at 249°C (ΔH = -781 kJ mol^{-1}) which may be due to the polymerization of the $CH_3CH{=}CHCOO$ ligands as suggested for **Complex 1**, as well as some other strong bond-forming processes.

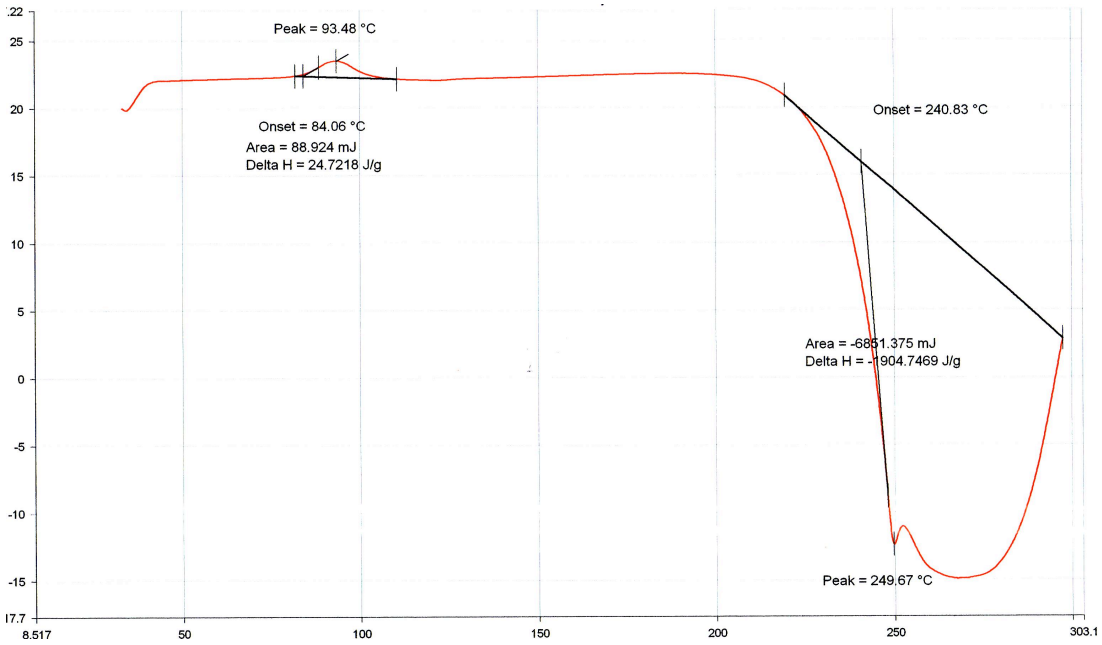

Figure 4.38 DSC of **Complex 5**

The **magnetic** data for the complex are: χ_g = 0.58 x 10^{-5}c.g.s., χ_m = 7.13 x 10^{-3} c.g.s., and χ_{dia} = -5.57 x 10^{-5} c.g.s. From these, the value of χ_m^{corr} is 7.19 x 10^{-3} c.g.s and that of μ_{eff} is 4.16 B.M. at 298 K. The value is slightly higher than the expected value for three unpaired electron (3.87 B.M.). The 2J value is +220 cm^{-1}. The results suggest ferromagnetic interaction in the complex, which is consistent with the proposed trimeric structure.

The **CV** voltammogram of **Complex 5** (**Figure 4.39**), scanned cathodically in the range (+1.0 V) – (-1.5 V), shows one cathodic peak at -0.80 V and an anodic peak at +0.31 V.

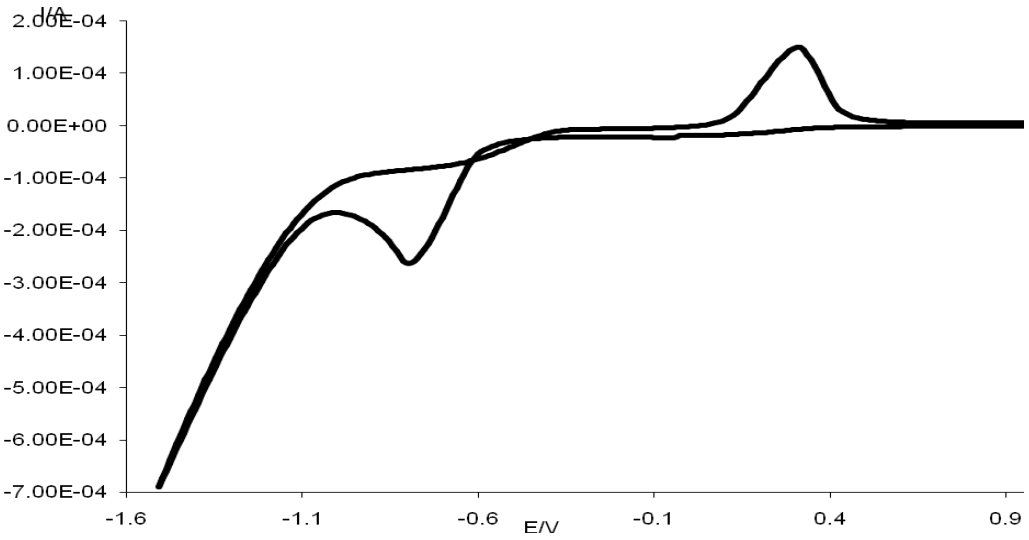

Figure 4.39 CV of **Complex 5**

The cathodic peak at -0.80 V is assigned to reduction of the mononuclear [Cu(II)] complex to mononuclear [Cu(I)] complex, which was then reoxidized to the mononuclear [Cu(II)] complex at +0.31 V. The redox process is shown below.

$$[\text{Cu(II)}] \underset{+0.31\ \text{V}}{\overset{-0.80\text{V}}{\rightleftharpoons}} [\text{Cu(I)}]$$

The values of ΔE and I_{pa}/I_{pc} ratio for [Cu(II)-Cu(I)] redox reaction are 1110 mV and 0.3 respectively. Thus, the result suggests that the trimeric structure of **Complex 5** "collapsed" in solution to monomers, which then undergoes quasireversible redox reaction similar to that of **Complex 2** ($K_2[Cu_2(p\text{-}OC_6H_4COO)_2(CH_3CH{=}CHCOO)_2(H_2O)_2]$; E_c = 0.84 V; E_a = +0.32 V; ΔE = 1160 mV; I_{pa}/I_{pc} = 1.5).

(b) $K[Cu_2(p\text{-}OC_6H_4COO)(CH_2{=}C(CH_3)COO)_3]$

The one-pot reaction involving *p*-HOC_6H_4COOH and $CH_2{=}C(CH_3)COOH$ (mol ratio = 1:3) formed a green powder (**Complex 6)**, obtained as the residue from the hot reaction mixture. It was sparingly soluble in methanol, ethanol and chloroform, and insoluble in most other common organic solvents.

The results from the **elemental analyses** give the C:H ratio of 9.7:1.0, which agrees with chemical formula $KCu_2C_{25}H_{31}O_{12}$ (formula weight = 409.9 g mol^{-1}; calculated C:H ratio = 9.6:1.0).

The **FTIR spectrum** of the complex (**Figure 4.40**) is different from those of the starting materials (**Figure 4.34** and **Figure 4.5**), and shows the presence of all of the expected functional groups as previously discussed, including a medium peak at 1644 cm^{-1} assigned to the free $CH_2=C(CH_3)COOH$. The ΔCOO value is 161 cm^{-1}, suggesting bridging carboxylate ligands.

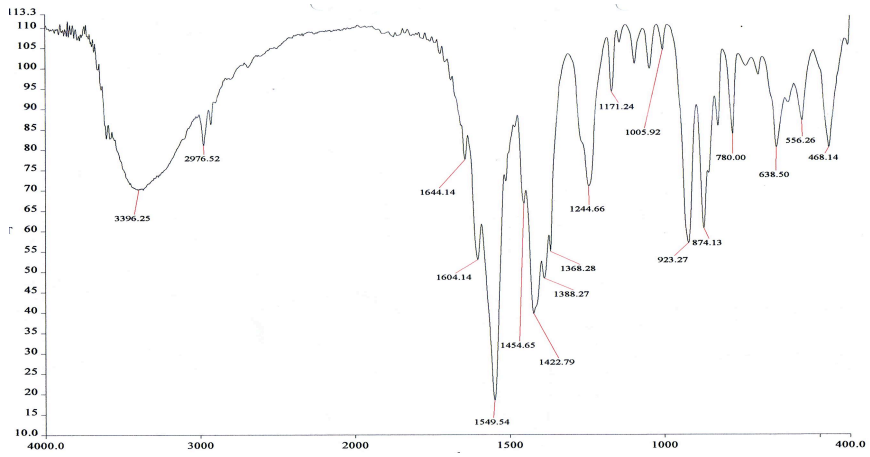

Figure 4.40 FTIR of **Complex 6**

The **UV-vis** spectra of the complex in the solid state (**Figure 4.41 (a)**) and as a solution in ethanol (with a few drops of acetic acid added to dissolve the solid; **Figure 4.41 (b)**), show a broad *d-d* band at 717 nm and 697 nm (ε_{max}= 212 $M^{-1}cm^{-1}$) respectively. The UV-vis spectrum of the solution also shows a shoulder at 380 nm. From these, it may be inferred that the complex is dimeric with square pyramidal Cu(II) centres in the solid state and in solution.

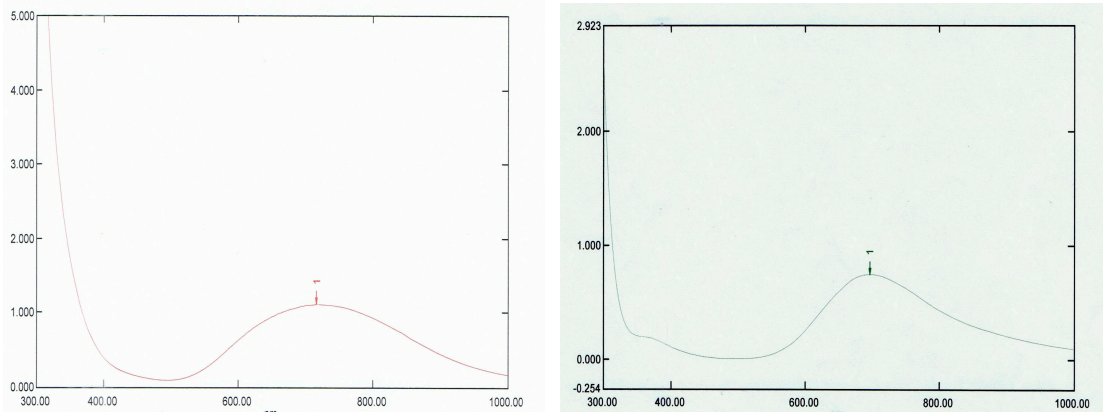

(a) (b)

Figure 4.41 UV-vis of **Complex 6** in (a) solid; and (b) solution

Combining the above results, the proposed structural formula for **Complex 6** is $K[Cu_2(p\text{-}OC_6H_4COO)(CH_2{=}C(CH_3)COO)_3(CH_3CH_2OH)(CH_2{=}C(CH_3)COOH)]$ (**Figure 4.42)**. The structure agrees with the chemical formula $KCu_2C_{25}H_{31}O_{12}$ from the elemental analyses, bridging carboxylates as inferred from FTIR, and binuclear complex and square-pyramidal Cu(II) as suggested from UV-vis spectra. Hence, it is the expected product from the reaction, and its yield is 80.5%.

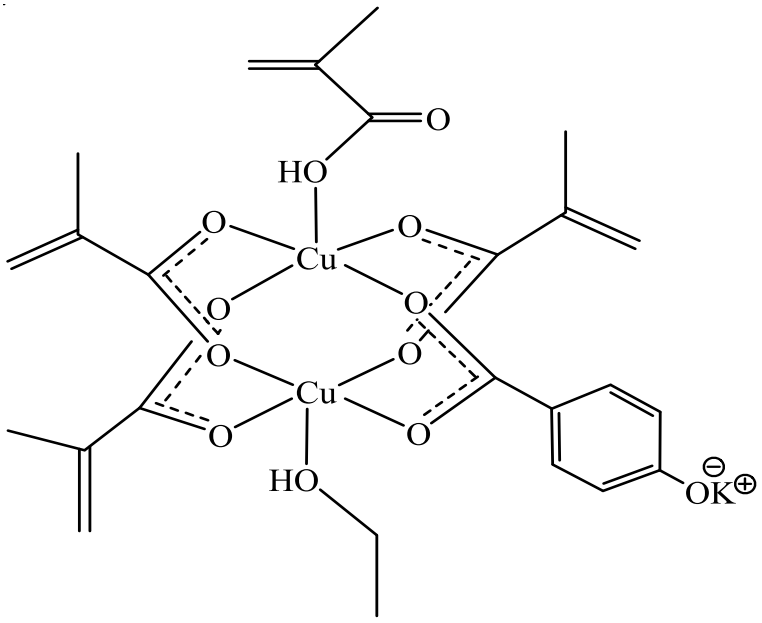

Figure 4.42 Proposed structural formula of **Complex 6**

The optical **band gap** energy for **Complex 6**, calculated as before from the onset λ value of 415 nm, is 2.99 eV. This is the same value obtained for **Complex 3 (**K[Cu_2(*p*-OC_6H_4COO)(CH_2=C(CH_3)COO)$_3$(CH_3CH_2OH)$_2$]**;** 2.99 eV). From this, it may be concluded that the photonic properties are not greatly affected by the linearity of the unsaturated alkylcarboxylate ligands.

The **TGA** thermogram (**Figure 4.43**) indicates that the decomposition temperature for **Complex 6** is 810°C. Thus, it is as thermally stable as **Complex 3** (K[Cu_2(*p*-OC_6H_4COO)(CH_3CH=CHCOO)$_3$(CH_3CH_2OH)(H_2O)]; T_{dec} = 817°C). The results seem to suggest that the isomeric unsaturated aliphatic carboxylate ligands do not affect the thermal stability of a complex, provided the geometry is similar.

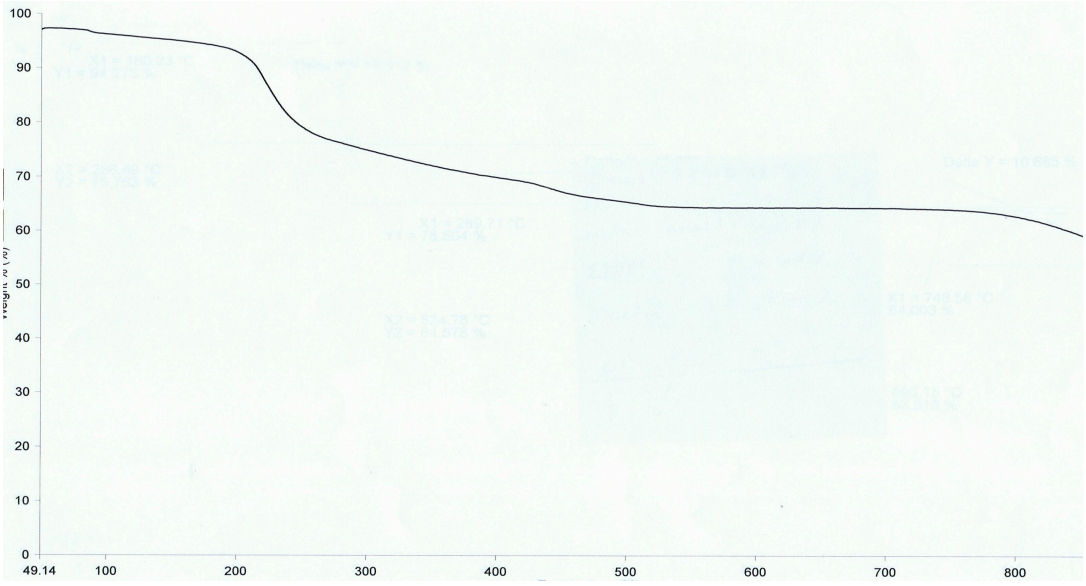

Figure 4.43 TGA of **Complex 6**

The thermogram also shows that the complex underwent the first weight loss of 5.0% at 84°C assigned to the evaporation CH_3CH_2OH (expected, 6.7%). The second weight loss of 16.0% at 189°C is assigned to the evaporation of CH_2=C(CH_3)COOH (expected, 12.5%). The complex did not decompose completely at temperatures above 810°C, and thus its formula weight could not be estimated.

The **DSC** scan (**Figure 4.44**) shows a weak endothermic peak at 93°C (ΔH = +8 kJ mol^{-1}) which may be due to the breaking of H-bond, as shown in **Figure 4.42**, and a broad endothermic peak at 200°C (52 kJ mol^{-1}) which may be due to the evaporation of $CH_2(CH_3)$=CHCOOH, as suggested from TGA.

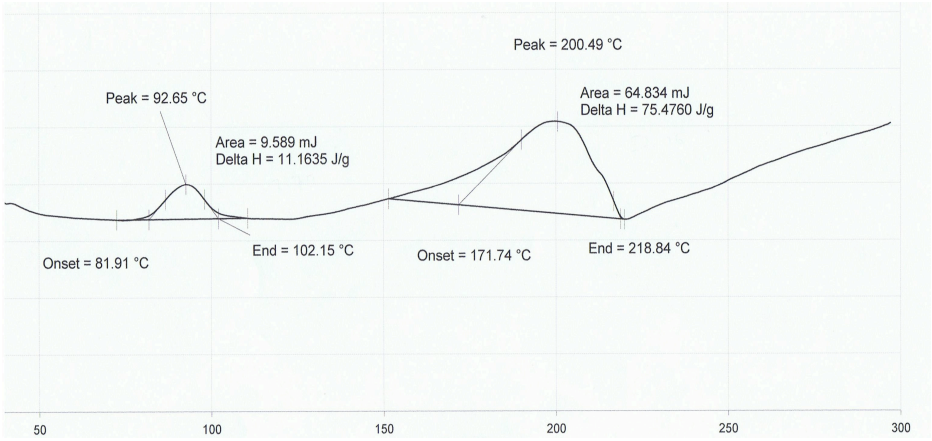

Figure 4.44 DSC of **Complex 6**

The **magnetic** data for **Complex 6** are: χ_g = 0.013 x 10^{-5}c.g.s., χ_m = 8.97 x 10^{-5} c.g.s., and χ_{dia} = -1.02 x 10^{-4} c.g.s. From these, the value of χ_m^{corr} is 1.91 x 10^{-4} c.g.s and that of μ_{eff} is 0.68 B.M. at 298 K. The 2J value is -1061 cm^{-1}. The values are similar to that of **Complex 3** (0.63 B.M.; -1163 cm^{-1}), and may be similarly explained. It further supports similar geometry for both complexes, and seems to suggest that isomeric unsaturated aliphatic carboxylate ligands do not affect the dipole moment of a complex.

The **CV** voltammogram for **Complex 6** (**Figure 4.45**), recorded cathodically from 1.0 V to -1.5 V, shows a cathodic peak at -0.79 V and an anodic peak at +0.20 V. The value for ΔE is 990 mV and for I_{pa}/I_{pc} ratio is 1.1. The results are similar to **Complex 3** (E_c = -0.72 V; E_a = +0.38 V; ΔE = 1100 mV; I_{pa}/I_{pc} = 1.0) and may be similarly explained. It also seems to suggest that isomeric unsaturated aliphatic carboxylate ligands do not affect the redox properties of a complex.

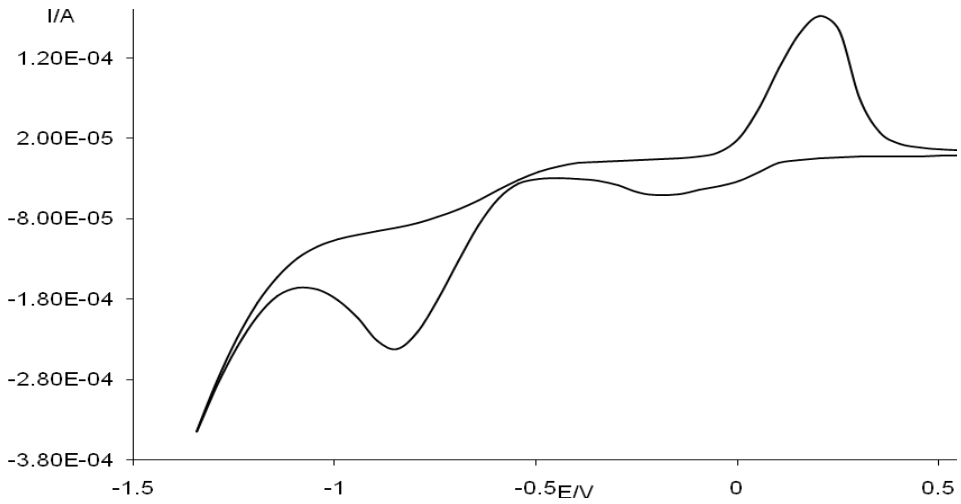

Figure 4.45 CV of **Complex 6**

(c) $K_3[Cu_2(p\text{-}OC_6H_4COO)_3(CH_2{=}C(CH_3)COO)]$

The one-pot reaction involving *p*-HOC_6H_4COOH with $CH_2{=}C(CH_3)COOH$ (mol ratio = 3:1) formed a brown powder (**Complex 7**), obtained as the residue from the hot reaction mixture. It was sparingly soluble in methanol, ethanol and chloroform, and insoluble in most other common organic solvents.

The results from the **elemental analyses** gave the C:H ratio of 11.1:1, which agrees with chemical formula $K_3Cu_2C_{29}H_{31}O_{14}$ (C:H ratio = 11.1:1).

Its **FTIR** spectrum of the complex (**Figure 4.46**), is different from those of the starting materials (**Figure 4.34** and **Figure 4.5**). It shows the presence of all of the expected functional groups as previously discussed, including two overlapping broad peak at 3450 cm^{-1} and 3359 cm^{-1} assigned to –OH group. The ΔCOO value is 147 cm^{-1}, suggesting bridging carboxylate ligands.

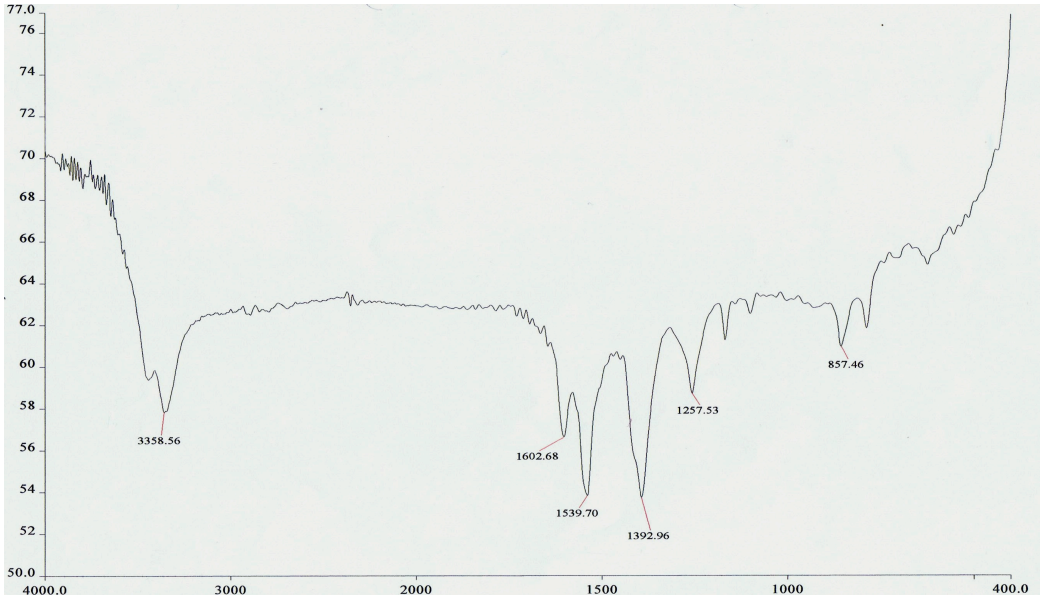

Figure 4.46 FTIR of **Complex 7**

The **UV-vis** spectra of the complex in the solid state (**Figure 4.47 (a)**) and as a solution in ethanol, with a few drops of acetic acid added to dissolve the solid (**Figure 4.47 (b)**), show a broad *d-d* band at 670 nm and 699 nm (ε_{max}= 338 M^{-1} cm^{-1}) respectively. The UV-vis spectrum of the solution also shows a shoulder at 380 nm. From these, it may be inferred that the complex is dimeric with square pyramidal Cu(II) centres in the solid state and in solution.

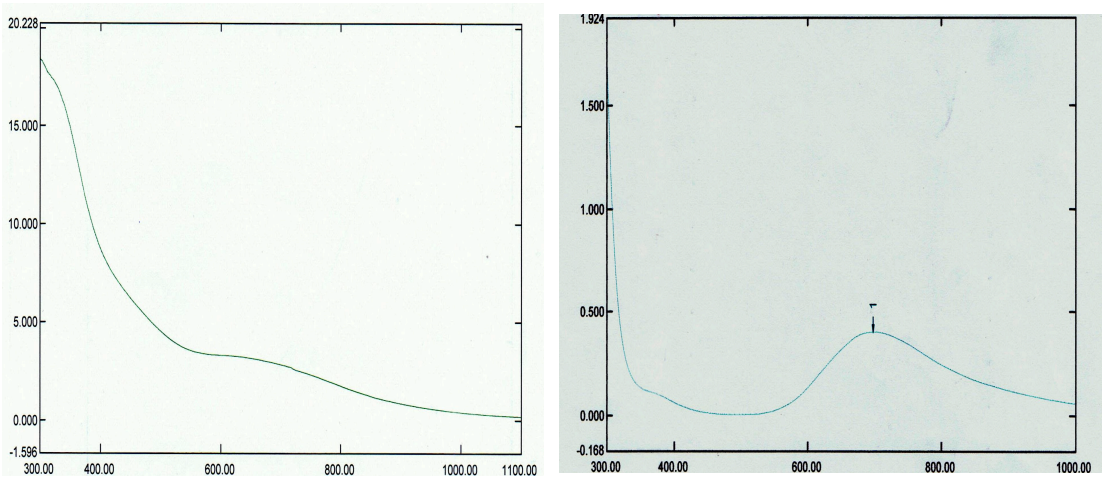

(a) (b)

Figure 4.47 UV-vis of **Complex 7** in (a) solid; and (b) solution

Combining the above results, **Complex 7** is proposed to have the structural formula of $K_3[Cu_2(p\text{-}OC_6H_4COO)_3(CH_2{=}C(CH_3)COO)(CH_3CH_2OH)_2].H_2O$ (**Figure 4.48**). The structure shows bridging carboxylates as inferred from FTIR, and binuclear complex and square-pyramidal Cu(II) as suggested from UV-vis spectra. Hence, it is the expected product from the reaction, and its yield was 66.2%.

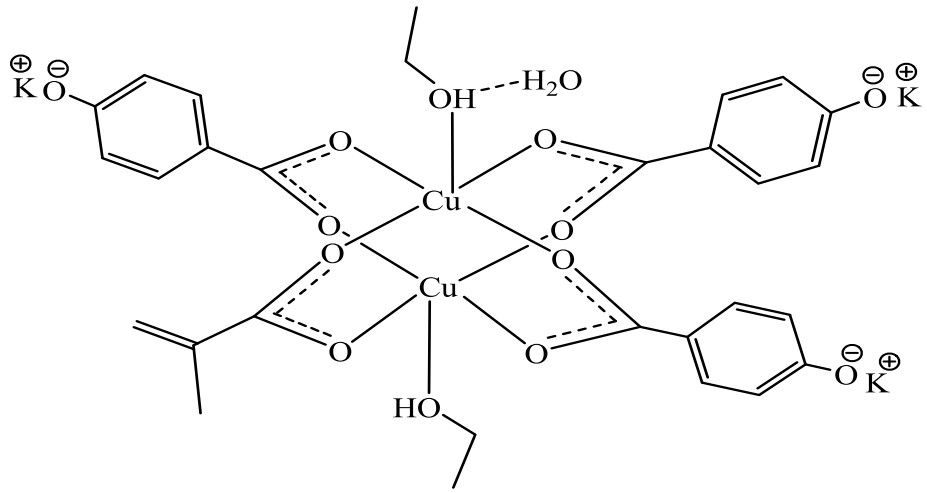

Figure 4.48 Proposed structural formula of **Complex 7**

The optical **band gap** energy for **Complex 7,** calculated as before from the onset λ value of 435 nm, is 2.89 eV. The value was comparable to all dimeric Cu(II) mixed-carboxylate complexes discussed above.

The **TGA** thermogram (**Figure 4.49**) shows that the decomposition temperature for **Complex 7** is 760°C. Thus, it is as thermally stable as **Complex 6** ($K[Cu_2(p\text{-}OC_6H_4COO)(CH_2(CH_3){=}CHCOO)_3(CH_3CH_2OH)(CH_2(CH_3){=}CHCOOH)]$; T_{dec} = 810°C). The result seems to suggest that the different ratio of $CH_2(CH_3){=}CHCOO$ ligand to *p*-OC_6H_4COO ligand does not have a significant effect on the thermal stability of these complexes.

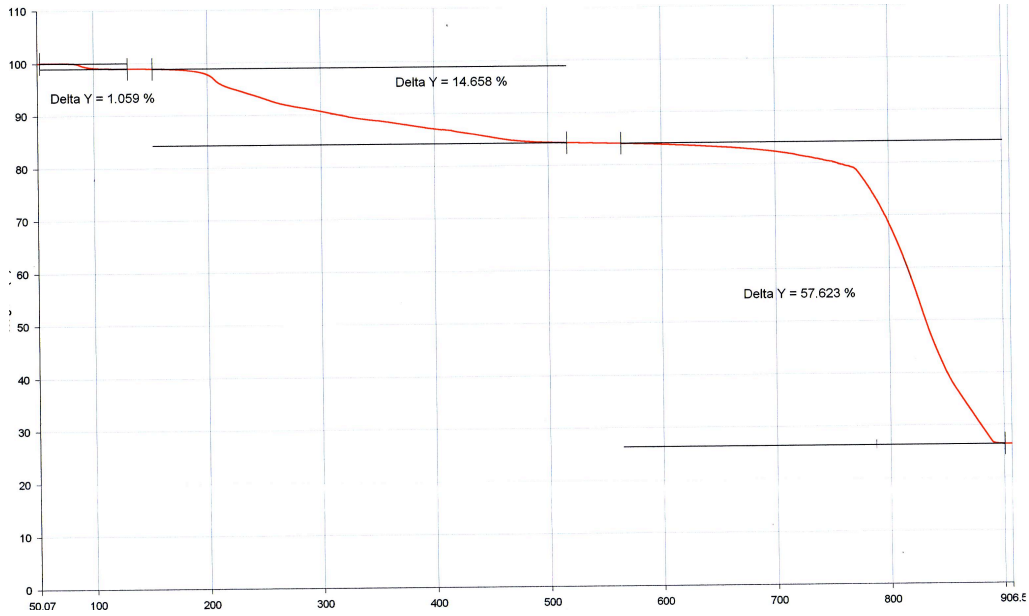

Figure 4.49 TGA of **Complex 7**

The thermogram also shows that the complex underwent the initial weight loss of 22.0% from 78°C to 760°C assigned to the evaporation of H_2O and CH_3CH_2OH, and to the decomposition of $CH_2(CH_3)$=CHCOO ligand (expected, 23.1%). The higher temperature than expected for the loss of these molecules may be due to the reaction of CH_3CH_2OH molecules to form involatile products [8], and polymerization of $CH_2(CH_3)$=CHCOO, as suggested earlier. The next weight loss of about 57.6% at 799°C is assigned to the decomposition of *p*-OC_6H_4COO (expected, 61.9%). Thus, as for **Complex 6**, it did not decompose completely at temperatures above 810°C, and thus its formula weight could not be estimated.

The **DSC** scan (**Figure 4.50**) shows a sharp endothermic peak at 89°C (ΔH = +24 kJ mol^{-1}) may be due to the breaking of H-bond, and a broad endothermic peak at 207°C (ΔH = +106 kJ mol^{-1}) which may be due to the dissociation of $CH_2(CH_3)$=CHCOO ligand. A broad exothermic peak immediately observed at peak temperature 258°C (ΔH = -48 kJ mol^{-1}) suggests the polymerization of $CH_2(CH_3)$=CHCOO ligand. Thus, the DSC results are in good agreement with those of TGA.

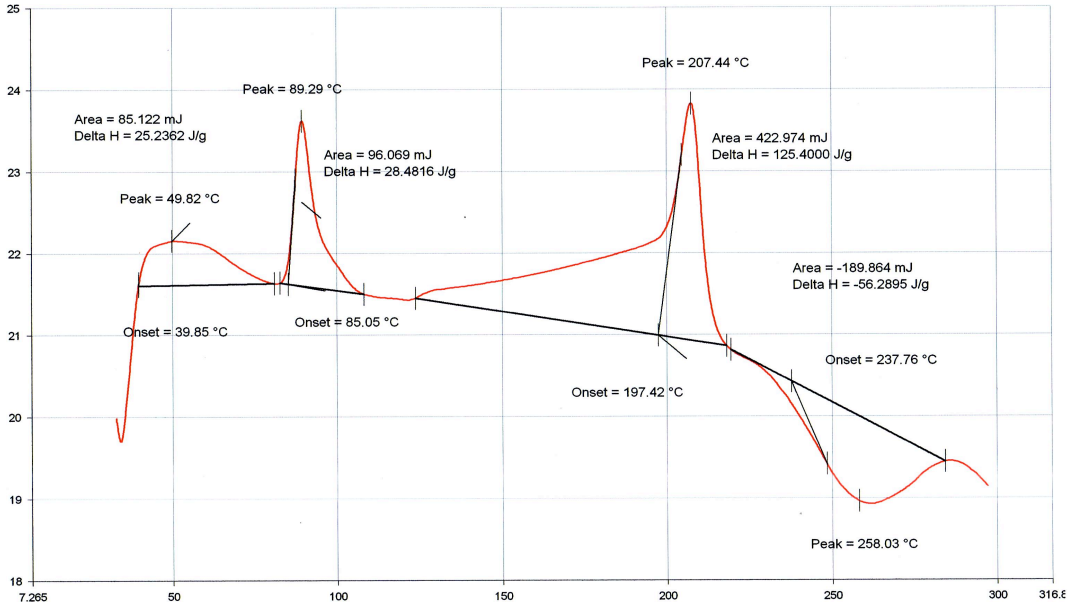

Figure 4.50 DSC of **Complex 7**

The **magnetic** data for **Complex 7** are: χ_g = 0.235 x 10^{-5}c.g.s., χ_m = 1.99 x 10^{-3} c.g.s., and χ_{dia} = -2.43 x 10^{-5} c.g.s. From these, the value of χ_m^{corr} is 2.02 x 10^{-3} c.g.s and that of μ_{eff} is 2.20 B.M. at 298 K. The 2J value is -255 cm^{-1}. The results suggest a significantly weaker antiferromagnetic interaction between the two Cu(II) centres compared to **Complex 6** (0.68 B.M.; -1061.2 cm^{-1}). Since both complexes adopt similar paddle-wheel structure, the difference may be due to a more effective electronic interaction through the alkylcarboxylate ligand compared to the arylcarboxylate ligand.

The **CV** voltammogram for **Complex 7** (**Figure 4.51**), recorded cathodically from +1.0 V to -1.5 V, shows a reduction peak at -0.78 V and an oxidation peak at +0.51 V. The value for ΔE is 1290 mV and for I_{pa}/I_{pc} ratio is 1.3. The results are similar to **Complex 6** (E_c = -0.79 V; E_a = +0.20 V; ΔE = 990 mV; I_{pa}/I_{pc} = 1.1), and may be similarly explained. It is further noted thatcompared to **Complex 6**, the mixed valence [Cu(II)Cu(I)] complex formed from **Complex 7** was reoxidised at a significantly higher potential, suggesting that it has higher stability, possibly due to a more tetrahedral geometry at [Cu(I)].

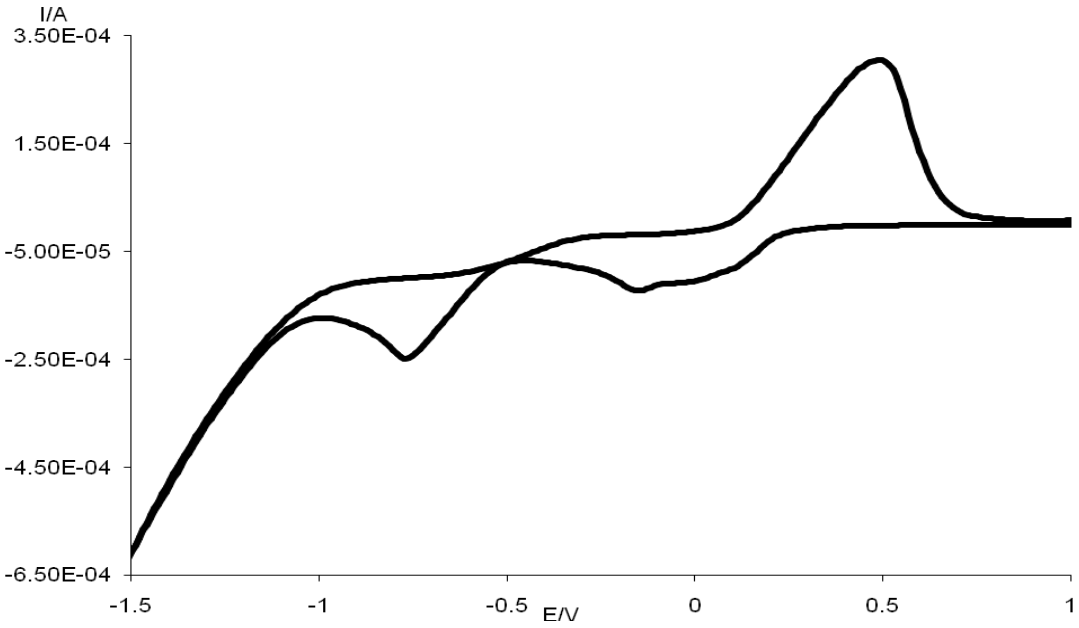

Figure 4.51 CV of **Complex 7**

(d) ***Summary***

The one-pot reaction involving different ratios of *p*-HOC_6H_4COOH and $CH_2(CH_3)$=CHCOOH was successfully used to prepare the intended ionic complex for n = 2 and 3, but not for n = 1.

Complex 5 was mononuclear, while **Complex 6** and **Complex 7** were dinuclear with square pyramidal geometry at the two Cu(II) centres. Their thermal stability cannot be correlated with nuclearity, geometry, and ratio of aromatic to unsaturated aliphatic carboxylates. The trimeric complex (**Complex 5**) has ferromagnetic interaction, while dinuclear paddle-wheel complexes (**Complex 6** and **Complex 7**) have antiferromagnetic interaction. The strongest antiferromagnetic interaction was exhibited by **Complex 6** which has a higher ratio of unsaturated aliphatic carboxylate ligand. All complexes were redox active.The analytical results are summarized in **Table 4.3**.

Table 4.3 Analytical results for complexes from the one-pot reaction

	Complex 5	**Complex 6**	**Complex 7**
Structural formula*	$\{K[Cu(OH)L'(L'H)]\}_3$	$K[Cu_2LL'_3(EtOH)(L'H)]$	$K_3[Cu_2L_3L'(EtOH)_2]$
ΔCOO/ cm^{-1}	130 (chelating)	161 (bridging)	147 (bridging)
λ_{max}/nm solid	730	717	670
solution ($\varepsilon_{max}/M^{-1}cm^{-1}$)	699 (207)	697 (212)	699 (338)
$T_{decomposition}/^oC$	720	810	799
μ_{eff} ($2J/cm^{-1}$)	4.15 (+220) ferromagnetic	0.63 (-1163) antiferromagnetic	2.20 (-255) antiferromagnetic
E_{pc}/V E_{pa}/V (I_{pa}/I_{pc})	-0.80 +0.31 0.3	-0.79 +0.20 1.1	-0.78 +0.51 1.3

* solvates are not shown; L, *p*-OC_6H_4COO; L', $CH_2(CH_3)$=CHCOO

4.3 Ligand-Exchange Reaction

The ligand-exchange reaction was used to synthesize ionic complex precursors of general formula $[Cu_2(p\text{-}HOC_6H_4COO)_n(RCOO)_{4-n}]$, where R is $CH_3CH{=}CH$, $CH_3(CH_2)_7CH{=}CH(CH_2)_7$, $(CH_3)_3C$, $CH_3(CH_2)_3CHC_2H_5$, or $CH_3(CH_2)_7CH(CH_2)_5CH_3$, and n = 1-3. The synthesis involved three steps:

Step 1: *Synthesis of* $[Cu_2(p\text{-}HOC_6H_4COO)_4]$

The metathesis reaction between $[Cu_2(CH_3COO)_4]$ and p-HOC_6H_4COOH formed two products: a green powder and a blue crystal. The reaction equation is shown below.

$$[Cu_2(CH_3COO)_4] + 4\ p\text{-}HOC_6H_4COOH \longrightarrow [Cu_2(p\text{-}HOC_6H_4COO)_4] + 4\ CH_3COOH$$

The green powder was obtained as the residue from the hot reaction. Its FTIR spectrum (**Figure 4.52)** agrees with that of $[Cu_2(p\text{-}HOC_6H_4COO)_4]$, the intended product.

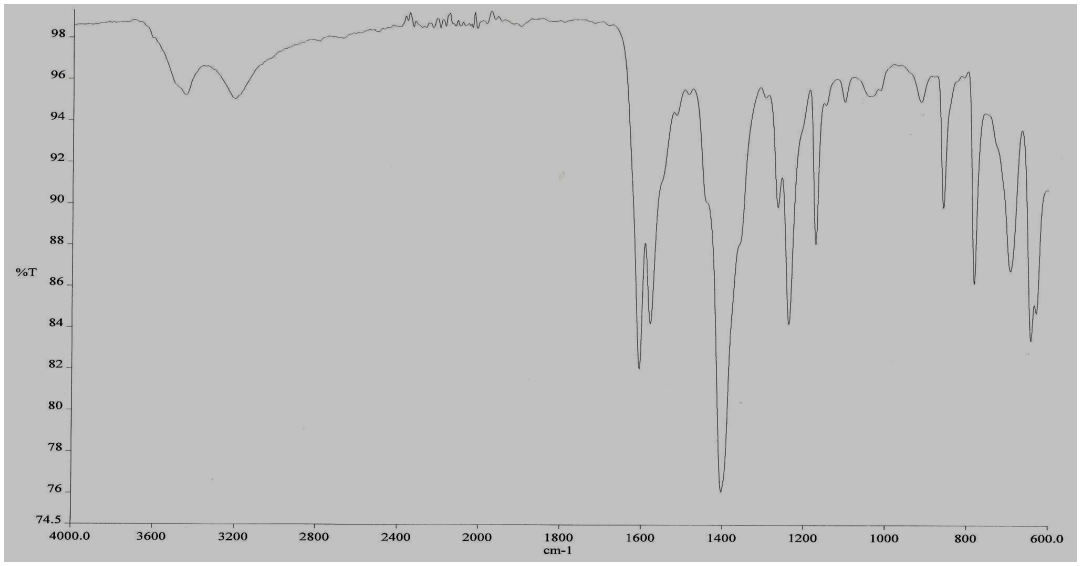

Figure 4.52 FTIR of $[Cu_2(p\text{-}HOC_6H_4COO)_4]$

The blue crystal was formed from the filtrate on standing at room-temperature for a month. Single crystal X-ray crystallography of the blue crystal (dimensions 0.30 x 0.26 x 0.20 mm; solved by direct methods and refined by full matrix least square in F^2 in the centrosymmetric space group $P2_1/c$) gave the chemical formula $[Cu(p\text{-}HOC_6H_4COO)_2(C_5H_5N)_2]$. An ORTEP presentation of the crystal is shown in **Figure 4.53,** and the packing pattern is shown in **Figure 4.54** [23].

The copper atom of the blue crystal structure is an inversion center and adopts a distorted octahedral geometry with the nitrogen atoms of the two pyridine ligands, trans to each other, and to the carboxylate O atoms of two bidentate 4-hydroxybenzoate ligands [Cu-O = 1.9706 (10) and 2.5204 (11) Å].

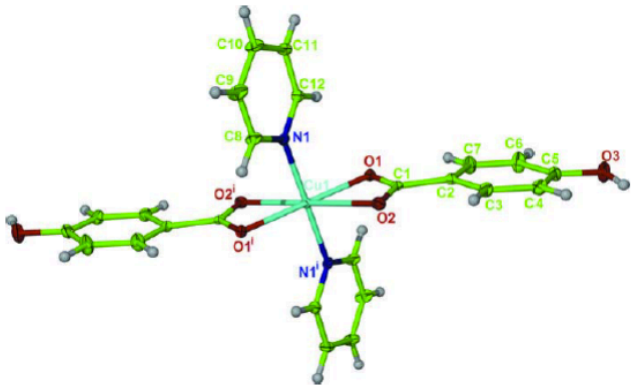

Figure 4.53 An ORTEP presentation of the blue crystal

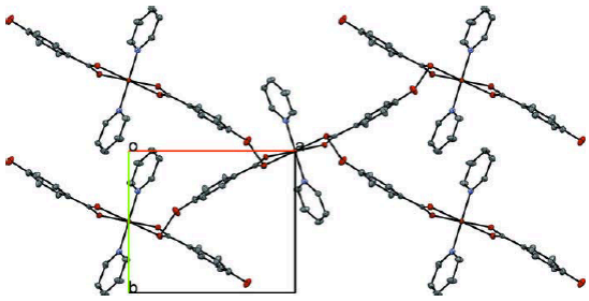

Figure 4.54 The packing pattern of blue crystal, viewed along the crystallographic *c*-axis

The crystal data and structure refinement of the crystal are shown in **Table 4.4,** while selected hydrogen bonding interaction data is shown in **Table 4.5**.

Table 4.4 Crystallographic and refinement details of blue crystal

Empirical formula	$Cu_2C_{24}H_{20}N_2O_6$
Formula weight	495.96
Temperature	100 K
Wavelength	0.71073 Å
Crystal system, space group	Monoclinic, $P2_1/c$
Unit cell dimension	a = 10.6715 (2) Å $\alpha = 90^o$ b = 8.5385 (1) Å $\beta = 109.124\ (1)^o$ c = 12.3988 (2) Å $\gamma = 90^o$
Volume	1067.41 (3) A^3
Z, Calculated density	2, 1.543 Mg/m^3
Absorption coefficient	1.07 mm^{-1}
F(000)	510
Crystal size	0.30 x 0.26 x 0.20 mm
Theta range for data collection	3.0 to 28.2 º
Limiting indices ($\pm h$, $\pm k$, $\pm l$)	-13/13, -11/11, -16/16
Reflections collected / unique	9756 / 2448 [R_{int} = 0.060]
Absorption correction	Multi-scan
Refinement method	Full-matrix least-squares on F^2
Data / restraints / parameters	2448 / 152 / 0
Goodness-of-fit on F^2	1.06
Final R indices [$I > 2\sigma(I)$]	R1 = 0.026, wR2 = 0.066
$\Delta\rho_{max}$ and $\Delta\rho_{min}$	0.38 and -0.32 e $Å^{-3}$

Table 4.5 Hydrogen bonds [Å and deg.] of blue crystal

D – H … A	D - H	H…A	D…A	D – H…A
O3–H3A…O2^i	0.84	1.87	2.7028(16)	171

Symmetry codes: (i) –x+1, y + 1/2, -z + 3/2.

Step 2: *Synthesis of [$Cu_2(RCOO)_4$]*

The second step was synthesis of [$Cu_2(RCOO)_4$] from [$Cu_2(CH_3COO)_4$] and RCOOH, also by the metathesis reaction. These complexes were discussed in the respective section below.

Step 3: *Ligand-exchange reaction*

The third step was reacting [$Cu_2(p\text{-}HOC_6H_4COO)_4$], prepared in Step 1, with [$Cu_2(RCOO)_4$], prepared in Step 2, in the correct ratio (1:1, 3:1 and 1:3 respectively) in ethanol in the presence of a few drops of pyridine to dissolve the starting materials. The equation for the expected reaction is:

$$n\ [Cu_2(p\text{-}HOC_6H_4COO)_4] + (4\text{-}n)\ [Cu_2(RCOO)_4]$$

$$\downarrow$$

$$2\ [Cu_2(p\text{-}HOC_6H_4COO)_n(RCOO)_{4-n}]$$

4.3.1 [$Cu_2(p\text{-}HOC_6H_4COO)_n(CH_3CH{=}CHCOO)_{4-n}$]

Three complexes with the expected formula [$Cu_2(p\text{-}HOC_6H_4COO)_n(CH_3CH{=}CHCOO)_{4-n}$], where n = 1-3, were obtained from the ligand-exchange reaction involving the correct mole ratios of [$Cu_2(p\text{-}HOC_6H_4COO)_4$] and [$Cu_2(CH_3CH{=}CHCOO)_4$]. These are discussed, starting with the symmetrical complexes (n = 2), and then the less symmetrical complexes (n = 1 followed by n = 3).

(a) [$Cu_2(p\text{-}HOC_6H_4COO)_2(CH_3CH{=}CHCOO)_2$]

The ligand-exchange reaction involving [$Cu_2(p\text{-}HOC_6H_4COO)_4$] with [$Cu_2(CH_3CH{=}CHCOO)_4$] (mol ratio = 1:1) formed two products: a purple powder and a green powder.

(i) Purple powder

The purple powder (**Complex 8**) formed as the residue from the hot reaction mixture in presence of a fe drops of pyridine. It was soluble in methanol, dimethylsulfoxide, and dimethylformamide, but insoluble in chloroform, acetone and toluene.

The results of **elemental analyses** gives the ratio of C:H:N equals to 15.2:1.0:1.6, which is in good agreement with that calculate for $Cu_2C_{35}H_{30}N_2O_{11}$ (formula weight, 781.7 $gmol^{-1}$; CHN ratio, 15.0:1.1:1.0).

Its **FTIR** spectrum (**Figure 4.55**) is different from those of the starting materials (**Figure 4.52** and **Figure 4.56**).

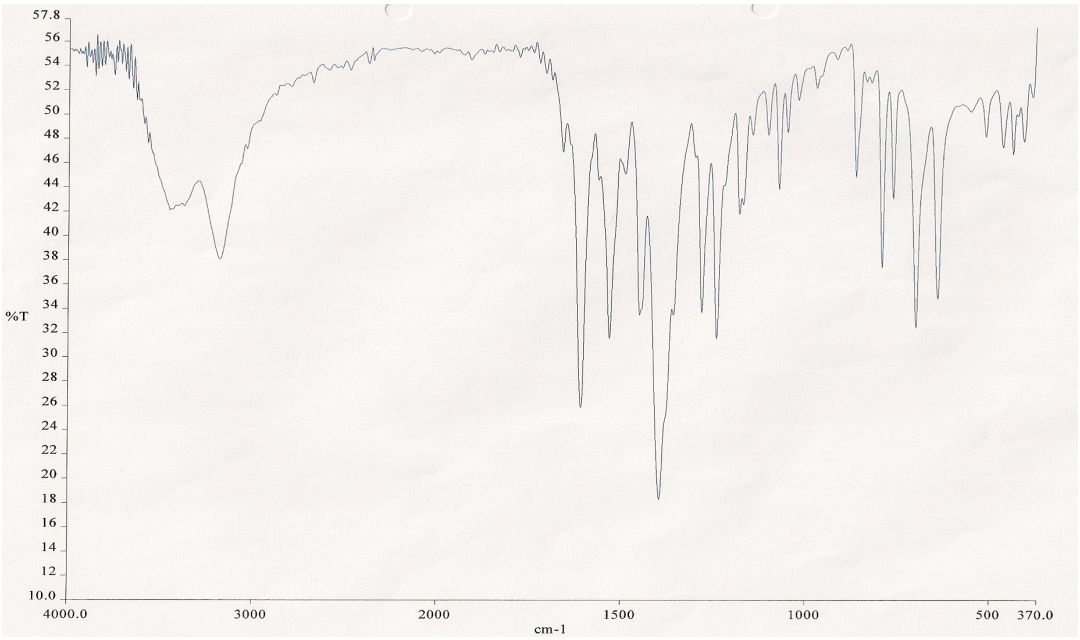

Figure 4.55 FTIR of **Complex 8**

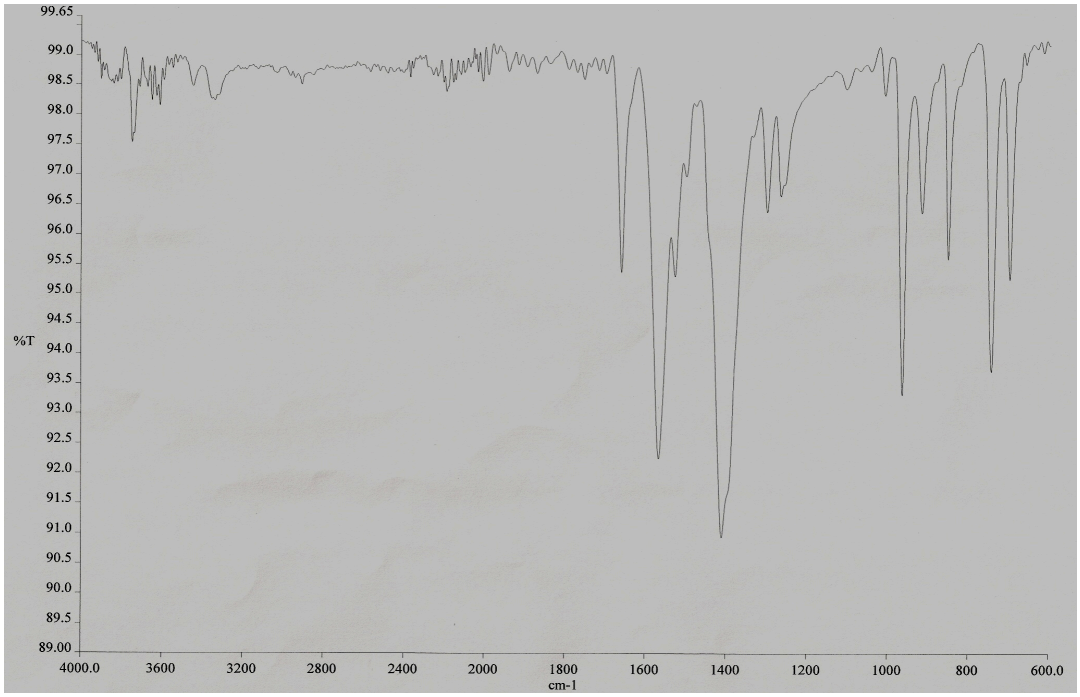

Figure 4.56 FTIR of $[Cu_2(CH_3CH{=}CHCOO)_4]$

The spectrum shows the presence of all of the expected functional groups as previously discussed, including peaks at 1394 and 759 cm^{-1} assigned to pyridine. The ΔCOO value is 135 cm^{-1}, suggesting bridging or chelating carboxylate ligands.

The **UV-vis** spectrum of **Complex 8** in the solid state (**Figure 4.57(a)**) shows two broad overlapping bands and 572 and 700 nm, while that of a solution in ethanol (**Figure 4.57(b)**) show a broad *d-d* band at 703 nm (ε_{max}= 197 $M^{-1}cm^{-1}$) respectively. These and the ε_{max} value suggest a dimeric complex with square planar and square pyramidal Cu(II) centres in the solid state, which changed to square pyramidal in solution.

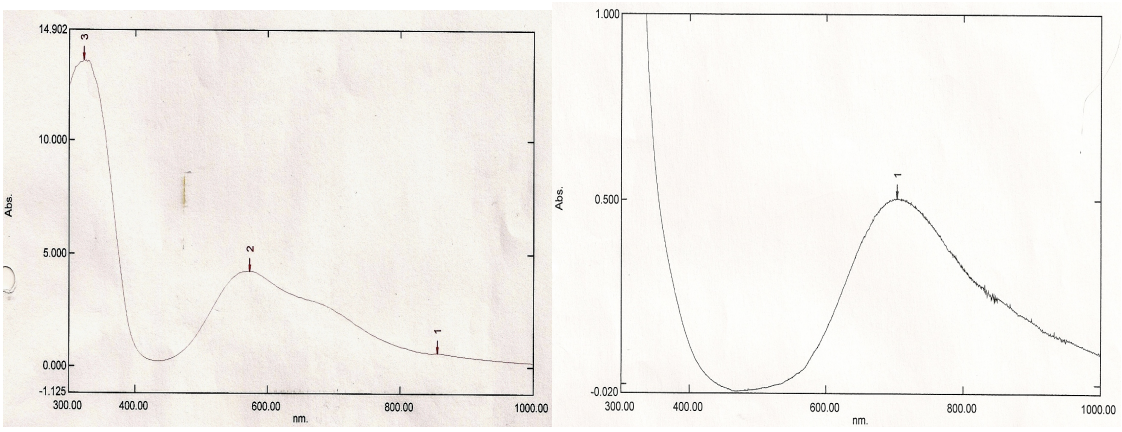

(a) (b)

Figure 4.57 UV-vis of **Complex 8** in (a) solid; and (b) solution

Combining the above analytical results, the proposed structural formula of **Complex 8** is $[Cu_2(p\text{-}HOC_6H_4COO)_3(CH_3CH{=}CHCOO)(C_5H_5N)].C_5H_5N$ (**Figure 4.58)**. Thus, it is not the intended complex from this reaction, and its yield was 46.5 %.

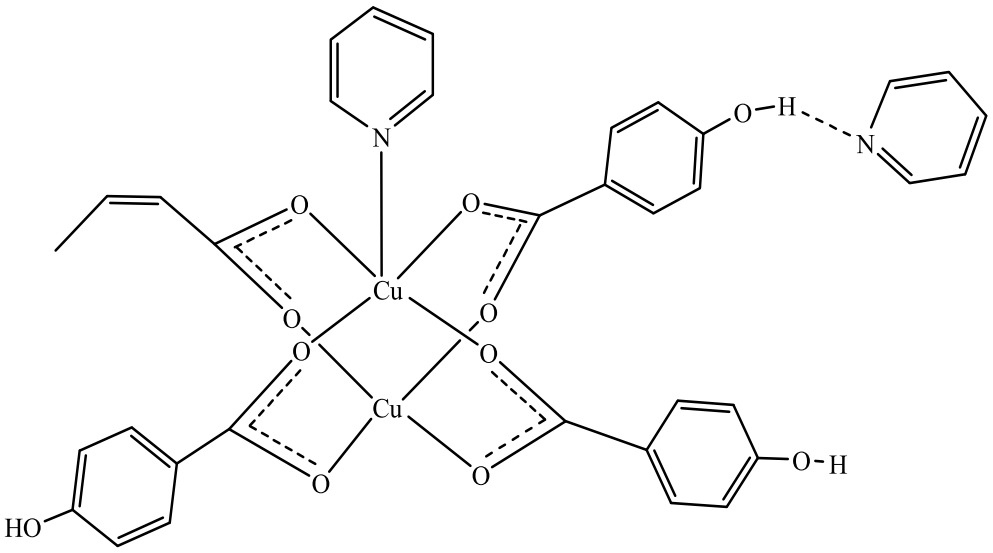

Figure 4.58 Proposed structural formula of **Complex 8**

The optical **band gap** energy for **Complex 8,** calculated as before from the onset λ value of 2.63 eV.

The **TGA** thermogram (**Figure 4.59**) shows that its decomposition temperature is 209^{o}C. Above this temperature, the combined experimental weight loss of 89.0% is accounted for by the decomposition of all of the carboxylate ligands and two pyridine molecules (expected 83.7%). It is noted that pyridine did not evaporate off at its boiling point (115^{o}C), as expected from the proposed structural formula. This is likely due to its coordination at the axial position and to the OH group of the arylcarboxylate ligand by hydrogen bonding.

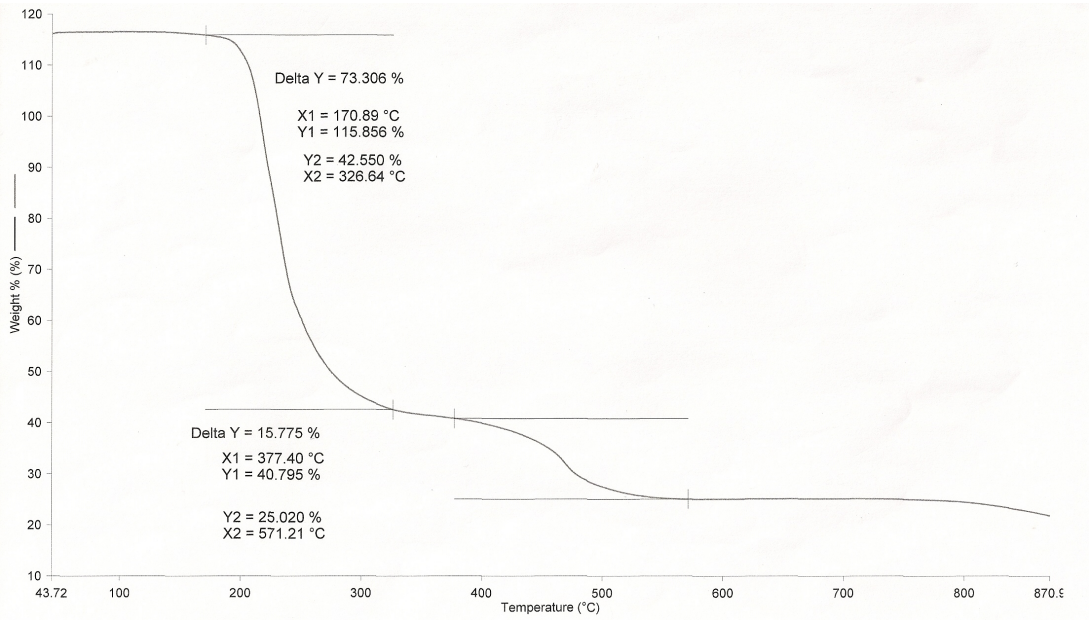

Figure 4.59 TGA of **Complex 8**

The amount of residue left at temperatures above 570^{o}C is 11.0%. The expected value, assuming either CuO or Cu_2O, is 20.4% and 18.8% respectively. The lower than expected value obtained seems to suggest loss of volatile Cu compound(s).

The **DSC** scan (**Figure 4.60**) shows a strong endothermic peak at 205^{o}C (ΔH = +199.7 kJ mol^{-1}) and a weak endothermic peak at 236^{o}C (+6 kJ mol^{-1}). Since the strong peak occurred just below its decomposition temperature (209^{o}C), it may be concluded that the complex melted at this temperature, and then immediately decomposed.

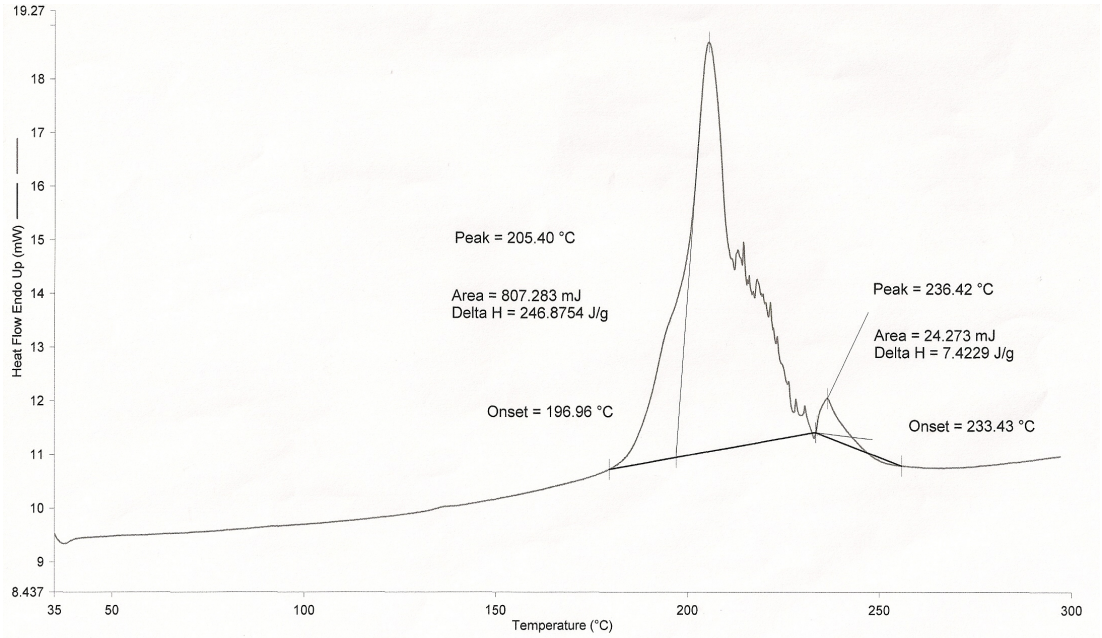

Figure 4.60 DSC of **Complex 8**

The **magnetic** susceptibility data for the complex are: $\chi_g = 0.332 \times 10^{-5}$ c.g.s., $\chi_m = 2.595 \times 10^{-3}$ c.g.s., and $\chi_{dia} = -1.640 \times 10^{-4}$ c.g.s. From the data, the value of χ_m^{corr} is 2.759×10^{-3} c.g.s and that of μ_{eff} is 2.57 B.M. at 298 K. The value is slightly lower than the spin-only value of 2.83 B.M. for two unpaired electrons. The 2J value is -100 cm^{-1}. Thus, it may be said that there is a weak electronic communication between the two Cu(II) centres. This may be due to the electron-donating –OH group of three *p*-HOC_6H_4COO ligands, which reduces the communication through the superexchange pathway.

The **CV** voltammogram (**Figure 4.61**), recorded cathodically from 1.5 V to -1.5 V, shows two cathodic peaks at -0.61 V and -0.88 V, and three anodic peak at +0.01 V, +0.44 V and +0.98 V.

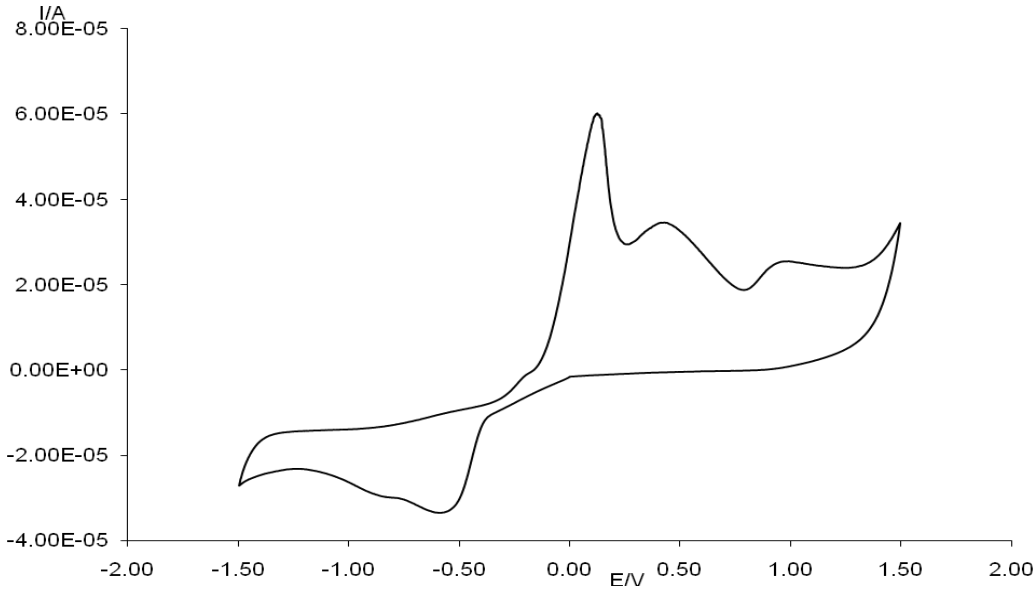

Figure 4.61 CV of **Complex 8**

The cathodic peak at -0.61 V is assigned to reduction of the binuclear [Cu(II)Cu(II)] complex to mixed-valence [Cu(II)Cu(I)] complex, which was further reduced to monovalent [Cu(I)Cu(I)] complex at -0.88 V. The dinuclear [Cu(I)Cu(I)] complex was then reoxidized to the mixed-valence [Cu(II)Cu(I)] complex at +0.44 V and then to the dinuclear [Cu(II)Cu(II)] complex at +0.98 V. The strong anodic peak at +0.01 V suggests dissolution of deposited Cu(0) on the electrode. To account for this, it is postulated that the [Cu(I)Cu(I)] complex formed disproportionated to mononuclear [Cu(II)] and [Cu(0)]. The electrochemical-chemical (EC) mechanism for the redox reactions are shown below (**Scheme 4.1**).

$$[Cu(II)Cu(II)] \underset{+0.98\ V}{\overset{-0.61\ V}{\rightleftharpoons}} [Cu(II)Cu(I)] \underset{+0.44\ V}{\overset{-0.88\ V}{\rightleftharpoons}} [Cu(I)Cu(I)]$$

$$[Cu(II)Cu(I)] \longrightarrow [Cu(II)] + [Cu(0)]$$

$$[Cu(0)] \xrightarrow{+0.01\ V} [Cu(I)]$$

Scheme 4.1 EC mechanism of **Complex 8**

From the cathodic and anodic potentials, the ΔE values for [Cu(II)Cu(II)]–[Cu(II)Cu(I)] and [Cu(II)Cu(I)]–[Cu(I)Cu(I)] redox reactions are 1588 mV and 1316 mV respectively. Thus the results show that **Complex 8** undergoes quasireversible redox reactions, indicating the occurrence of extensive structural reorganisation.

The I_{pa}/I_{pc} ratio for [Cu(II)Cu(II)]–[Cu(II)Cu(I)] and [Cu(II)Cu(I)]–[Cu(I)Cu(I)] redox reactions are 1.0 and 1.5 respectively. From these, it may be concluded that the mixed valence [Cu(II)Cu(I)] complex is chemically stable, while the monovalent [Cu(I)Cu(I)] complex is less chemical stable. This is consistent with its disproportionation suggested above.

(ii) Green powder

The green powder (**Complex 9**) deposited from the filtrate on standing at room temperature for a week. It was soluble in all common organic solvents, except for toluene.

The C:H:N ratio from the **elemental analyses** is 11.2:1:1. This agrees with the chemical formula $CuC_{13}H_{17}NO_5$ (formula weight, 330.8 g mol^{-1}; calculated C:H:N ratio, 11.2:1.2:1).

The **FTIR** spectrum (**Figure 4.62**) is similar to that of one of the starting materials of the reaction, namely $[Cu_2(CH_3CH{=}CHCOO)_4]$ (**Figure 4.56**), but with peaks assigned to pyridine at 1400 and 761 cm^{-1}. The ΔCOO value is 159 cm^{-1}, suggesting bridging carboxylate ligands.

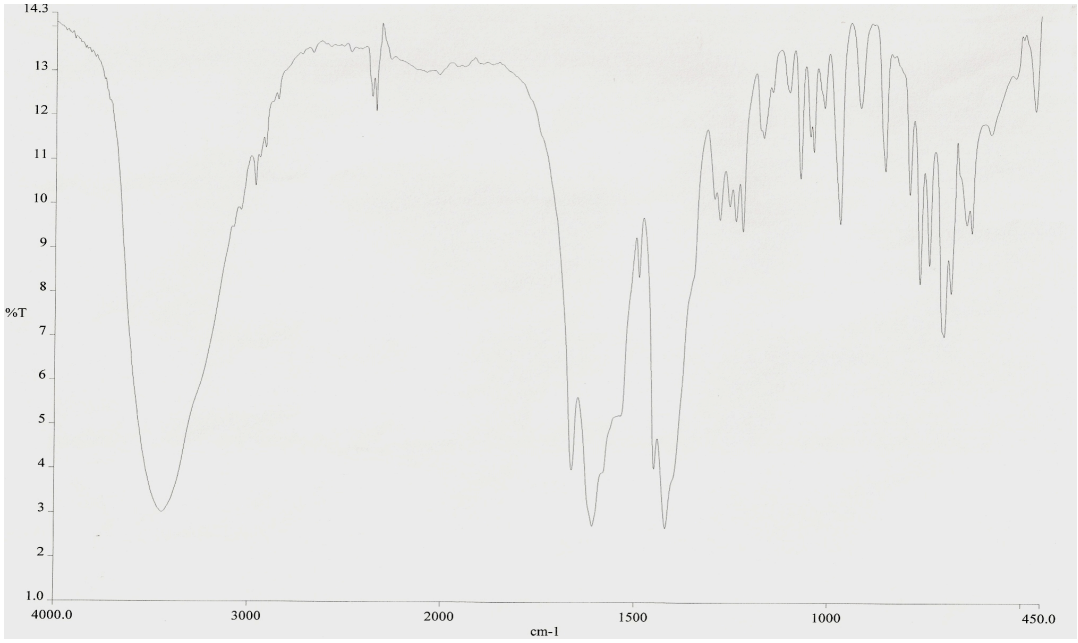

Figure 4.62 FTIR of **Complex 9**

The **UV-vis** spectrum for the complex in the solid state (**Figure 4.63(a)**) and as a solution in ethanol (**Figure 4.63(b)**) show a broad *d-d* band at 717 nm and 706 nm (ε_{max}= 1.14 x 10^3 $M^{-1}cm^{-1}$) respectively. From these, it may be inferred that the complex is dimeric with square pyramidal Cu(II) centres.

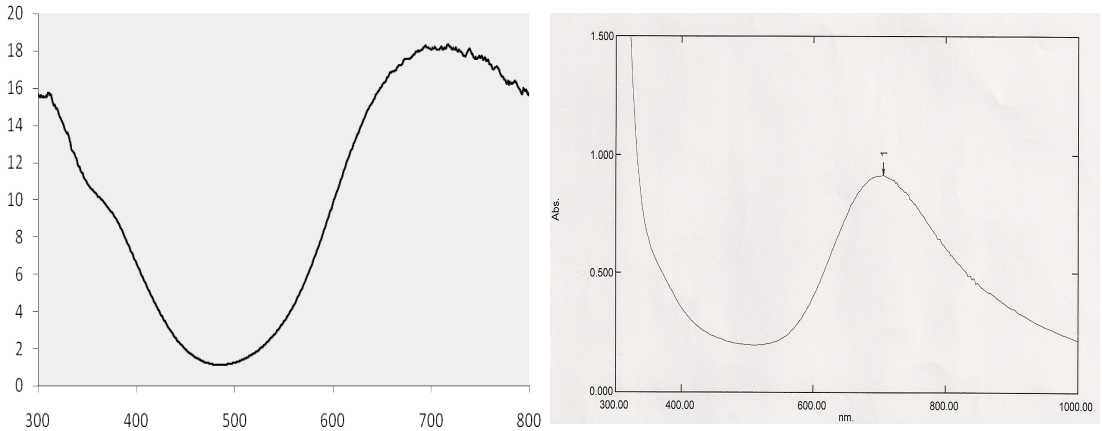

Figure 4.63 UV-vis of **Complex 9** in (a) solid; and (b) solution

Combining the above results, the proposed structural formula for the complex is $[Cu_2(CH_3CH{=}CHCOO)_4(C_5H_5N)_2].2H_2O$ (**Figure 4.64)**. It shows bridging carboxylates as inferred from FTIR, and binuclear complex with square-pyramidal Cu(II) as

suggested from UV-vis. Thus, it is **not** the intended product from the reaction. It is actually a complex formed between the unreacted starting material ($[Cu_2(CH_3CH=CHCOO)_4]$) with pyridine.

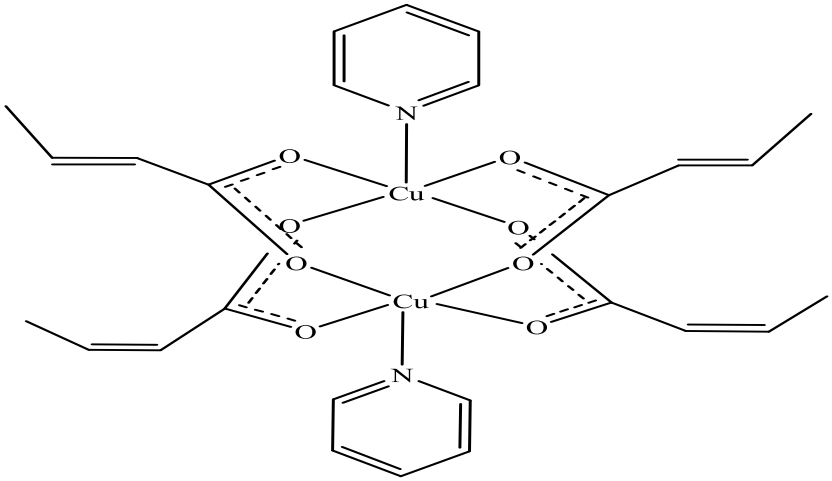

Figure 4.64 Proposed structural formula of **Complex 9** (non-coordinated H_2O molecules are not shown)

(b) $[Cu_2(p\text{-}HOC_6H_4COO)(CH_3CH=CHCOO)_3]$

The ligand-exchange reaction involving $[Cu_2(p\text{-}HOC_6H_4COO)_4]$ with $[Cu_2(CH_3CH=CHCOO)_4]$ (mol ratio =1:3) formed two products: a blue powder and a green powder.

(i) Blue powder

The blue powder (**Complex 10**) was the residue from the hot reaction mixture. It was soluble in methanol, tetrahydrofuran, dimethyl sulfoxide, dimethylformamide, and sparingly soluble in chloroform and acetone.

The results from the **elemental analyses** gave the C:H:N ratio equals 13.5:1.0:1.4, which are in good agreement with the chemical formula $Cu_2C_{31}H_{36}O_{10}N_2$ (calculated C:H:N ratio = 13.3:1.3:1.0).

The **FTIR** spectrum (**Figure 4.65**) is different from those of the starting materials (**Figure 4.52** and **Figure 4.56**). This indicates that there was a reaction between [Cu_2(*p*-$HOC_6H_4COO)_4$] and [$Cu_2(CH_3CH{=}CHCOO)_4$]. It shows the presence of all of the expected functional groups as previously discussed. The ΔCOO value is 167 cm^{-1}, suggesting bridging carboxylate ligands.

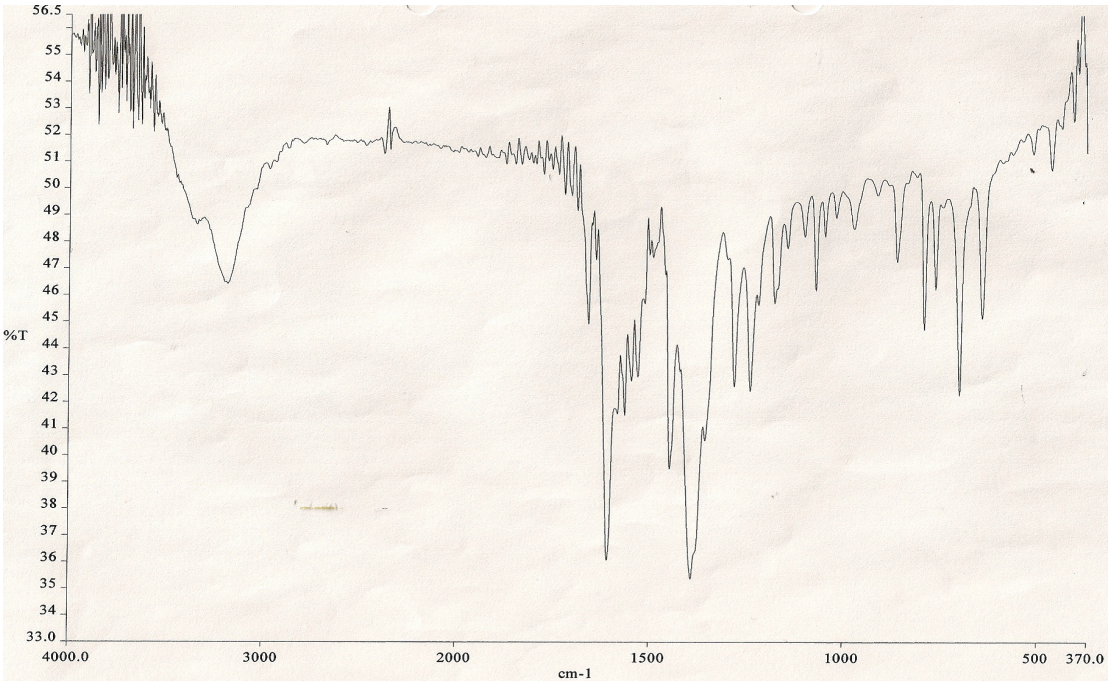

Figure 4.65 FTIR of **Complex 10**

The **UV-vis** spectrum of **Complex 10** in the solid state (**Figure 4.66(a)**) and as a solution in methanol (**Figure 4.66(b)**) shows a broad *d-d* band at 683 nm and 703 nm (ε_{max}= 230 $M^{-1}cm^{-1}$) respectively. These suggest a dimeric complex with square pyramidal Cu(II) centres in both the solid state and in solution.

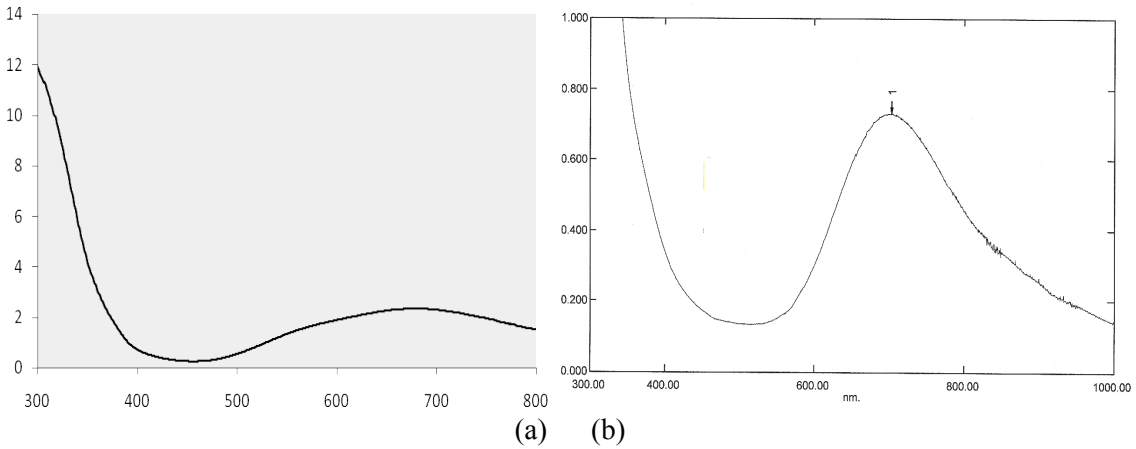

(a) (b)

Figure 4.66 UV-vis of **Complex 10** (a) solid; (b) solution

Combining the above results, **Complex 10** is proposed to have the structural formula $[Cu_2(p\text{-}HOC_6H_4COO)(CH_3CH{=}CHCOO)_3(C_5H_5N)_2].CH_3CH_2OH$ (**Figure 4.67**). The structure is consistent with the chemical formula of $Cu_2C_{31}H_{36}O_{10}N_2$ based on the elemental analyses, the bridging carboxylate ligands as inferred from FTIR, and binuclear complex and square-pyramidal Cu(II) as suggested from UV-vis. Hence, it is the intended product of the reaction, and its yield was 45.1%.

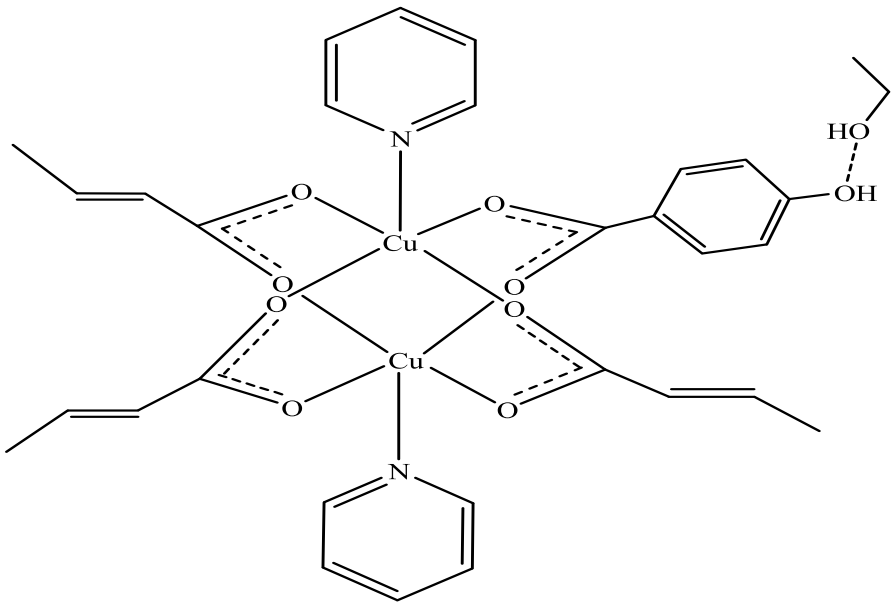

Figure 4.67 Proposed structural formula of **Complex 10**

The optical **band gap** energy for **Complex 10,** calculated as before from the onset λ value of 537 nm, is 2.31 eV. The value is lower than that of **Complex 8** (E_g = 2.63 eV; $[Cu_2(p\text{-}HOC_6H_4COO)_3(CH_3CH{=}CHCOO)(C_5H_5N)].C_5H_5N$). The results seem to suggest that presence of a higher ratio of arylcarboxylate ligand to linear alkylcarboxylate ligand resulted in a complex with a wider band gap energy. This may be due to resonance stabilization of *pi* electrons in the aromatic ring.

The **TGA** thermogram (**Figure 4.68**) shows that **Complex 10** decomposes at temperatures above 178°C. Thus it is less thermally stable than **Complex 8** ($[Cu_2(p\text{-}HOC_6H_4COO)_3(CH_3CH{=}CHCOO)].2C_5H_5N$; T_{dec} = 209°C). This is expected as the former complex has greater number of alkylcarboxylate ligands and strong axial ligations by pyridine molecules.

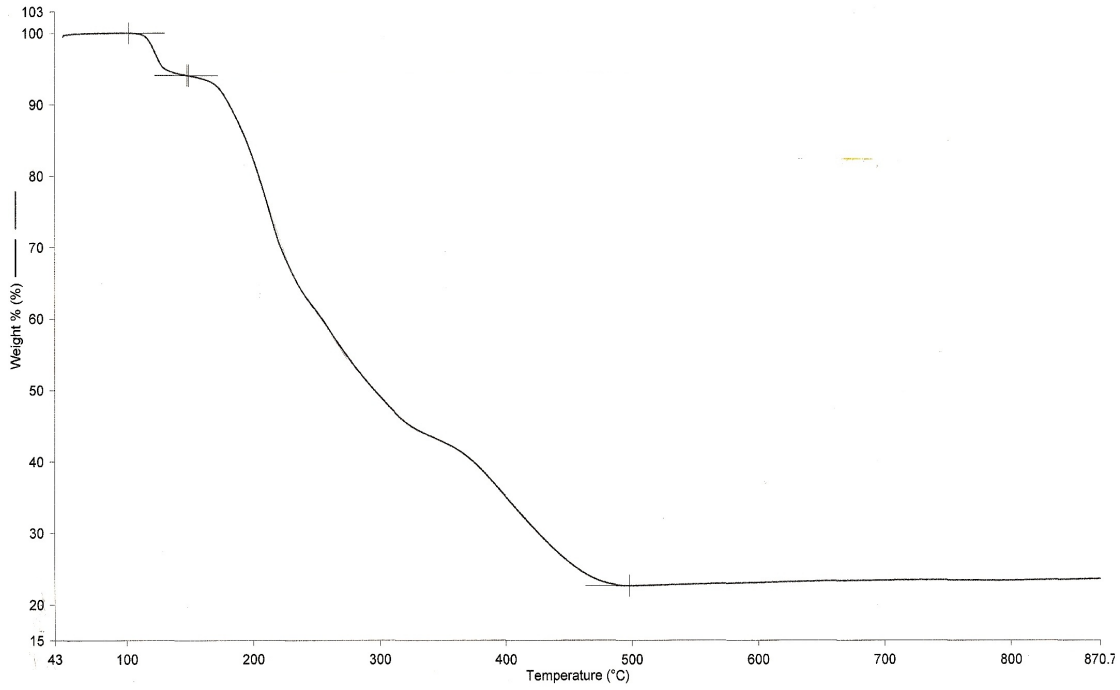

Figure 4.68 TGA of **Complex 10**

The thermogram also shows an initial weight loss of 5.9% at 120°C, assigned to the evaporation of non-coordinated CH_3CH_2OH molecule (expected 6.0%). The higher than expected temperature at which this occurred (bpt CH_3CH_2OH = 87°C) supports the suggestion that the molecule is H-bonded to the complex, as shown in **Figure 4.67**. The complex then suffered a total weight loss of 71.1% from 178°C to 500°C, assigned to the decomposition of the ligands (expected 70.6%).

The amount of residue at temperatures above 500°C is 23.0%. The expected value, assuming that the residue is CuO, is 21.7%. Thus, the complex may be said to undergo an almost complete decomposition of all of the organic ligands.

The **DSC** scan (**Figure 4.69**) shows an endotherm at 102°C (ΔH = + 37.8 kJ mol^{-1}), assigned to dissociation of axially-coordinated C_5H_5N and H-bonded CH_3CH_2OH molecules. This is followed by overlapping endotherms at 197°C (ΔH = 199 kJ mol^{-1}), which may be due to the decomposition of the carboxylate ligands to carbon dioxide and other volatiles.

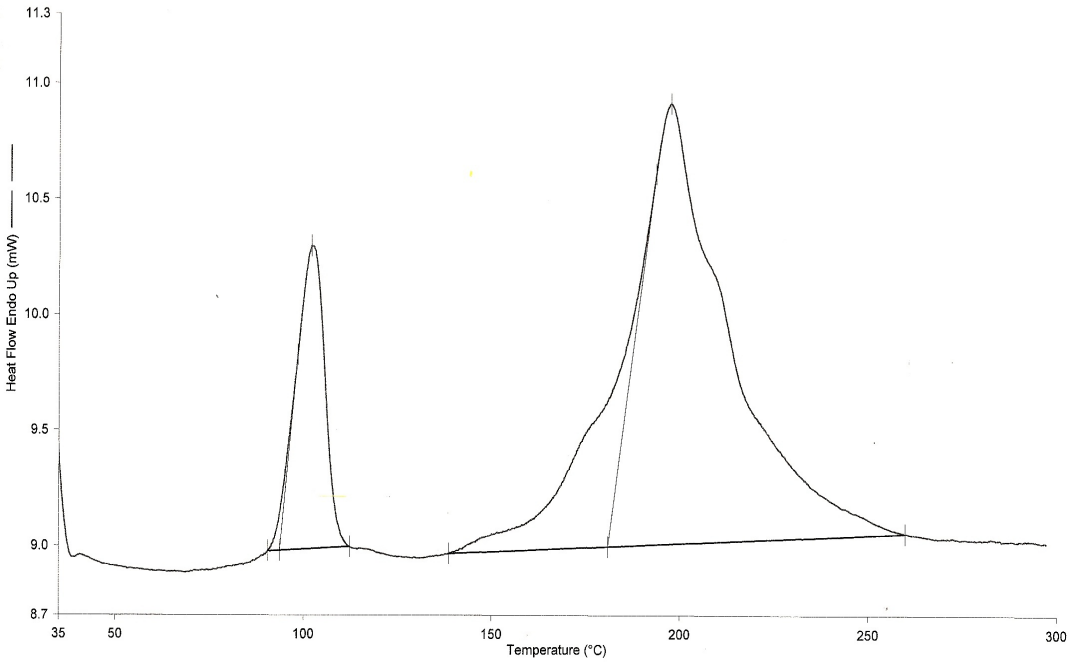

Figure 4.69 DSC of **Complex 10**

The μ_{eff} value, calculated from its magnetic susceptibility data (χ_g, 0.429 x 10^{-5}c.g.s., χ_m, 3.14 x 10^{-3}c.g.s.; χ_{dia}, -1.97 x 10^{-4}; and χ_m^{corr} , 3.34 x 10^{-3}), is 2.83 B.M. at 298 K. The value is in good agreement with the spin-only value of 2.83 B.M. for two unpaired electrons expected for the dimeric copper(II) complex with no magnetic interaction between the two copper(II) ions. The 2J value is 50 cm^{-1}. This suggests a weak ferromagnetic interaction between the two Cu(II) centres.

A possible explanation for the observed magnetic properties for **Complex 10** may be due to the stronger Cu-pyridine axial bonds which results in weaker Cu-OOCR equatorial bonds (as suggested from TGA). Thus, the geometry at each Cu(II) centre is less planar (more tetrahedrally distorted), and leads to a reduced overlap between the magnetic x^2-y^2 orbital of Cu(II) and that of the ligands for effective superexchange pathway.

The **CV** voltammogram (**Figure 4.70**), recorded cathodically from 1.5 V to -1.5 V, shows two cathodic peaks at -0.51 V and -0.93 V, and two anodic peaks at +0.28 V and +0.44 V. It is to be noted that the peak at +0.97 V was seen in the background scan and therefore it is not considered as an oxidation peak for the **Complex 10**.

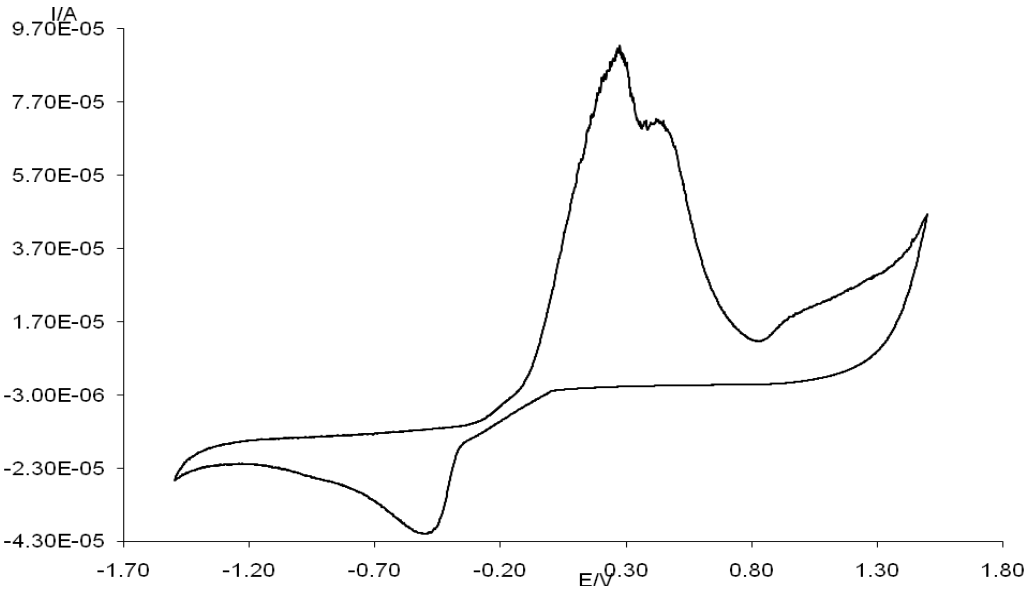

Figure 4.70 CV of **Complex 10**

The cathodic peak at -0.51 V is assigned to reduction of the binuclear [Cu(II)Cu(II)] complex to mixed-valence [Cu(II)Cu(I)] complex, which was further reduced to monovalence [Cu(I)Cu(I)] complex at -0.93 V. The dinuclear [Cu(I)Cu(I)] complex formed was then reoxidized to the mixed-valence [Cu(II)Cu(I)] complex at +0.28 V and then to the dinuclear [Cu(II)Cu(II)] complex at +0.44 V. The redox process is shown in **Scheme 4.2**.

$$[Cu(II)Cu(II)] \underset{+0.44\ V}{\overset{-0.51V}{\rightleftharpoons}} [Cu(II)Cu(I)] \underset{+0.28\ V}{\overset{-0.93V}{\rightleftharpoons}} [Cu(I)Cu(I)]$$

Scheme 4.2 Redox process of **Complex 10**

From the cathodic and anodic potentials, the ΔE values for [Cu(II)Cu(II)]–[Cu(II)Cu(I)] and [Cu(II)Cu(I)]–[Cu(I)Cu(I)] couples are 948 mV and 1204 mV, and the I_{pa}/I_{pc} ratio are 1.8 and 145, respectively. Thus the results show that **Complex 10** undergoes quasireversible redox reactions, and that mixed valence [Cu(II)Cu(I)] complex, and especially the monovalent [Cu(I)Cu(I)] complex, are chemically unstable.

(ii) Green powder

The green powder was obtained from the filtrate on standing at room temperature for a week. It was soluble in all common organic solvents, except for toluene.

The results from the **elemental analyses** give the C:H:N ratio equals 10.7:1.0:1.1. This agrees with the chemical formula $CuC_{13}H_{15}O_4N$ (C:H:N ratio is 11.1:1.1:1.0), and is similar to that of **Complex 9 (**$[Cu_2(CH_3CH{=}CHCOO)_4].2C_5H_5N$**).** Additionally, the FTIR spectrum of the green powder (**Figure 4.71**) is similar with that of **Complex 9** (**Figure 4.62**). Thus, the green powder formed in this reaction is not a new complex; it is in fact **Complex 9** (formed from the reaction between the unreacted $[Cu(CH_3CH{=}CHCOO)_4]$ with pyridine).

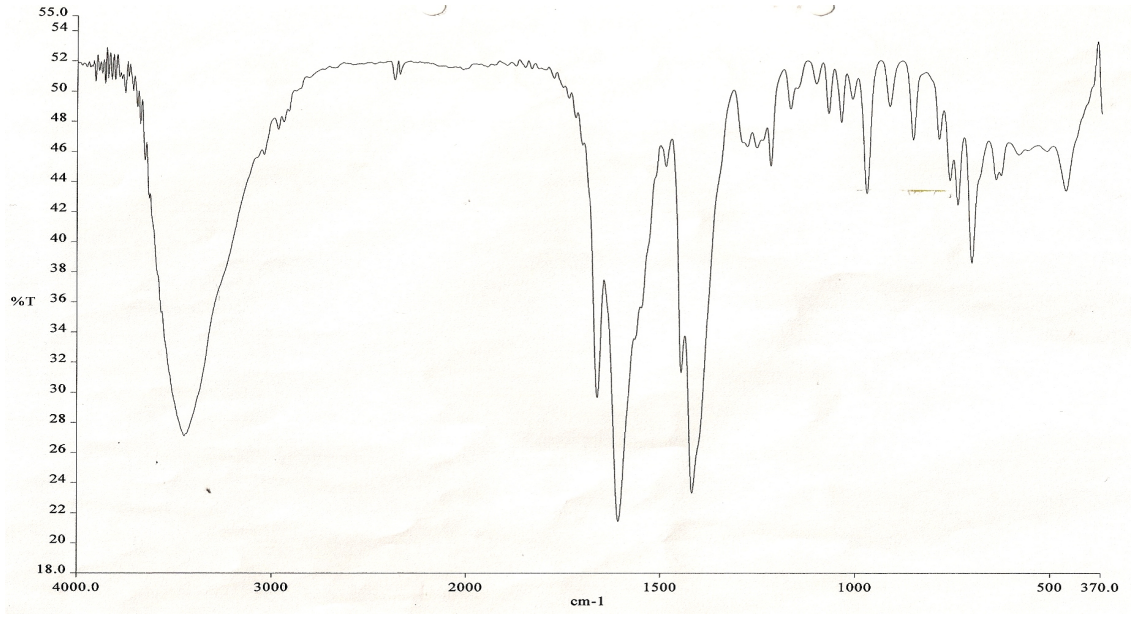

Figure 4.71 FTIR spectrum of **green powder**

(c) $[Cu_2(p\text{-}HOC_6H_4COO)_3(CH_3CH{=}CHCOO)]$

The ligand-exchange reaction involving $[Cu_2(p\text{-}HOC_6H_4COO)_4]$ and $[Cu_2(CH_3CH{=}CHCOO)_4]$ (mol ratio = 3:1) formed two products: a purple powder and a green powder.

(i) Purple powder

The purple powder was the residue from the hot reaction mixture. It was soluble in methanol, dimethyl sulfoxide, and dimethylformamide but insoluble in chloroform, acetone and toluene.

The results from the **elemental analyses** for the purple powder gave the C:H:N ratio equals to 15.8:1.0:1.6, which is similar to that of **Complex 8** ($[Cu_2(p\text{-}HOC_6H_4COO)_3(CH_3CH{=}CHCOO)(C_5H_5N)_2]$). Additionally, its **FTIR** spectrum (**Figure 4.72**) is similar with that of **Complex 8** (**Figure 4.55**). Therefore, it is safe to assume that both "complexes" are the same, and hence it is the intended product from the reaction.

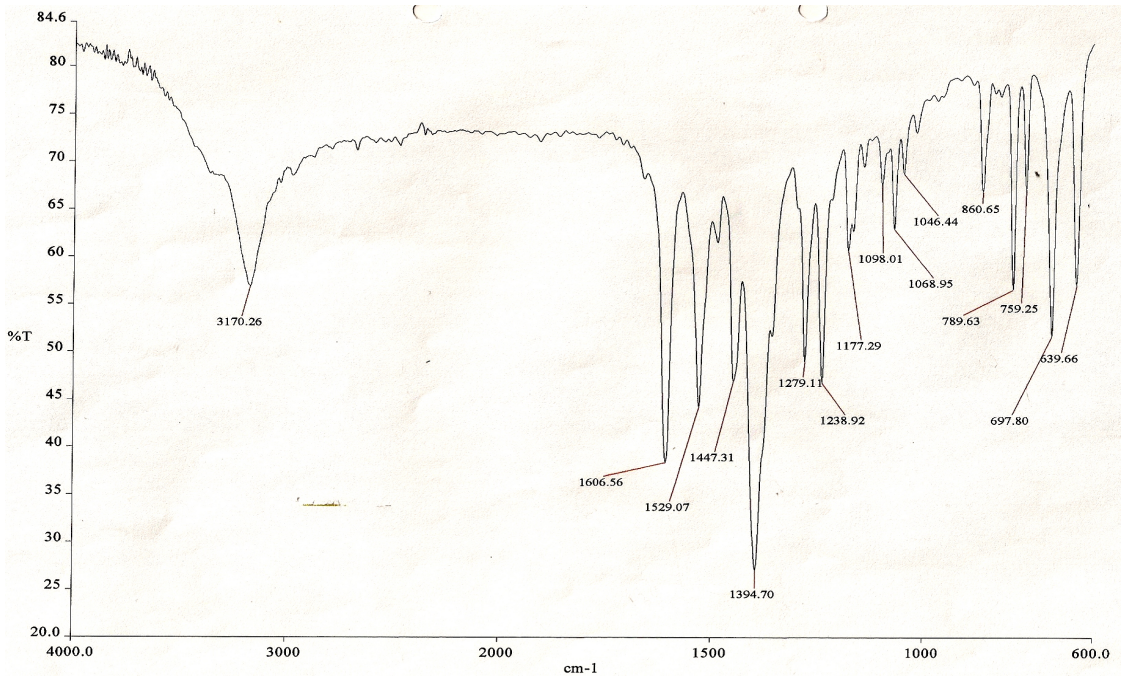

Figure 4.72 FTIR spectrum of ***purple powder***

(ii) Green powder

The green powder was obtained from the filtrate after a week at room temperature. It was soluble in all common organic solvents, except toluene. The results from the **elemental analyses** give the C:H:N ratio equals 10.0:1.0:1.1. This agrees with the

chemical formula $CuC_{13}H_{15}O_4N$ (formula weight = 330.8 g mol^{-1}, C:H:N ratio = 11.1:1.1:1.0), which is the same as **Complex 9 (**$[Cu_2(CH_3CH{=}CHCOO)_4].2C_5H_5N$). This is further confirmed by the similarity between the FTIR spectrum of the green powder (**Figure 4.73**) with that of **Complex 9** (**Figure 4.62**). Thus, the green powder is formed from the reaction of $[Cu_2(CH_3CH{=}CHCOO)_4]$ (one of the starting materials) with pyridine.

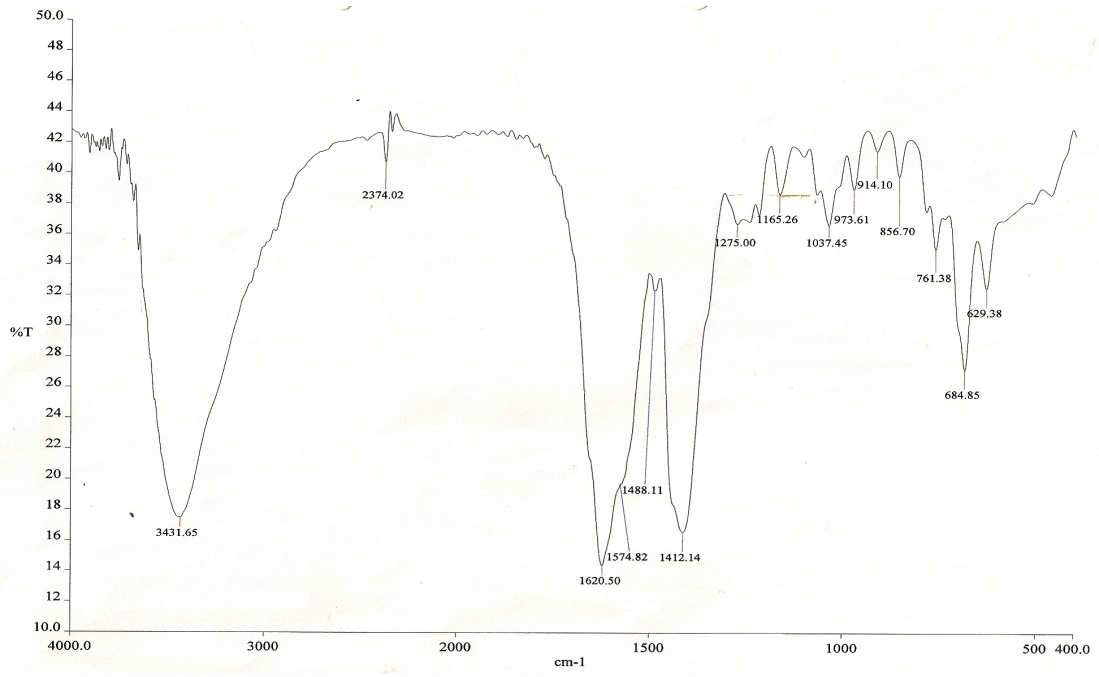

Figure 4.73 FTIR spectrum of ***green powder***

(d) Summary

The ligand-exchange reaction involving different ratios of $[Cu_2(p\text{-}HOC_6H_4COO)_4]$ and $[Cu_2(CH_3CH{=}CHCOO)_4]$ was successfully used to prepare $[Cu_2(p\text{-}HOC_6H_4COO)_n(CH_3CH{=}CHCOO)_{4-n}]$, where n = 1 and 3, but not for n = 2. The complex obtained from the filtrate of $[Cu_2(CH_3CH{=}CHCOO)_4]$ (the starting material) with C_5H_5N.

The complexes were dinuclear with square pyramidal geometry at the two Cu(II) centres. **Complex 8** (n = 3) is more thermally stable and is antiferromagnetic, while

Complex 10 (n = 1) is ferromagnetic. All complexes showed quasireversible redox reaction. The mixed-valence complexes formed were more chemically stable compared to the monovalence complex. The analytical results are summarized in the **Table 4.6**.

Table 4.6 Analytical results for complexes from the ligand-exchange reaction

	Complex 8	**Complex 9**	**Complex 10**
Structural formula*	$[Cu_2(C_5H_5N)_2L_3L']$	$[Cu_2L'_4(C_5H_5N)_2]$	$[Cu_2LL'_3(C_5H_5N)_2]$
ΔCOO/ cm^{-1}	135 (bridging)	159 (bridging)	167 (bridging)
λ_{max}/nm solid	572	717	683
solution ($\varepsilon_{max}/M^{-1}cm^{-1}$)	703 (197)	706 (1.14×10^3)	703 (230)
$T_{decomposition}/^oC$	209	#	178
μ_{eff} (2J)	2.57 (-100) antiferromagnetic	#	2.83 (+50) ferromagnetic
E_{pc}/V E_{pa}/V (I_{pc}/I_{pa})	-0.61; -0.88 +0.01; +0.44; +0.98 (1.0,1.5)	#	-0.51; -0.93 +0.28; +0.44 (1.8, 145)

* solvates are not shown; L = *p*-HOC_6H_4COO; L' = $CH_3CH{=}CHCOO$; # Not reported

4.3.2 $[Cu_2(p\text{-}HOC_6H_4COO)(CH_3(CH_2)_7CH{=}CH(CH_2)_7COO)_3]$

The ligand-exchange reaction between $[Cu_2(p\text{-}HOC_6H_4COO)_4]$ and $[Cu_2(CH_3(CH_2)_7CH{=}CH(CH_2)_7COO)_4]$ (mol ratio = 1:3) formed a dark green semi-solid (**Complex 11**) from the hot reaction mixture. It was soluble in all common organic solvents, except dimethylsulfoxide and acetone.

The result of **elemental analyses** (C, 65.3%; H, 10.4%) is in good agreement with that calculated for $Cu_2C_{61}H_{108}O_{11}$ (formula weight, 1144.5 g mol^{-1}; C, 64.0%; H, 9.4%).

The **FTIR** spectrum (**Figure 4.74**) is different from those of the starting materials (**Figure 4.52** and **Figure 4.75**). From this, it may be suggested that a reaction occurred between $[Cu_2(p\text{-}HOC_6H_4COO)_4]$ and $[Cu_2(CH_3(CH_2)_7CH{=}CH(CH_2)_7COO)_4]$ to form a product. Additionally, the spectrum shows the presence of all of the expected functional groups as previously discussed, including two sharp peaks at 2926 cm^{-1} and 2855 cm^{-1} assigned to the long aliphatic carbon chain. The ΔCOO value is 159 cm^{-1}, suggesting bridging carboxylate ligands.

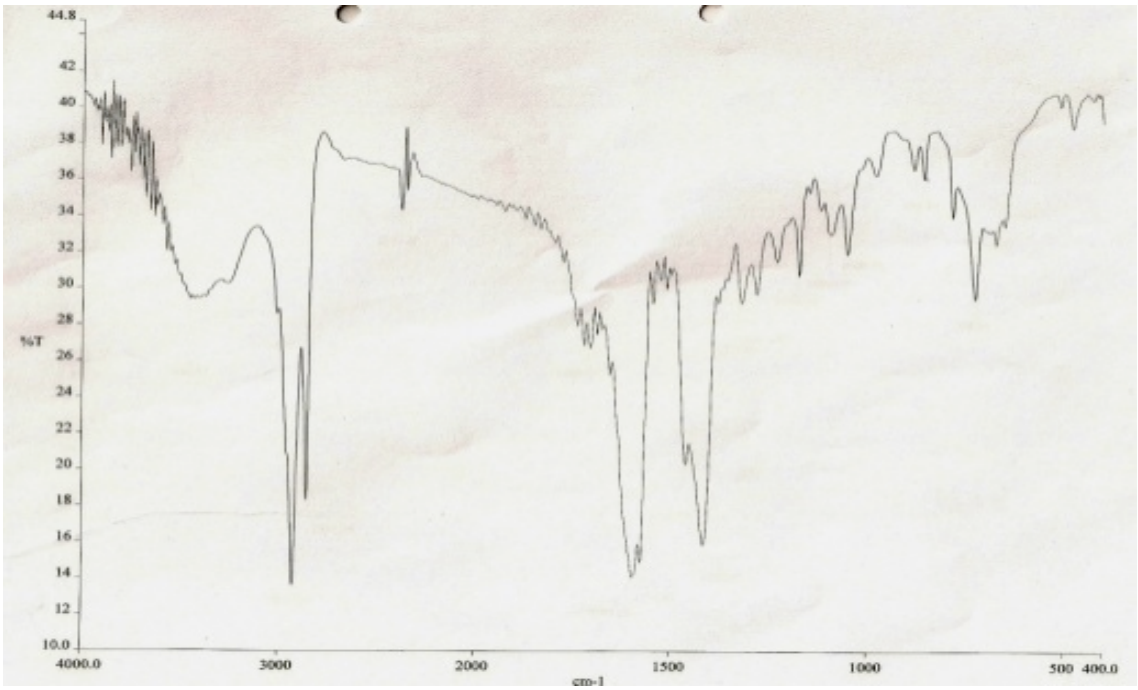

Figure 4.74 FTIR spectrum of **Complex 11**

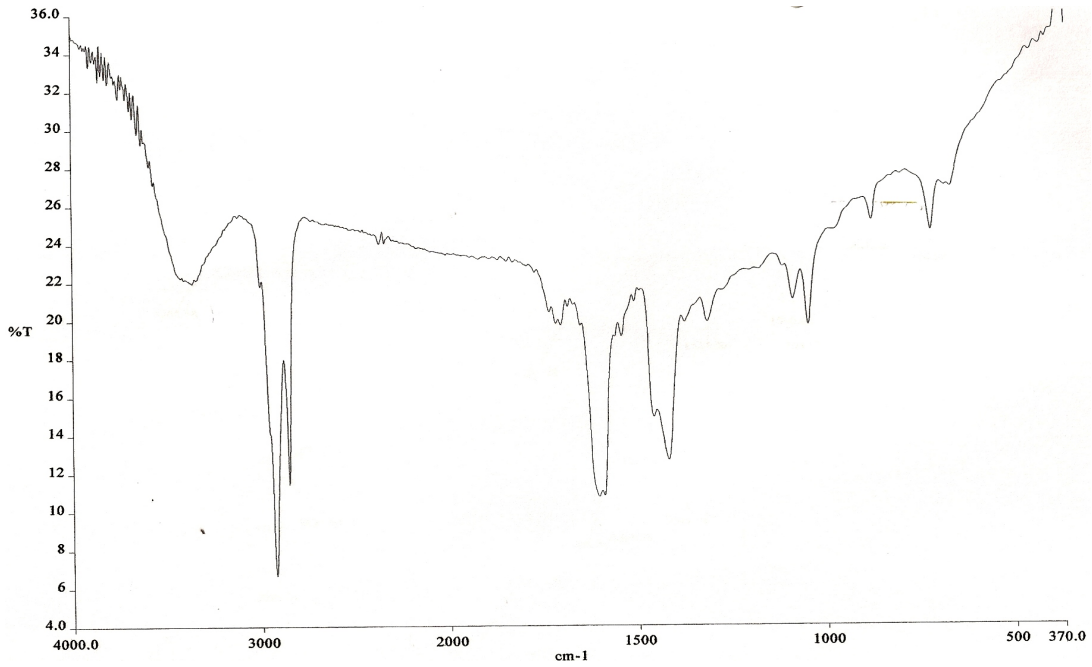

Figure 4.75 FTIR spectrum of $[Cu_2(CH_3(CH_2)_7CH{=}CH(CH_2)_7COO)_4]$ (starting material)

Its **UV-vis** spectrum in methanol (**Figure 4.76**) shows a broad *d-d* band at 690 nm (ε_{max}= 452 $M^{-1}cm^{-1}$) and a shoulder at 360 nm. These suggests a dimeric complex with square-pyramidal Cu(II) centres.

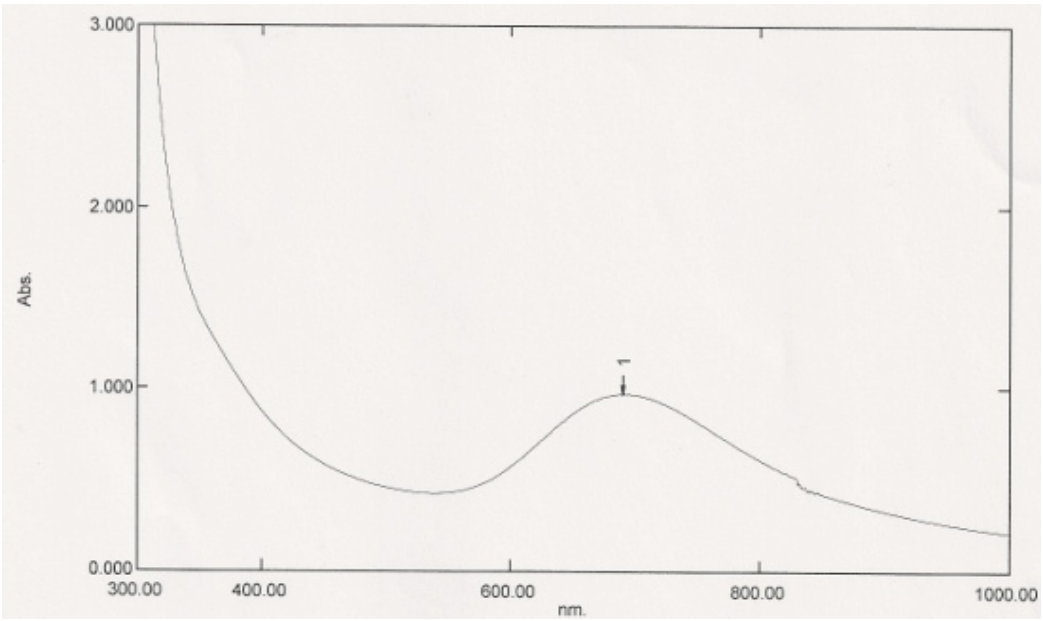

Figure 4.76 UV-vis spectrum of **Complex 11** in methanol

Combining the above results, **Complex 11** is proposed to have the structural formula $[Cu_2(p\text{-}HOC_6H_4COO)(CH_3(CH_2)_7CH{=}CH(CH_2)_7COO)_3(H_2O)_2]$ (**Figure 4.77**).

The chemical formula ($Cu_2C_{61}H_{108}O_{11}$) is in agreement with the results of the elemental analyses, and it shows bridging carboxylates as inferred from FTIR, and square pyramidal Cu(II) binuclear complex with dimer-dimer Cu-O_{axial} linkages as suggested from UV-vis. Thus, it is the intended product from the reaction, and its yield was 69.2%.

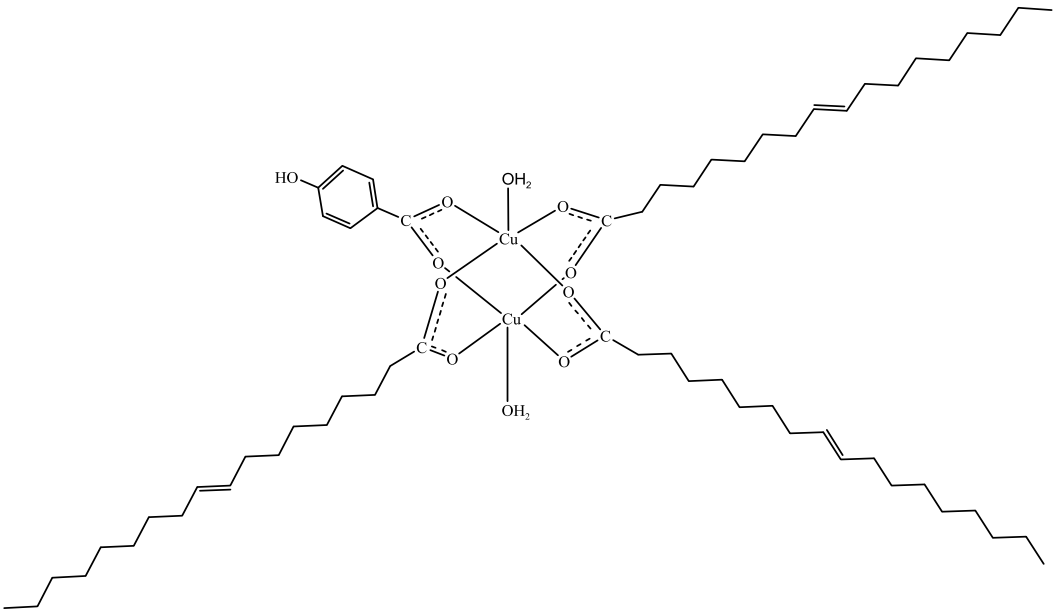

Figure 4.77 Proposed structural formula of **Complex 11**

The value of **Eg** for **Complex 11,** calculated as before from onset λ value of 542 nm, is 2.29 eV. This is similar to that of **Compex 10** ([Cu_2(*p*-HOC_6H_4COO)(CH_3CH=$CHCOO)_3(C_5H_5N)_2$].CH_3CH_2OH; E_g = 2.31 eV). The results seem to suggest that the length of unsaturated alkylcarboxylate ligand and the different axial neutral ligands has insignificant effect on the photonic properties of these dinuclear copper(II) mixed-carboxylates.

The **TGA** thermogram (**Figure 4.78**) shows that the decomposition temperature for **Complex 11** is 201^oC. Thus, it is more thermally stable than **Complex 10** ([Cu_2(*p*-HOC_6H_4COO)(CH_3CH=$CHCOO)_3(C_5H_5N)_2$].CH_3CH_2OH; T_{dec} = 178^oC), which has a shorter alkyl chain. The difference may be related with the formation of less volatile

$CH_3(CH_2)_7CH=CH(CH_2)_7COOH$ from **Complex 11**, or to a weaker RCOO-Cu equatorial bonds in **Complex 10** as a result of stronger C_5H_5N-Cu axial bonds.

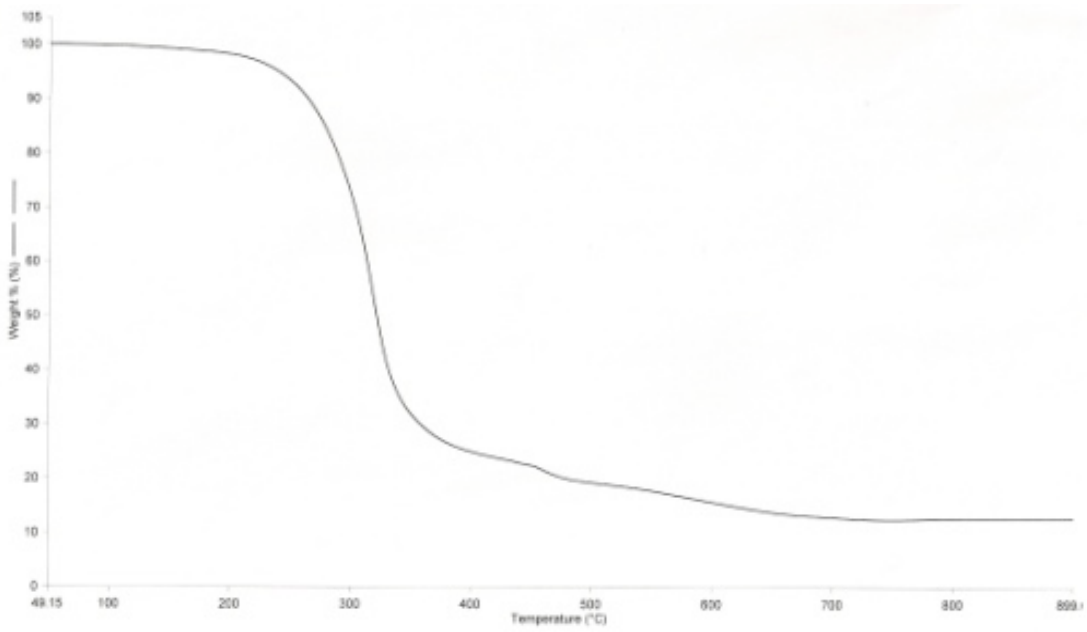

Figure 4.78 TGA of **Complex 11**

The thermogram also shows that the complex decomposed in two steps. The first step at 201°C involved a weight loss of 73% and is assigned to the decomposition of $CH_3(CH_2)_7CH=CH(CH_2)_7COO$ (expected 76%). The second step at 445°C involved a weight loss of 12% and is assigned to the decomposition of the *p*-HOC_6H_4COO ligand (expected 12%).

The amount of residue at temperatures above 686°C was 15%. Assuming that it is pure CuO, the estimated formula mass of **Complex 11** is 1060 g mol^{-1}. This is in good agreement with the value calculated based on the chemical formula from the CHN results (1112.6 g mol^{-1}).

The **DSC** scan (**Figure 4.79**) shows a broad endotherm at 51°C (ΔH = +26.6 kJ mol^{-1}), assigned to the breaking of Cu-OH_2(axial) bonds (**Figure 4.77**). This is followed by a very broad and weak endotherm from about 73°C to about 188°C ($\Delta H_{combined}$ =

+74.9 kJ mol^{-1}), assigned to the breaking of van der Waals forces between the long alkylcarboxylate chains. Finally, overlapping broad endotherms at onset temperature of 200°C ($\Delta H_{combined}$ = +74.9 kJ mol^{-1}) are assigned to the decomposition of the ligands, as this occurs at the decomposition temperature of the complex (Td = 201°C from TGA).

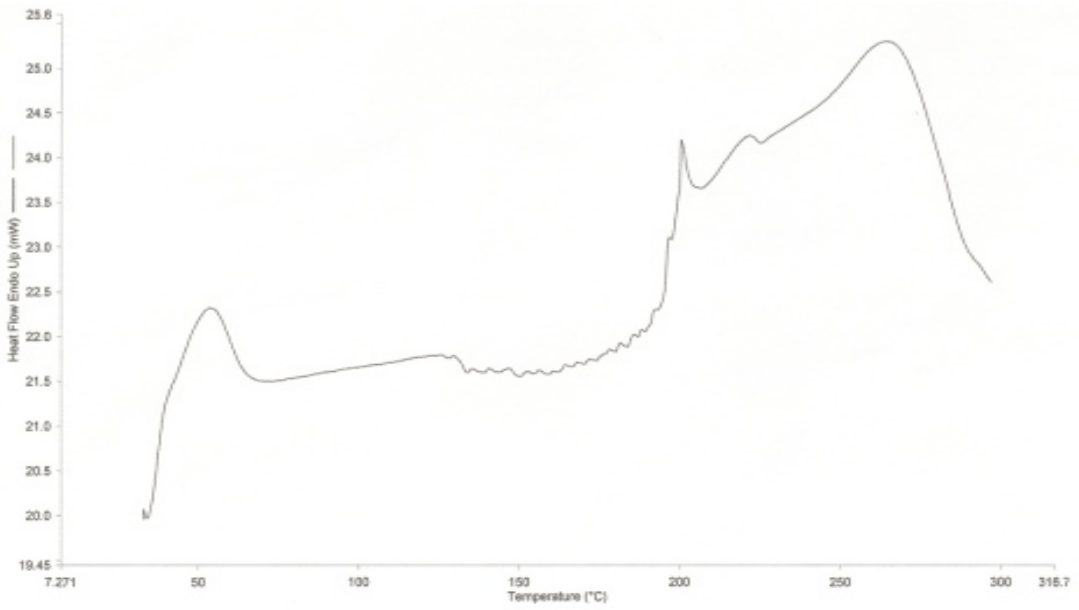

Figure 4.79 DSC of **Complex 11**

The **magnetic** susceptibility of the complex could not be determined by the Gouy method as it was a semi-solid at room temperature.

The **CV** voltammogram (**Figure 4.80**), scanned cathodically in the potential range -2.0 V to +2.0 V, shows one reduction peak at -1.27 V, and two oxidation peaks at +0.83 V and +1.68 V.

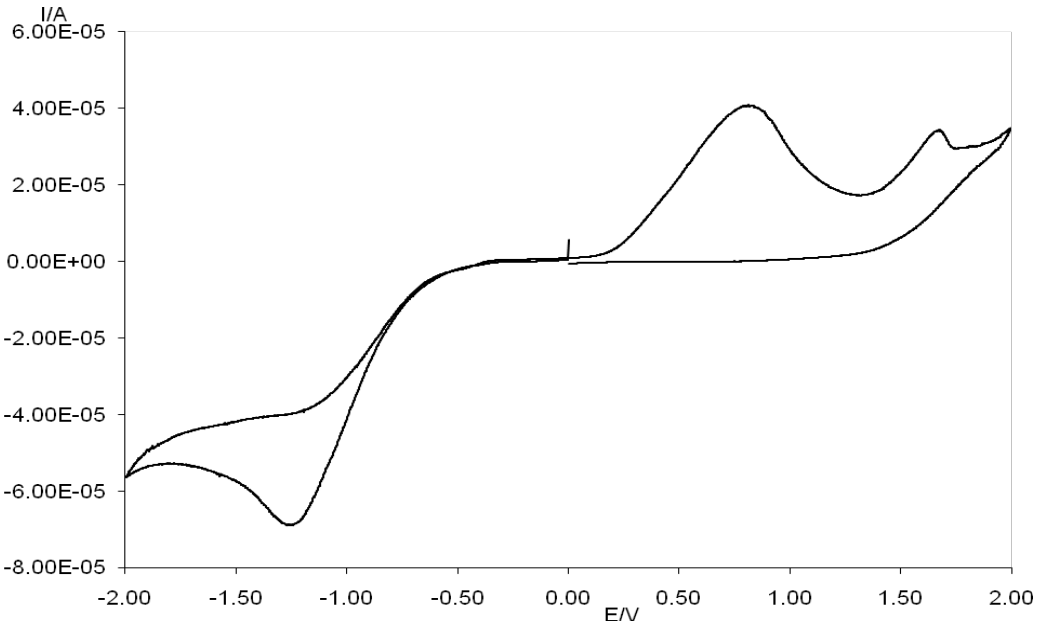

Figure 4.80 CV of **Complex 11**

The cathodic peak at -1.27 V is assigned to the one-step reduction of binuclear [Cu(II)Cu(II)] complex to [Cu(I)Cu(I)] complex, suggesting the absence of electronic interaction between the two Cu(II) centres. It is further noted that the normally observed values for the reduction of [Cu(II)Cu(II)] to [Cu(II)Cu(I)] is about -0.5 V, and that of [Cu(II)Cu(I)] to [Cu(I)Cu(I)] is about -1 V [10, 24, 25]. The high value for the reduction potential for **Complex 11** may be due to the insulating layer formed by three long and nonlinear alkylcarboxylates ligands, which "prevented" the electrons from the electrode to reach the Cu(II) centres.

The dinuclear [Cu(I)Cu(I)] complex was reoxidized, also in one step, to [Cu(II)Cu(II)] complex at +0.83 V. The anodic peak at +1.68 V may be due to the oxidation of the ligand, either at the C=C bond or the aromatic -OH. The redox process is shown below.

$$[\text{Cu(II)Cu(II)}] \underset{+0.83\ \text{V}}{\overset{-1.27\ \text{V}}{\rightleftharpoons}} [\text{Cu(I)Cu(I)}]$$

From the cathodic and anodic potentials, the ΔE value is 2100 mV, indicating a quasireversible redox reaction. The I_{pa}/I_{pc} ratio is 0.6, indicating that the [Cu(I)Cu(I)] complex formed was chemically unstable. However, the absence of anodic stripping at about 0 V associated with the oxidation of [Cu(0)] means that the [Cu(I)Cu(I)] complex did not disproportionate to [Cu(II)] and [Cu(0)].

4.3.3 [Cu_2(p-HOC_6H_4COO)($(CH_3)_3CCOO$)$_3$]

The ligand-exchange reaction between [Cu_2(*p*-HOC_6H_4COO)$_4$] and [$Cu_2((CH_3)_3CCOO)_4$] (mol ratio =1:3) formed two products: a greenish-brown powder and a green crystal.

(a) Greenish-brown powder

The greenish-brown powder (**Complex 12)** was obtained as the residue from the hot reaction mixture. It was sparingly soluble in all organic solvents.

The results from the **elemental analyses** give the C:H:N ratio of 28.0:4.0:1.0, which agrees with the chemical formula $Cu_2C_{32}H_{47}NO_{11}$ (formula weight = 784.8 g mol^{-1}, calculated C:H:N ratio = 27.4:3.4:1.0).

The **FTIR** spectrum (**Figure 4.81**) is different from those of the starting materials (**Figure 4.52** and **Figure 4.82**), indicating a reaction has occurred between [Cu_2(*p*-$HOC_6H_4CO_2$)$_4$] and [$Cu_2(C(CH_3)_3CO_2)_4$] under the stated conditions.

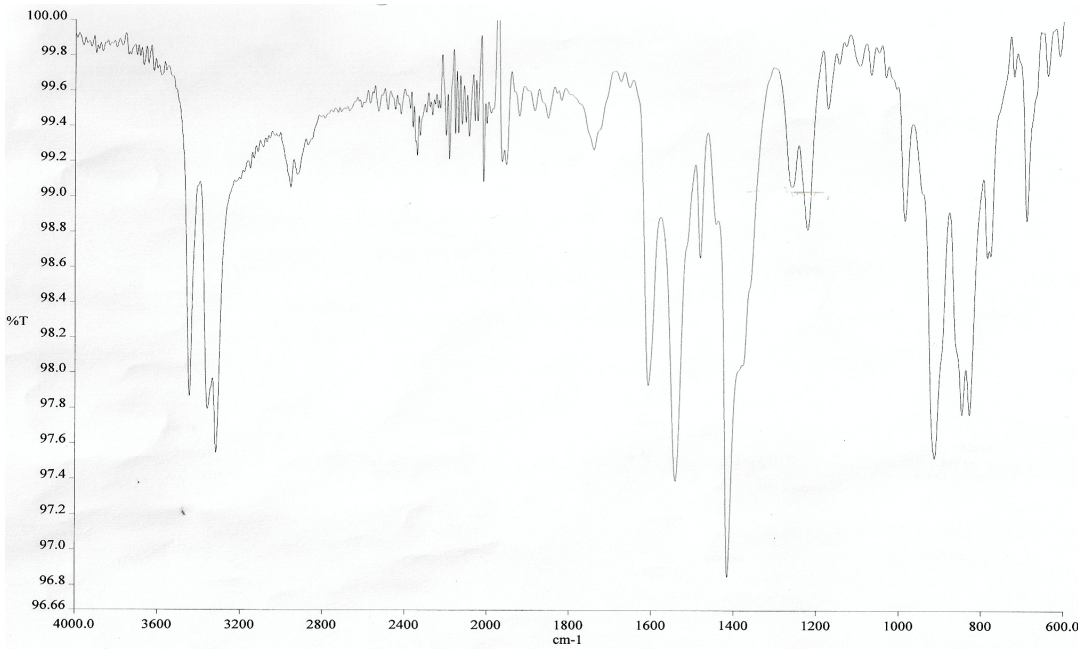

Figure 4.81 FTIR of **Complex 12**

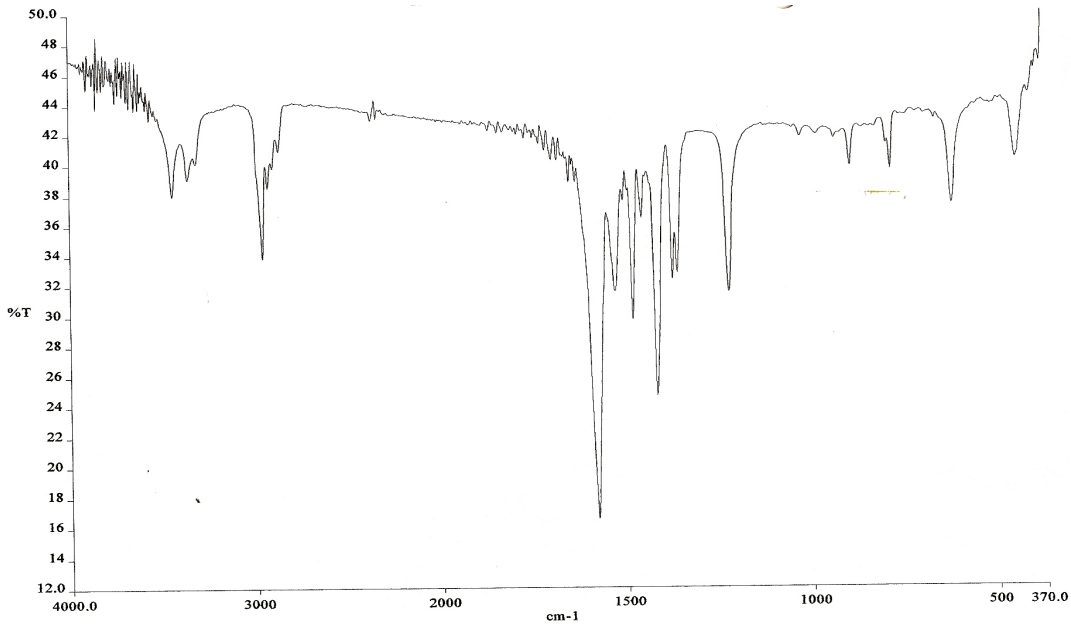

Figure 4.82 FTIR of $[Cu_2((CH_3)_3CCOO)_4]$ (starting material)

The spectrum also shows the presence of all of the expected functional groups as previously discussed. The ΔCOO values are 127 cm^{-1} and 225 cm^{-1}, suggesting chelating, bridging and monodentate carboxylate ligands respectively.

Its **UV-vis** spectrum of a dark brown "solution" formed when the solid was dissolved in methanol (partially soluble; **Figure 4.83**) shows a continuously increasing absorbtion from 1000 nm to 300 nm. This suggests extensive delocalisation of electrons. However, the electronic spectrum for the sample in the solid state could not be recorded due to insufficient amount. Therefore, the geometry and nuclearity of the complex cannot be deduced from its spectrum.

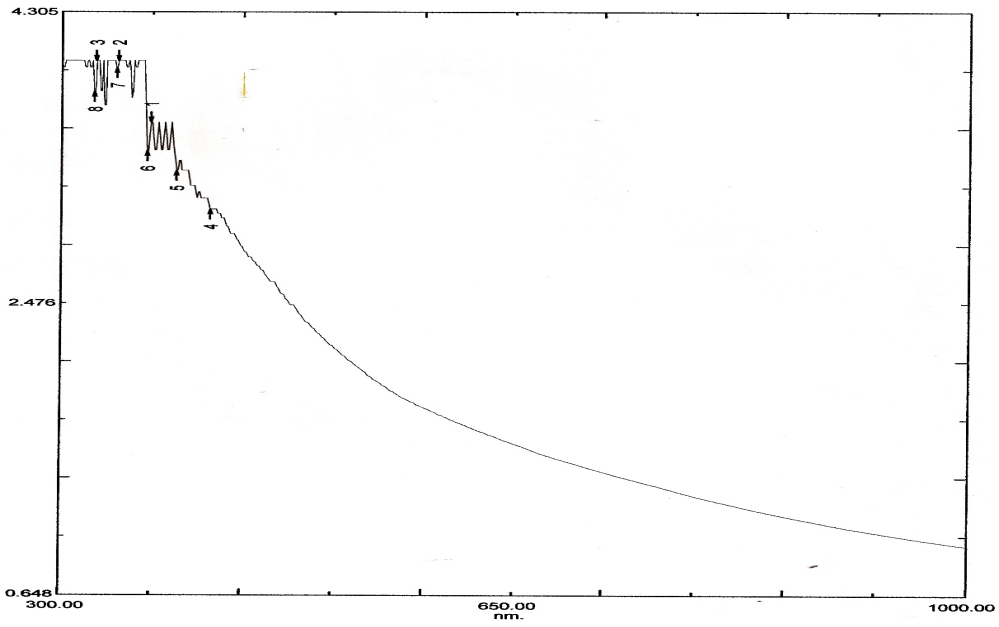

Figure 4.83 UV-vis of **Complex 12** in solution

Combining the above results, **Complex 12** is proposed to have the structural formula $(C_5H_5NH)[Cu_2((CH_3)_3CCOO)_4(p\text{-}HOC_6H_4COO)]$ (**Figure 4.84)**. The proposed structure shows tetrahedral Cu(II) inferred from its greenish-brown colour, the chemical formula $Cu_2C_{32}H_{47}NO_{11}$ which agrees with the results of the elemental analyses, and bridging/chelating and monodentate carboxylates as inferred from FTIR. Thus, its yield was 13.8%, but it is **not** the intended product from the reaction.

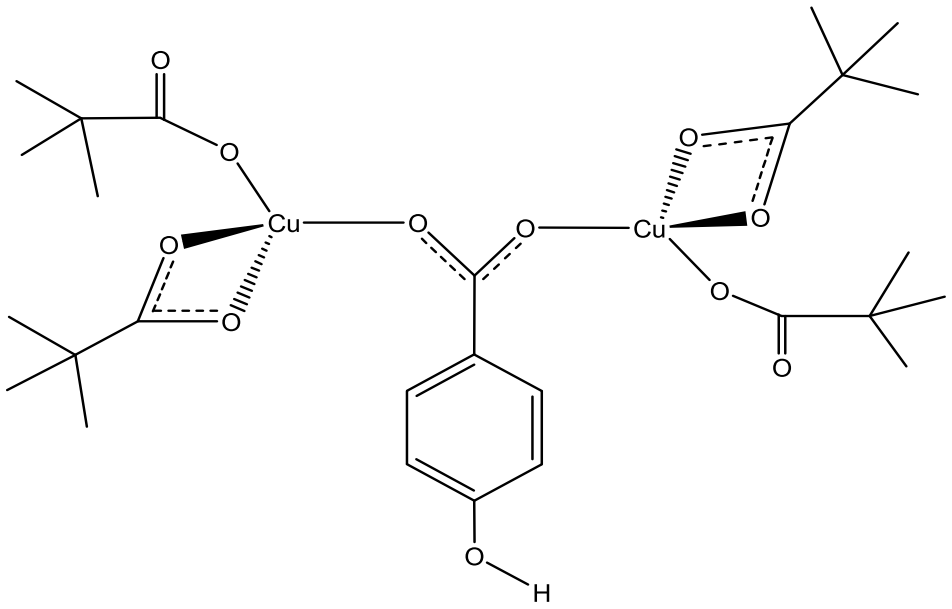

Figure 4.84 Proposed structural formula of **Complex 12** (pyridinium ion is not shown)

The **TGA** thermogram (**Figure 4.85**) shows that the decomposition temperature for **Complex 12** is 170°C. Thus, it is as thermally stable as **Complex 10** ($[Cu_2(p\text{-}HOC_6H_4COO)(CH_3CH{=}CHCOO)_3(C_5H_5N)_2].CH_3CH_2OH$; T_{dec} = 178°C). The results seem to infer that the thermal stability of these mixed-carboxylate complexes is independent on the degree of saturation of the alkylcarboxylate ligand used.

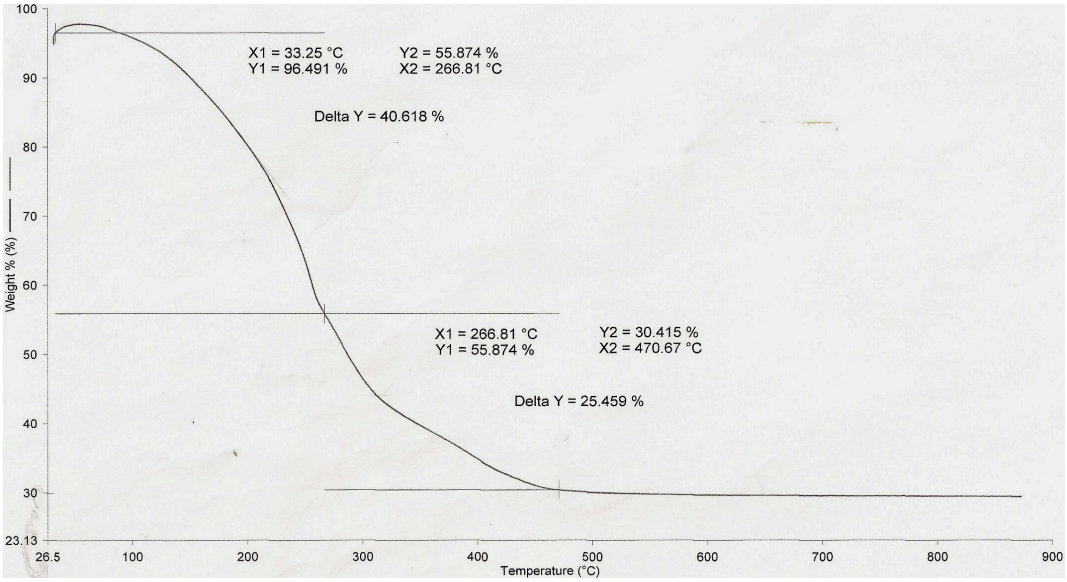

Figure 4.85 TGA of **Complex 12**

The thermogram also shows that the complex suffered an initial weight loss of 11.0% at 110°C, assigned to the evaporation of C_5H_5N (expected 10.1%). The next weight loss of 57% at 170°C is attributed to the decomposition of the ligands (expected 73.6%). The amount of residue at temperatures above 471°C is 32% (expected, assuming CuO, 20.3%). The result suggests incomplete decomposition of the carboxylate ligands.

The **DSC** scan (**Figure 4.86**) shows a weak endotherm at onset temperature 49°C (ΔH = +3.9 kJ mol^{-1}), assigned to the rotational energy about the ligand connecting the two tetrahedral Cu(II) centres. This is followed by a very broad, strong and overlapping endotherms in the temperature range of 105°C to 281°C ($\Delta H_{combined}$ = +3466.3 kJ mol^{-1}), assigned to the combined energy needed to overcome the van der Waals forces between $-C(CH_3)_3$, H-bonds (Refer to **Figure 4.84**), the breaking of $(CH_3)_3CCOO$-Cu and Cu-(*p*-HOC_6H_4COO)-Cu bonds, and decomposition of the ligands.

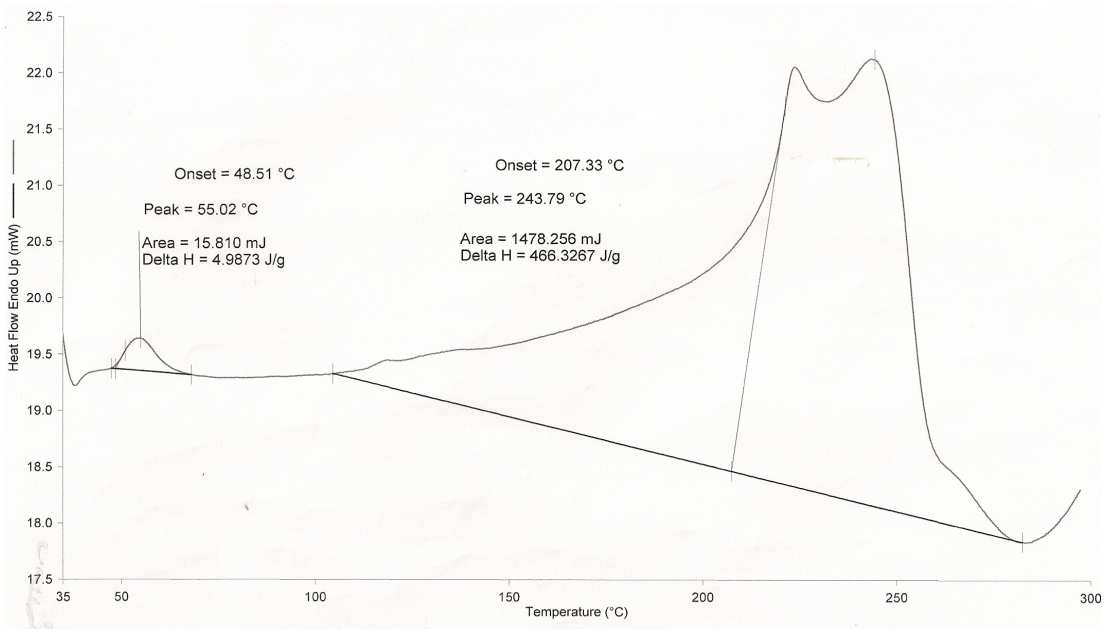

Figure 4.86 DSC of **Complex 12**

The value of μ_{eff}, calculated as before from the values of χ_g (1.32 x 10^{-5}c.g.s.), χ_m (9.88 x 10^{-3}c.g.s.), χ_{dia}, (-2.75 x 10^{-4} c.g.s) and hence χ_m^{corr} (1.02 x 10^{-2} c.g.s), is 4.94 B.M. at 298 K. The value of 2J is +357 cm^{-1}. These results suggest strong ferromagnetic interaction between the two copper(II) centres, which is consistent with the proposed structural formula.

The **CV** voltammogram (**Figure 4.87**), recorded cathodically from 0 V in the potential range of -1.3 V to +1.0 V, shows three reduction peaks at -0.19 V, -0.86 V and -1.02 V, and two oxidation peaks at -0.19 V, and +0.09 V. The third oxidation peak at 0.62 V is not considered as it was also observed in the blank.

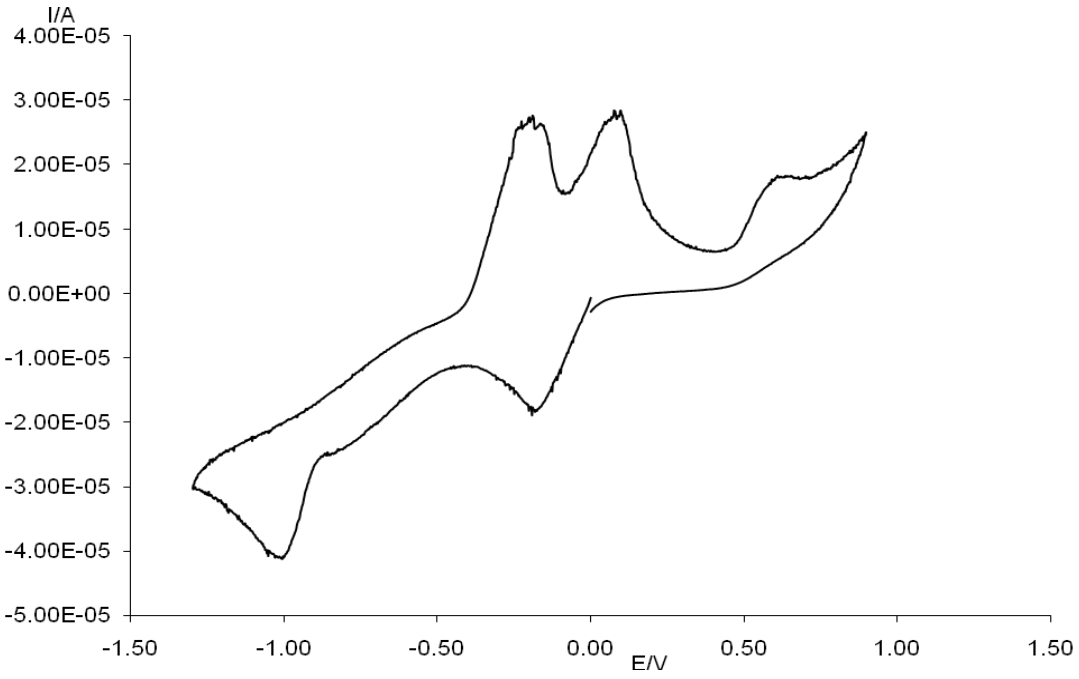

Figure 4.87 CV of **Complex 12**

The three cathodic peaks at -0.19, -0.86 V and -1.02 V are assigned to the reduction of [Cu(II)Cu(II)] to [Cu(I)Cu(I)], [Cu(II)] to [Cu(I)], and [Cu(I)] to [Cu(0)] complexes, respectively. It is postulated that [Cu(II)Cu(II)] complex was reduced at the same potential (-0.19 V) as the two centres have the same geometry. The [Cu(II)Cu(II)]

complex and [Cu(I)Cu(I)] complex formed then dissociated to two [Cu(II)] and two [Cu(I)] complexes respectively. The mononuclear [Cu(II)] complex was then reduced to [Cu(I)] complex at -0.86 V. Finally, the [Cu(I)] complex formed was reduced to [Cu(0)] at -1.02 V. The [Cu(0)] complex formed was then oxidized to [Cu(I)] at -0.19 V, which was then oxidized to [Cu(II)] at +0.09 V. The electrochemical-chemical-electrochemical (ECE) mechanism for the redox reactions are summarized in **Scheme 4.3.**

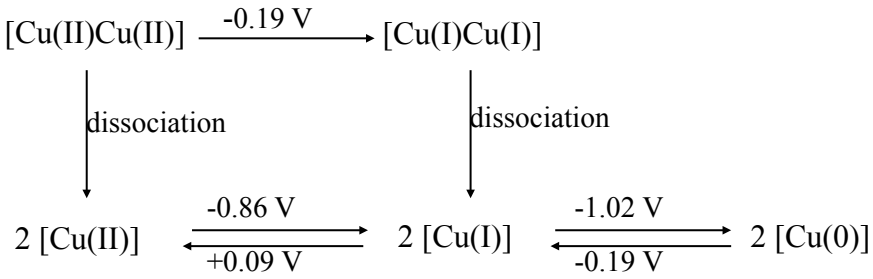

Scheme 4.3 The ECE mechanism of **Complex 12**

(b) Complex 13

Green crystals (**Complex 13**) deposited out of the filtrate after standing at room temperature for a month. Its yield was 87.5%, and it was soluble in all organic solvents.

The results of **elemental analyses** (C, 52.2%; H, 6.8%; N, 4.2%) are in good agreement with those calculated for $CuC_{15}H_{23}NO_4$ (formula weight, 344.9 g mol^{-1}; C, 52.2%; H, 6.7%; N, 4.1%).

The crystal structure of **Complex 13** (chemical formula $[Cu_2((CH_3)_3CCOO)_4(C_5H_5N)_2)]$), a crystal with dimensions 0.32 x 0.26 x 0.16 mm) was solved by direct methods and refined by full matrix least square in F^2 in the centrosymmetric space group $P2_1/n$. An ORTEP presentation of the crystal is shown in **Figure 4.88,** and the packing pattern is shown in **Figure 4.89** [26].

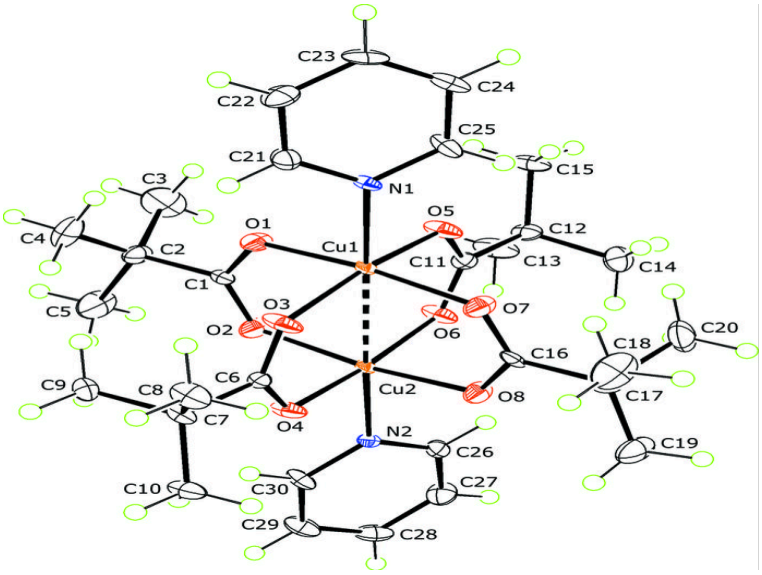

Figure 4.88 An ORTEP presentation of **Complex 13**

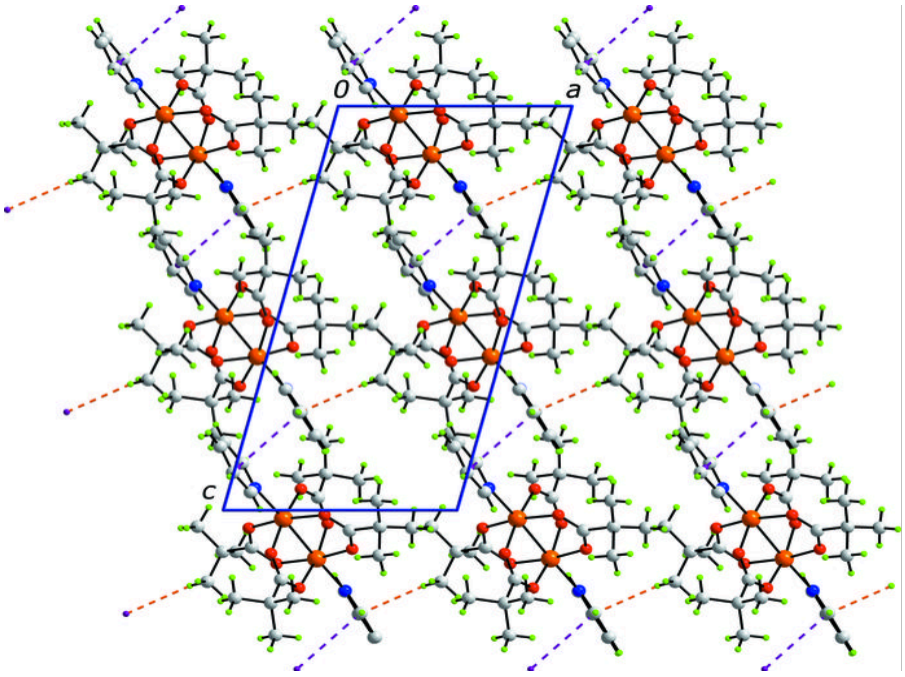

Figure 4.89 The packing pattern of **Complex 13**, viewed along the crystallographic *b*-direction.

The structure of **Complex 13** represents a monoclinic polymorph of the previously reported triclinic form [27]. Each carboxylate group is bidentate bridging and distorted octahedral geometry about each Cu(II) centre is completed by a pyridine N atom and the other Cu atom [Cu … Cu = 2.6139 (7) Å]. In the crystal, molecules are connected into supramolecular chains via π-π interactions formed by the pyridine rings

[centroid-centroid distance = 3.552 (3) Å] and these are connected into a two-dimensional array in the ac plane by C-H … π contacts. One of the tertbutyl groups is disordered over two orientations in a 0.734 (6): 0.266 (6) ratio.

From the above results, it may be concluded that the ligand-exchange reaction between $[Cu_2(p\text{-}HOC_6H_4COO)_4]$ with $[Cu_2((CH_3)_3CCOO)_4]$ (mole ratio 1:3) did not form the intended complex, $[Cu_2(p\text{-}HOC_6H_4CO_2)(CH_3)_3CCOO)_3]$ under our experimental conditions.

The crystal data and structure refinement of the crystal are shown in **Table 4.7,** while selected bond lengths, bond angles and hydrogen bonding interaction data are shown in **Table 4.8** and **Table 4.9** respectively.

Table 4.7 Crystallographic and refinement details of **Complex 13**

Empirical formula	$Cu_2C_{30}H_{46}N_2O_8$
Formula weight	689.80
Temperature	100 K
Wavelength	0.71073 Å
Crystal system, space group	Monoclinic, $P2_1/n$
Unit cell dimension	a = 9.4758 (9) Å α = 90º b = 20.0192 (12) Å β = 104.515 (3)º c = 18.6136 (10) Å γ = 90º
Volume	3418.3 (4) A^3
Z, Calculated density	4, 1.340 Mg/m^3
Absorption coefficient	1.29 mm^{-1}
F(000)	1448
Crystal size	0.32 x 0.26 x 0.16 mm
Theta range for data collection	2.2 to 28.4 º
Limiting indices ($\pm h$, $\pm k$, $\pm l$)	-11/11, -25/25, -23/23
Reflections collected / unique	28775 / 7077 [R_{int} = 0.060]
Absorption correction	Multi-scan
Refinement method	Full-matrix least-squares on F^2
Data / restraints / parameters	7077 / 404 / 12
Goodness-of-fit on F^2	1.13
Final R indices [I > 2σ(I)]	R1 = 0.058, wR2 = 0.156
$\Delta\rho_{max}$ and $\Delta\rho_{min}$	1.26 and -0.75 e $Å^{-3}$

Table 4.8 Selected bond lengths [Å] of **Complex 13**

Cu1 – O7	1.950(3)	Cu2 – O6	1.962(3)
Cu1 – O1	1.956(3)	Cu2 – O4	1.968(3)
Cu1 – O3	1.976(3)	Cu2 – O8	1.976(3)
Cu1 – O5	1.987(3)	Cu2 – O2	1.978(3)
Cu1 – N1	2.157(3)	Cu2 – N2	2.157(3)

Table 4.9 Hydrogen bonds [Å and deg.] of **Complex 13**

D – H … A	D - H	H…A	D…A	D – H…A
C3–H3c…*Cg1*^{i}	0.98	2.90	3.609(7)	130
C19b – H19f…Cg2^{ii}	0.98	2.644	3.554(19)	154

Symmetry codes: (i) x- 1, y, z; (ii) x + 1, y, z. Cg1 and Cg2 are the centroids of the N1, C21 – C25 and N2, C26 – C30 rings respectively.

4.3.4 [Cu_2(p-HOC_6H_4COO)($CH_3(CH_2)_3CH(C_2H_5)COO)_3$]

The ligand-exchange reaction between [Cu_2(*p*-$HOC_6H_4COO)_4$] and [$Cu_2(CH_3(CH_2)_3CH(C_2H_5)COO)_4$] (mol ratio =1:3) gave a green solid (**Complex 14**) which deposited out of the hot reaction mixture. It was soluble in all organic solvents.

The results of elemental analyses (C, 52.4%; H, 7.5%) are in good agreement with that calculated for $Cu_2C_{33}H_{60}O_{12}$ (formula weight, 775.9 g mol^{-1}; C, 51.0%; H, 7.7%).

The **FTIR** spectrum (**Figure 4.90**) is different from those of the starting materials (**Figure 4.52** and **Figure 4.91**), indicating a reaction between [Cu_2(*p*-$HOC_6H_4COO)_4$] and [$Cu_2(CH_3(CH_2)_3CH(C_2H_5)COO)_4$] occurred to form a product. It shows the presence of all of the expected functional groups as previously discussed, including two sharp peaks at 2971 cm^{-1} and 2932 cm^{-1} assigned to the aliphatic carbon chain. The ΔCOO value is 161 cm^{-1}, suggesting bridging carboxylate ligands.

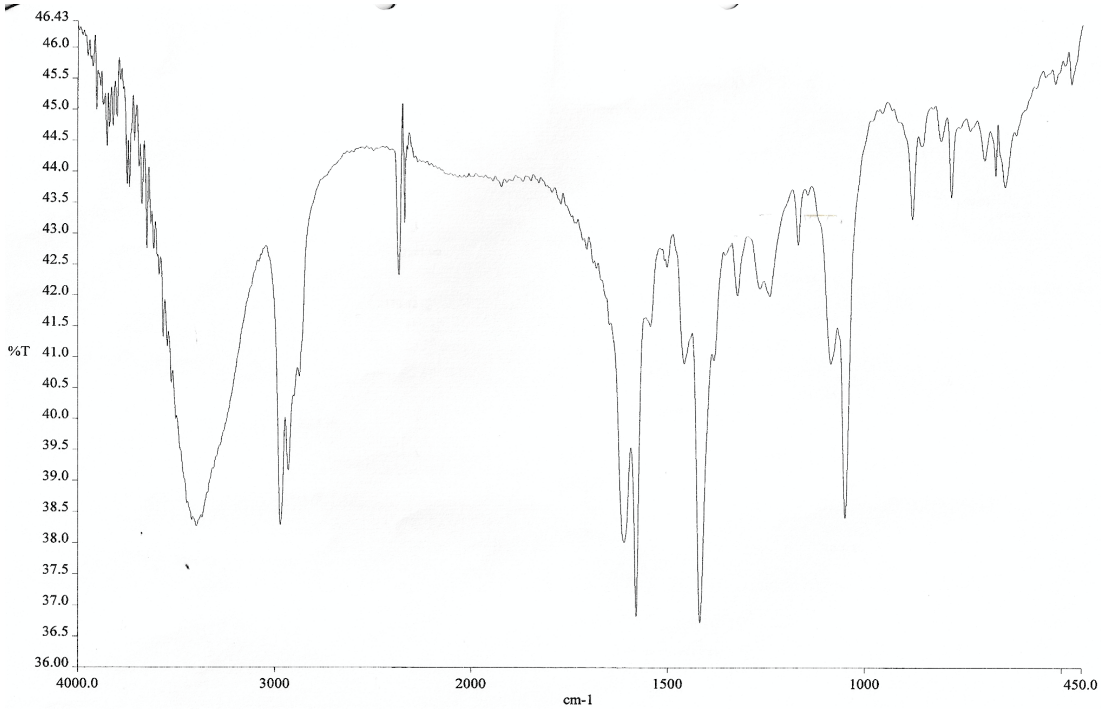

Figure 4.90 FTIR of **Complex 14**

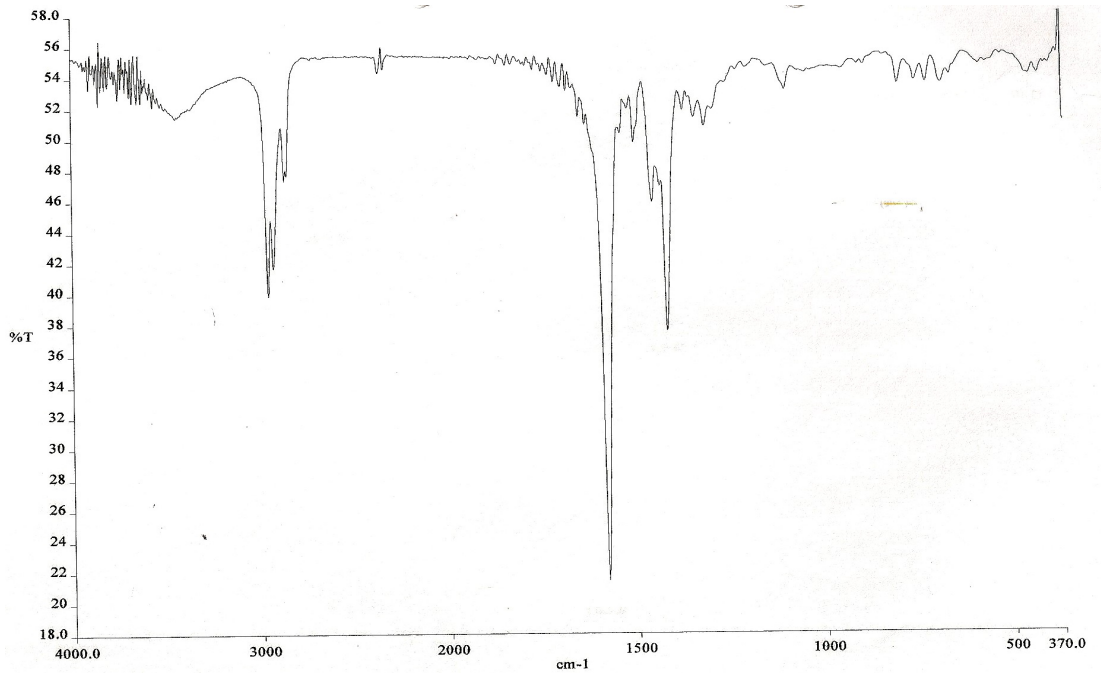

Figure 4.91 FTIR of $[Cu_2(CH_3(CH_2)_3CH(C_2H_5)COO)_4]$ (starting material)

The **UV-vis** spectra of the complex in the solid state (**Figure 4.92(a)**) and as a solution in methanol (**Figure 4.92(b)**) show a broad *d-d* band at 682 nm and 675 nm

(ε_{max}= 946 $M^{-1}cm^{-1}$) respectively. These suggest a dimeric complex with square pyramidal Cu(II) centres in both the solid state and in solution.

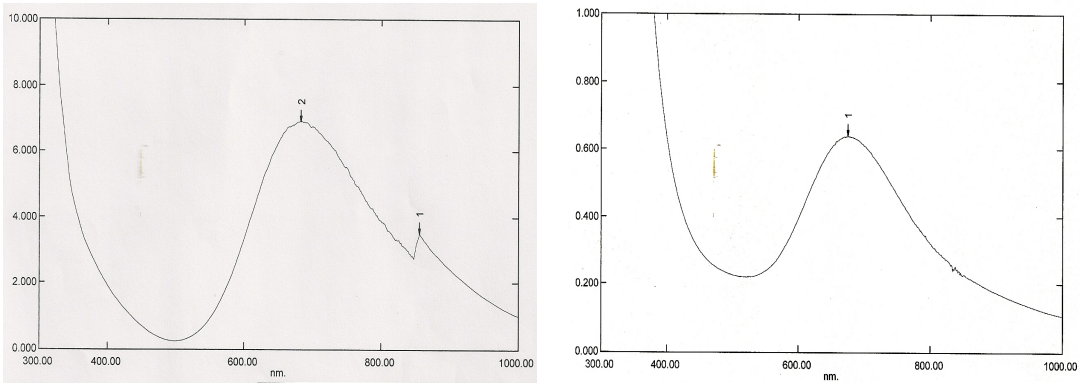

(a) (b)

Figure 4.92 UV-vis of **Complex 14** in (a) solid; (b) solution

Combining the above results, **Complex 14** is proposed to have the structural formula $[Cu_2(p\text{-}HOC_6H_4COO)(CH_3(CH_2)_3CH(C_2H_5)COO)_3(H_2O)_2].CH_3CH_2OH$ (**Figure 4.93**). The formula agrees with the chemical formula $Cu_2C_{33}H_{60}O_{12}$ from the elemental analyses, bridging carboxylates as inferred from FTIR, and binuclear complex with square pyramidal geometry at Cu(II) centre as suggested from UV-vis. Therefore, the complex is the expected product from the reaction, and its yield was 23.7%.

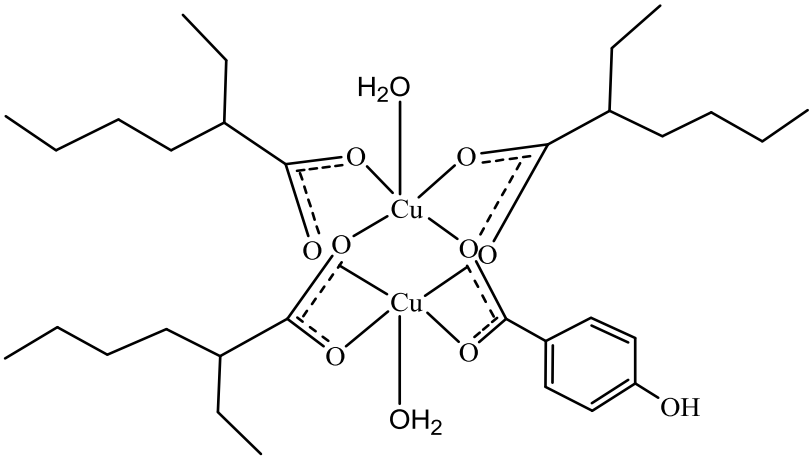

Figure 4.93 Proposed structural formula of **Complex 14 (**CH_3CH_2OH solvates are not shown; two dimers are shown to show square pyramidal Cu(II) centres)

The value of $\mathbf{E_g}$ for **Complex 14,** calculated as before from the onset λ value of 542 nm, is 2.29 eV. This is comparable to **Complex 10** ([Cu_2(*p*-HOC_6H_4COO)(CH_3CH=$CHCOO)_3(C_5H_5N)_2$].CH_3CH_2OH; 2.31 eV) and Complex 11 (Cu_2(*p*-HOC_6H_4COO)($CH_3(CH_2)_7CH$=$CH(CH_2)_7COO)_3(H_2O)_2$; 2.29 eV). It is noted that these complexes have the same arylcarboxylate:alkylcarboxylate ratio (1:3).

The **TGA** thermogram (**Figure 4.94**) shows that the decomposition temperature for **Complex 14** is 220°C. Thus, it is as thermally stable as the **Complex 11** ([Cu_2(*p*-HOC_6H_4COO)($CH_3(CH_2)_7CH$=$CH(CH_2)_7COO)_3$]; T_{dec} = 201°C). The results seem to suggest that unsaturated alkylcarboxylate ligands formed less thermally stable complexes compared to saturated alkylcarboxylate ligands.

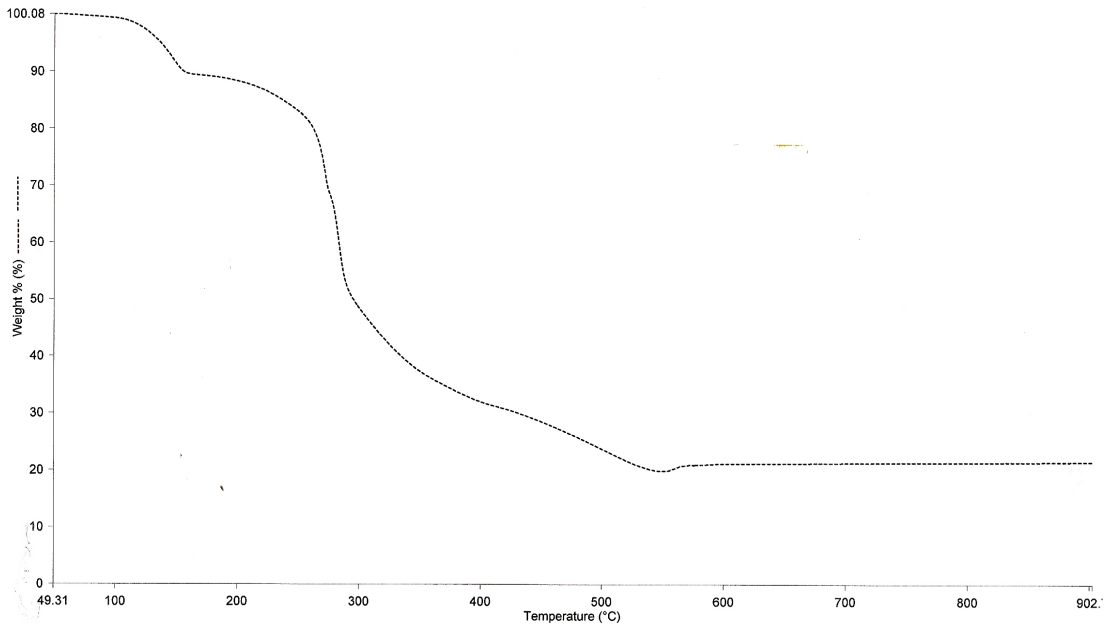

Figure 4.94 TGA of **Complex 14**

The thermogram also shows that the complex decomposed in two steps. The initial weight loss of 10% at 103°C is assigned to the evaporation of two axially-coordinated H_2O molecules and non-coordinated H-bonded CH_3CH_2OH molecule

(expected, 10.6%). The next weight loss of 69% at 220°C is attributed to the decomposition of all of the carboxylate ligands (expected, 73%).

The amount of residue at temperatures above 570°C is 21%, and assuming that it is pure CuO, the estimated formula mass of **Complex 14** is 761 g mol^{-1}. This is in good agreement with the value calculated from the proposed chemical formula (775.9 g mol^{-1}).

The **DSC** scan (**Figure 4.95**) shows a broad endothermic peak at 89°C (ΔH = +11.9 kJ mol^{-1}), assigned to the breaking of H-bond between CH_3CH_2OH and –OH group of the arylcarboxylate ligand (**Figure 4.93**). The two endotherms at 217°C (ΔH = +33.7 kJ mol^{-1}) and 263°C (ΔH = +52.6 kJ mol^{-1}), are assigned to the decomposition of the ligands as they coincide with its decomposition temperature from TGA (T_d = 220°C).

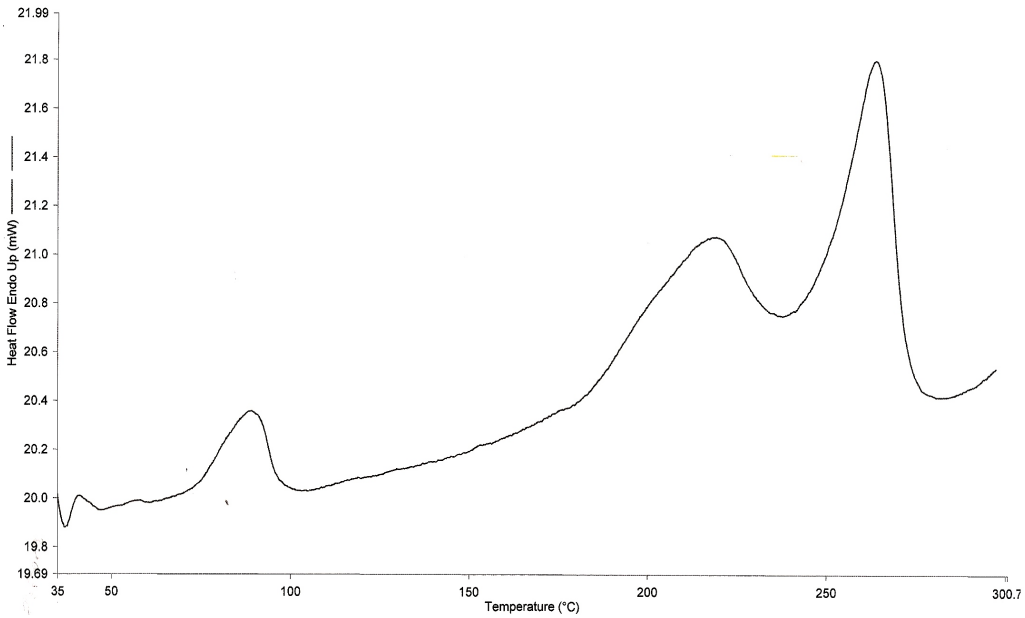

Figure 4.95 DSC of **Complex 14**

The value of μ_{eff}, calculated as before (χ_g, 0.189 x 10^{-5}c.g.s.; χ_m, 1.40 x 10^{-3}c.g.s.; χ_{dia}, -3.10 x 10^{-4} c.g.s; and χ_m^{corr} 1.71 x 10^{-3} c.g.s), is 2.03 B.M. at 298 K. The 2J value is

-319 cm^{-1}. These suggest a strong antiferromagnetic interaction between the two Cu(II) centres, which is as expected based on the proposed structural formula.

The **CV** voltammogram (**Figure 4.96**), scanned cathodically in the potential range -1.6 V to +1.6 V, shows two overlapping reduction peaks at -0.87 V and -1.07, and two overlapping oxidation peaks at +0.36 V and +0.54 V.

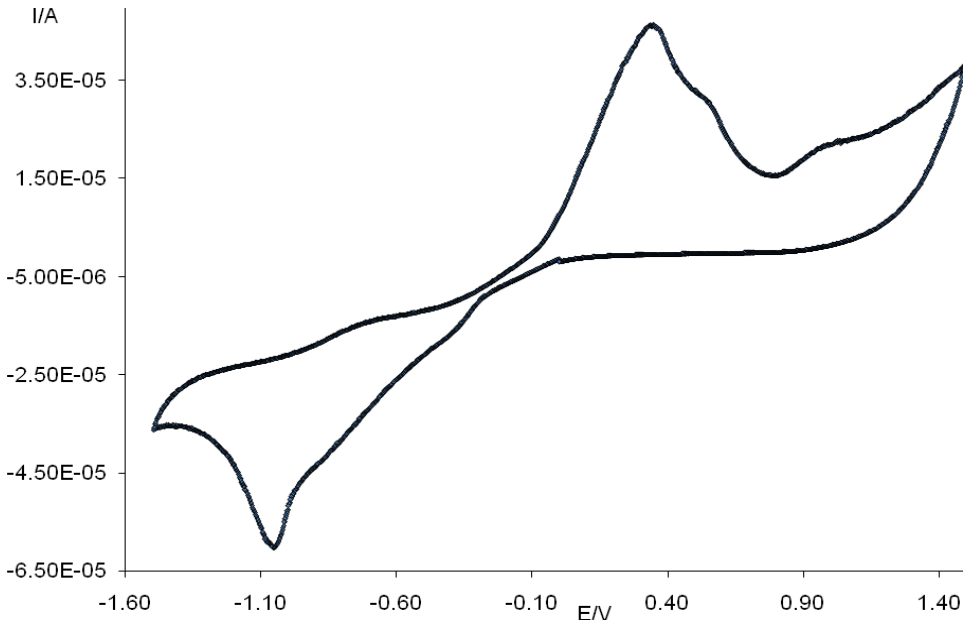

Figure 4.96 CV of **Complex 14**

The cathodic peak at -0.87 V is assigned to the reduction of the binuclear [Cu(II)Cu(II)] complex to mixed-valence [Cu(II)Cu(I)] complex, which was further reduced to monovalence [Cu(I)Cu(I)] complex at -1.07 V. The dinuclear [Cu(I)Cu(I)] complex formed was then reoxidized to the mixed-valence [Cu(II)Cu(I)] complex at +0.36 V and then to the dinuclear [Cu(II)Cu(II)] complex at +0.54 V. The redox processes are shown in **Scheme 4.4**.

$$[Cu(II)Cu(II)] \underset{+0.36\ V}{\overset{-0.87V}{\rightleftharpoons}} [Cu(II)Cu(I)] \underset{+0.54\ V}{\overset{-1.07V}{\rightleftharpoons}} [Cu(I)Cu(I)]$$

Scheme 4.4 Redox process of **Complex 14**

The lower redox potentials compared to **Complex 11** (E_c = - 1.27 V, E_a = + 0.83 V) may be due to the smaller insulating layer (shorter and branched carbon chains in **Complex 14**), as previously proposed.

The values of ΔE and I_{pa}/I_{pc} ratio for [Cu(II)Cu(II)]–[Cu(II)Cu(I)] couple are 1230 mV and 1.1 respectively, while those for [Cu(II)Cu(I)]–[Cu(I)Cu(I)] couple are 1610 mV and 0.5 respectively. Thus the results show that **Complex 14** undergo quasireversible redox reactions, and that the mixed-valence [Cu(II)Cu(I)] complex was chemically stable while the monovalent [Cu(I)Cu(I)] complex was chemically unstable.

4.3.5 $[Cu_2(p\text{-}HOC_6H_4COO)(CH_3(CH_2)_7CH((CH_2)_5CH_3)COO)_3]$

The ligand-exchange reaction between $[Cu_2(p\text{-}HOC_6H_4COO)_4]$ and $[Cu_2(CH_3(CH_2)_7CH((CH_2)_5CH_3)COO)_4]$ (mol ratio =1:3) formed two products: a dark turquoise powder and a green liquid.

(a)Dark turquoise powder

The dark turquoise powder (**Complex 15)** was obtained as the residue from the hot reaction mixture. It was soluble in methanol, ethanol, tetrahydrofuran, chloroform and toluene, sparingly soluble in dimethylformamide and acetone, and insoluble in dimethylsulfoxide.

The results of **elemental analyses** (C, 62.0%; H, 9.4%) are in good agreement with those calculated for $Cu_2C_{55}H_{102}O_{11}$ (formula weight, 1065.1 g mol^{-1}; C, 62.0%; H, 9.6%).

The **FTIR** spectrum (**Figure 4.97**) is different from those of the starting materials (**Figure 4.52** and **Figure 4.98**). This indicates that a reaction occurred between $[Cu_2(p\text{-}HOC_6H_4COO)_4]$ and $[Cu_2(CH_3(CH_2)_7CH((CH_2)_5CH_3)COO)_4]$ under the stated condition. The spectrum also shows the presence of all of the expected functional

groups as previously discussed, and the ΔCOO value of 166 cm^{-1} suggests bridging carboxylate ligands.

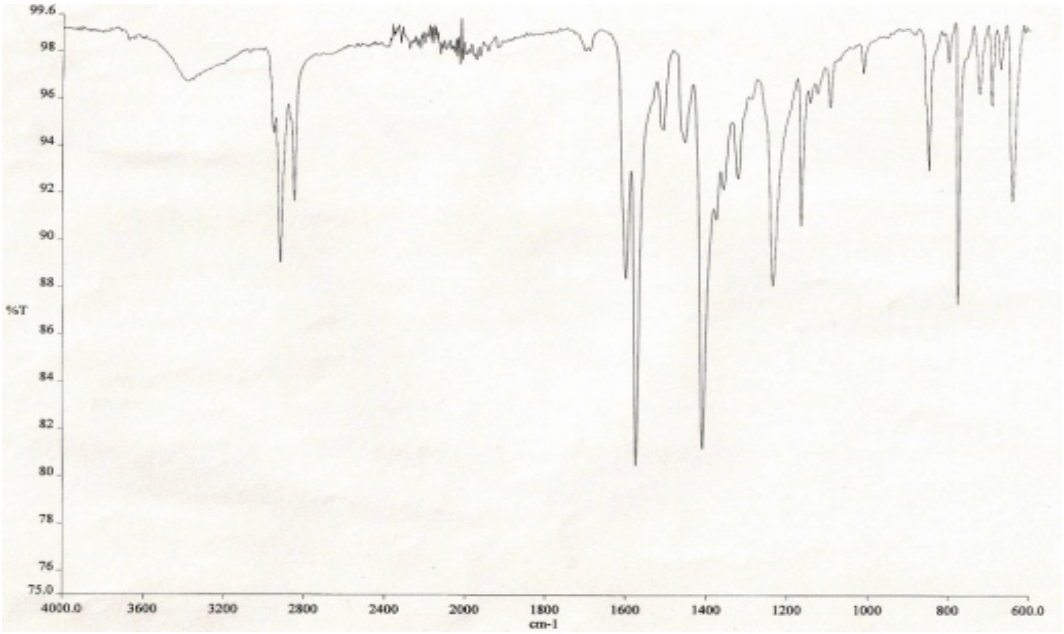

Figure 4.97 FTIR spectrum of **Complex 15**

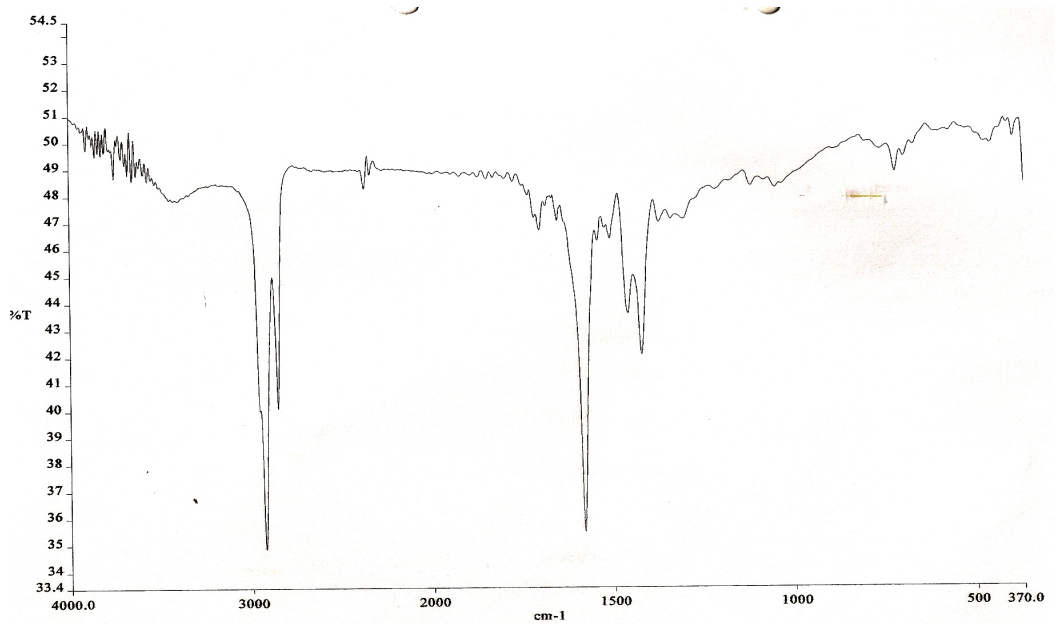

Figure 4.98 FTIR spectrum of $[Cu_2(CH_3(CH_2)_7CH((CH_2)_5CH_3)COO)_4]$ (starting material)

Its **UV-vis** spectra in the solid state (**Figure 4.99(a)**) and as a solution in methanol (**Figure 4.99(b)**), show a broad *d-d* band at 670 nm and 668 nm (ε_{max} = 618 $M^{-1}cm^{-1}$) respectively, suggesting a dimeric complex with square-pyramidal Cu(II) centres.

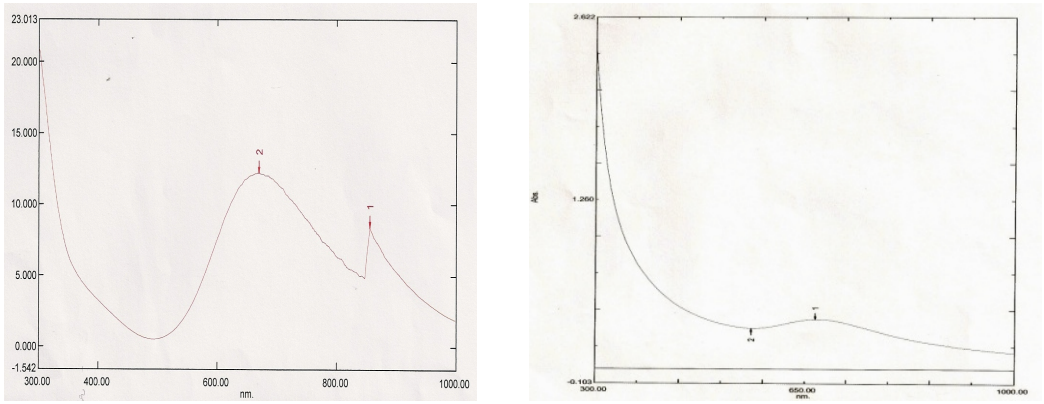

(a) (b)

Figure 4.99 UV-vis of **Complex 15** (a) solid; (b) solution

Combining the above results, **Complex 15** is proposed to have the structural formula $[Cu_2(p\text{-}HOC_6H_4COO)(CH_3(CH_2)_7CH((CH_2)_5CH_3)COO)_3(H_2O)_2]$ (**Figure 4.100**). The formula agrees with the chemical formula $Cu_2C_{55}H_{104}O_{11}$ from the elemental analyses, shows bridging carboxylates as inferred from FTIR, and binuclear complex with square pyramidal geometry at Cu(II) centre as suggested from UV-vis. Therefore, **Complex 15** is the expected product from the reaction, and its yield was 45.4%.

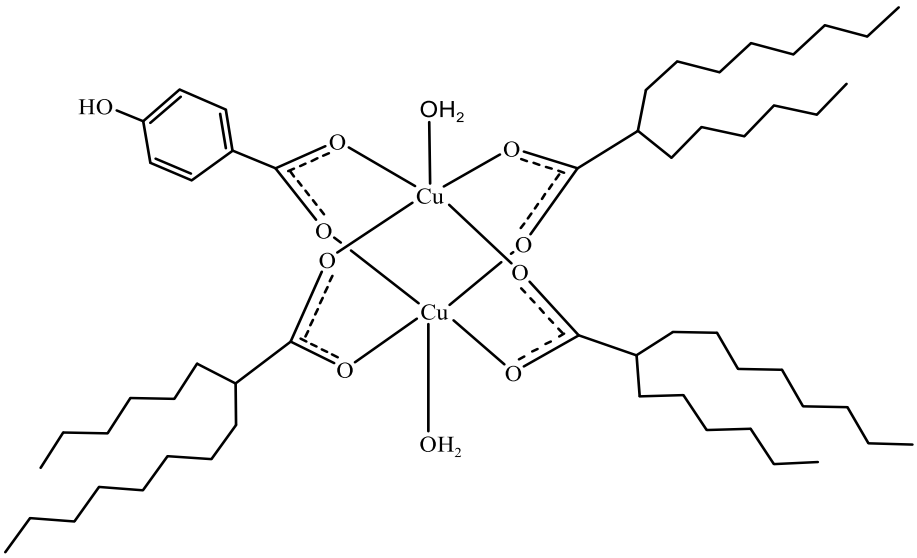

Figure 4.100 Proposed structural formula of **Complex 15**

The optical **band gap** energy for **Complex 15,** calculated as before from the onset λ value of 570 nm, is 2.18 eV. The value was lower than that of **Complex 10**, **Complex 11** and **Complex 14** (2.31 eV, 2.29 eV and 2.29 eV respectively). The results seem to suggest that a long and branched saturated alkylcarboxylates ligand formed copper(II) mixed-carboxylate complexes with lower band gaps. A possible explanation is that these ligands, which are stonger bases compared to the corresponding linear ligands, form stronger Cu-OOCR coordination bonds, which then increases the HOMO energy ($d_{x^2-y^2}$ orbital).

The **TGA** thermogram (**Figure 4.101**) shows that the decomposition temperature for **Complex 15** is 225°C. Thus, it is as thermally stable as **Complex 14** ($[Cu_2(p\text{-}HOC_6H_4COO)(CH_3(CH_2)_3CH(C_2H_5)COO)_3(H_2O)_2].C_2H_5OH$; T_{dec} = 220°C). This supports the previous conclusion that the thermal stability of these mixed-carboxylate complexes is independent on the chain length of the alkylcarboxylate ligand used.

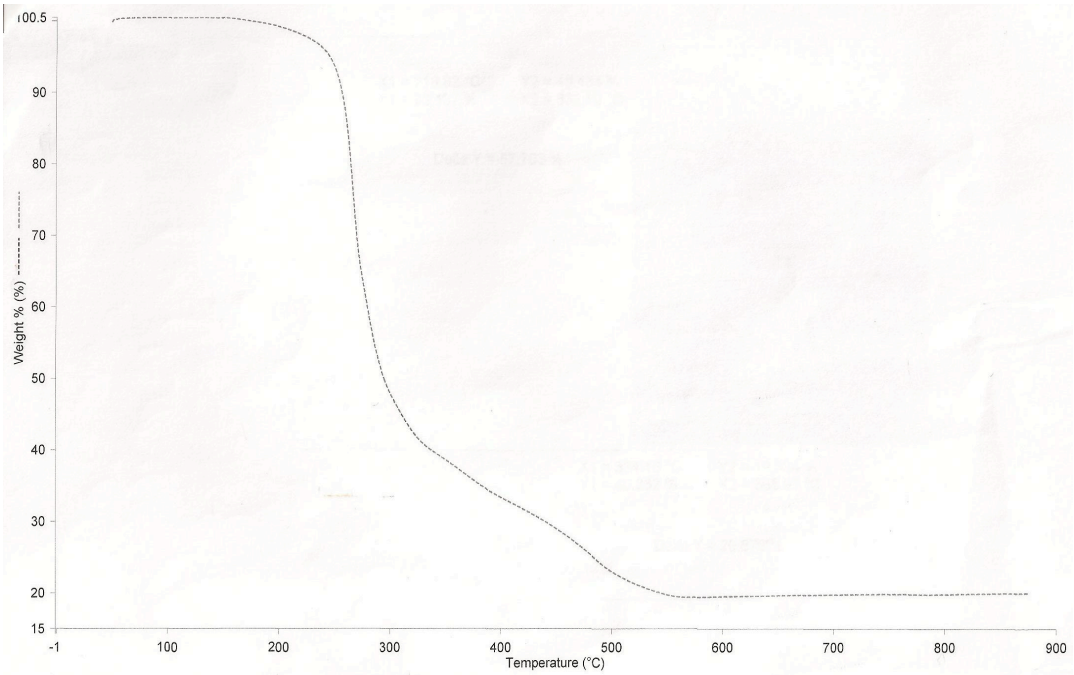

Figure 4.101 TGA of **Complex 15**

The thermogram also shows a total weight loss of 80.7% at 225^{o}C attributed to the decomposition of all carboxylates ligand (expected, 84.7). The amount of residue at temperatures above 569^{o}C is 19.3%, while the expected value, assuming that the residue is pure CuO, is 14.9%. Thus, the complex may be said to undergo incomplete decomposition at this temperature.

The **DSC** scan (**Figure 4.102**) shows a weak endotherm at onset temperature 146^{o}C (ΔH = +1.5 kJ mol^{-1}). Also observed is a sharp endothermic peak at 260^{o}C (ΔH = +170.9 kJ mol^{-1}) which is above its decomposition temperature from TGA (220^{o}C). It also shows a very broad endotherm with a maximum below room temperature, suggesting some bond breaking processes occurring before the complex decomposed.

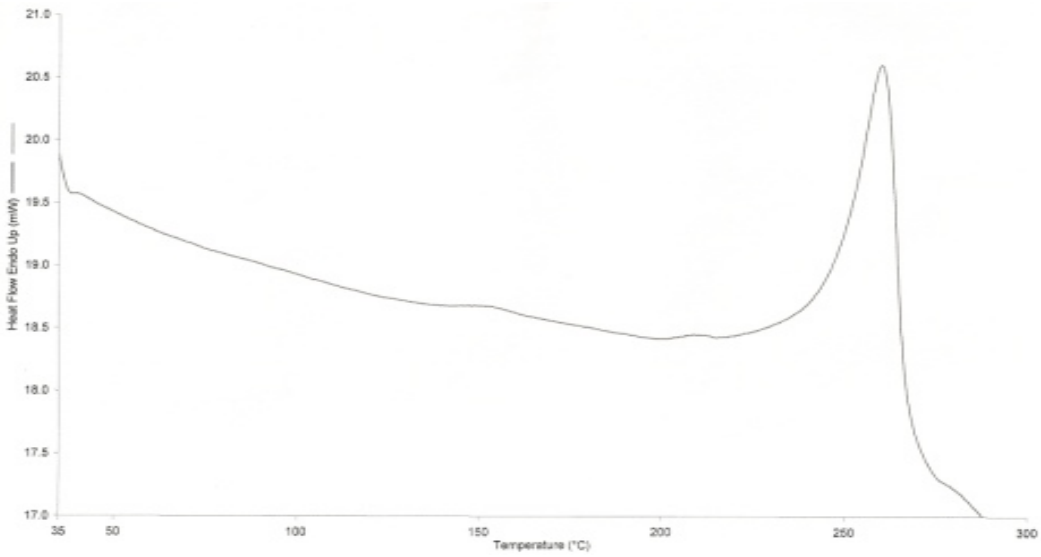

Figure 4.102 DSC of **Complex 15**

The value of μ_{eff}, calculated as before (χ_g, 0.152 x 10^{-5}c.g.s.; χ_m, 1.57 x 10^{-3}c.g.s.; χ_{dia}, -5.61 x 10^{-4} c.g.s; and χ_m^{corr} 2.13 x 10^{-3} c.g.s), is 2.26 B.M. at 298 K. The value of 2J is -232 cm^{-1}. These are comparable with those of **Complex 14** ($[Cu_2(p\text{-}HOC_6H_4COO)(CH_3(CH_2)_3CH(C_2H_5)COO)_3(H_2O)_2].CH_3CH_2OH$; 2.03 B.M.; -319 cm^{-1}), and seems to suggest that the magnetic properties of these mixed-carboxylate complexes are independent on the chain length of the alkylcarboxylate ligands used. The **CV** voltammogram (**Figure 4.103**), scanned cathodically in the potential range -2.2 V to +2.0 V, shows a reduction peak at -1.29 V and an oxidation peak at +0.67 V. The values of ΔE and I_{pa}/I_{pc} ratio for [Cu(II)Cu(II)]–[Cu(I)Cu(I)] couple are 1960 mV and 0.3. These are comparable with **Complex 11** ($[Cu_2(p\text{-}HOC_6H_4COO)(CH_3(CH_2)_7CH{=}CH(CH_2)_7COO)_3]$ (E_c = -1.27 V; E_a = +0.83 V; ΔE = 2100 mV; I_{pa}/I_{pc} = 0.6), and may be similarly assigned and explained. The CV results seem to suggest that the redox properties of these mixed-carboxylate complexes are independent on the degree of saturation of the alkylcarboxylate ligands used.

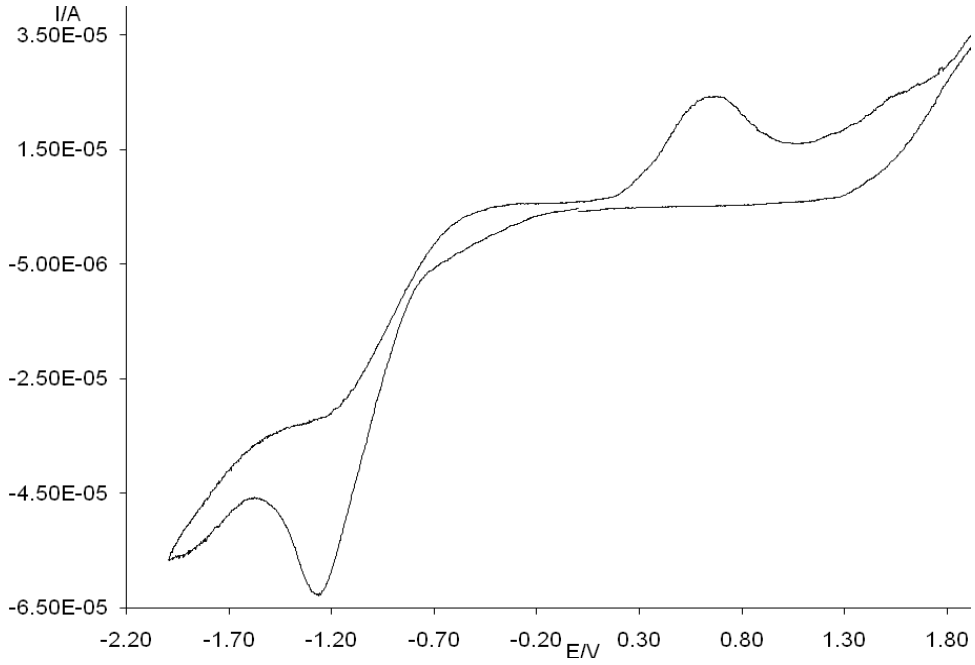

Figure 4.103 CV of **Complex 15**

$$[Cu(II)Cu(II)] \underset{+0.67\ V}{\overset{-1.29\ V}{\rightleftharpoons}} [Cu(I)Cu(I)]$$

(b) Green liquid

The green liquid **(Complex 16)** was obtained after the solvent was completely removed from the filtrate. The result of elemental analyses (C, 67.8%; H, 11.0%) agrees with the chemical formula of $Cu_2C_{64}H_{124}O_8$ or $[Cu_2(CH_3(CH_2)_7CH((CH_2)_5CH_3)COO)_4]$ (formula weight, 1148.8 g mol^{-1}; C, 66.9%; H, 10.9%) [28]. Therefore, it is not the expected complex from the reaction, and was not further analysed and characterised

4.3.6 Summary

The ligand-exchange reaction was successfully used to prepare $[Cu_2(p\text{-}HOC_6H_4COO)(RCOO)_3]$ where R = $CH_3(CH_2)_7CH{=}CH(CH_2)_7$ (**Complex 11**), $CH_3(CH_2)_3CH(C_2H_5)$ (**Complex 14**), and $CH_3(CH_2)_7CH(CH_2)_5$ (**Complex 15**), but not for $[Cu_2(p\text{-}HOC_6H_4COO)((CH_3)_3CCOO)_3]$.

Except for **Complex 12**, (C_5H_5N)([Cu_2(*p*-HOC_6H_4COO)((CH_3)$_3CCOO$)$_4$]), these complexes were dinuclear with square pyramidal geometry at the two Cu(II) centres. **Complex 12** was dinuclear with tetrahedral geometry at the Cu(II) centres.

The thermal stability of these complexes increases in the following order: **Complex 12** < **Complex 11** < **Complex 14**, **Complex 14**. **Complex 12** is strongly ferromagnetic and showed irreversible redox reaction, while **Complex 13** and **Complex 14** are antiferromagnetic and showed quasireversible redox reaction. The analytical results are summarized in **Table 4.10**.

Table 4.10 Complexes from the ligand-exchange reaction

	Complex 11	**Complex 12**	**Complex 14**	**Complex 15**
Structural formula*	[$Cu_2L(R)_3(H_2O)_2$]	[$Cu_2L(R')_3$]	[$Cu_2L(R'')_3(H_2O)_2$]	[$Cu_2L(R''')_3(H_2O)_2$]
ΔCOO/ cm^{-1}	159 (bridging)	127 (chelating) 225 (monodentate)	161 (bridging)	166 (bridging)
λ_{max}/nm solid	#	#	682	670
solution (ε_{max}/ $M^{-1}cm^{-1}$)	690 (452)	-	675 (946)	668 (618)
T_{dec}/°C	201	170	220	225
μ_{eff} (2J)	#	5.03 (+125) ferromagnetic	2.03 (-319) antiferromagnetic	2.26 (-232) antiferromagnetic
E_{pc}/V E_{pa}/V (I_{pc}/I_{pa})	-1.27 +0.83 (0.6)	-0.19; -0.86; -1.02 -0.19; +0.09 (#)	-0.87; -1.07 +0.36; +0.54 (1.1, 0.5)	-1.29 +0.67 (0.3)

* solvates are not shown; R = $CH_3(CH_2)_7CH{=}CH(CH_2)_7COO$; R' = $(CH_3)_3CCOO$; R'' = $CH_3(CH_2)_3CH(C_2H_5)COO$; R''' = $CH_3(CH_2)_7CH(CH_2)_5COO$; # Not applicable

4.4 Conversion to Ionic Complex

Complex 11 $[Cu_2(p\text{-}HOC_6H_4COO)(CH_3(CH_2)_7CH{=}CH(CH_2)_7COO)_3]$ was chosen to react with KOH (mol ratio = 1:1) in an attempt to form the corresponding ionic complex, $K[Cu_2(p\text{-}OC_6H_4COO)(CH_3(CH_2)_7CH{=}CH(CH_2)_7COO)_3]$. The product obtain was a pale green powder (**Complex 17**) from the hot reaction mixture. It was partially soluble in all common organic solvents.

The product(s) from the filtrate was not isolated and characterized as the colour of the solution was colourless, inferring absence of Cu(II) complex(es).

The results from the **elemental analyses** give the C:H ratio equals 6.0:1.0, which agrees with the chemical formula $Cu_2C_{36}H_{72}O_8$ (formula weight = 760.04 g mol^{-1}; calculated C:H ratio = 5.9:1.0).

The **FTIR** spectrum (**Figure 4.104**) is different from those of the starting material (**Figure 4.74**). This suggests $[Cu_2(p\text{-}HOC_6H_4COO)(CH_3(CH_2)_7CH{=}CH(CH_2)_7COO)_3]$ reacted with KOH. Additionally, the spectrum shows the presence of all of the expected functional groups as previously discussed. The ΔCOO value is 134 cm^{-1}, suggesting bridging carboxylate ligands. The 'clean' spectrum indicates the complex adopt the symmetrical *trans*- structure.

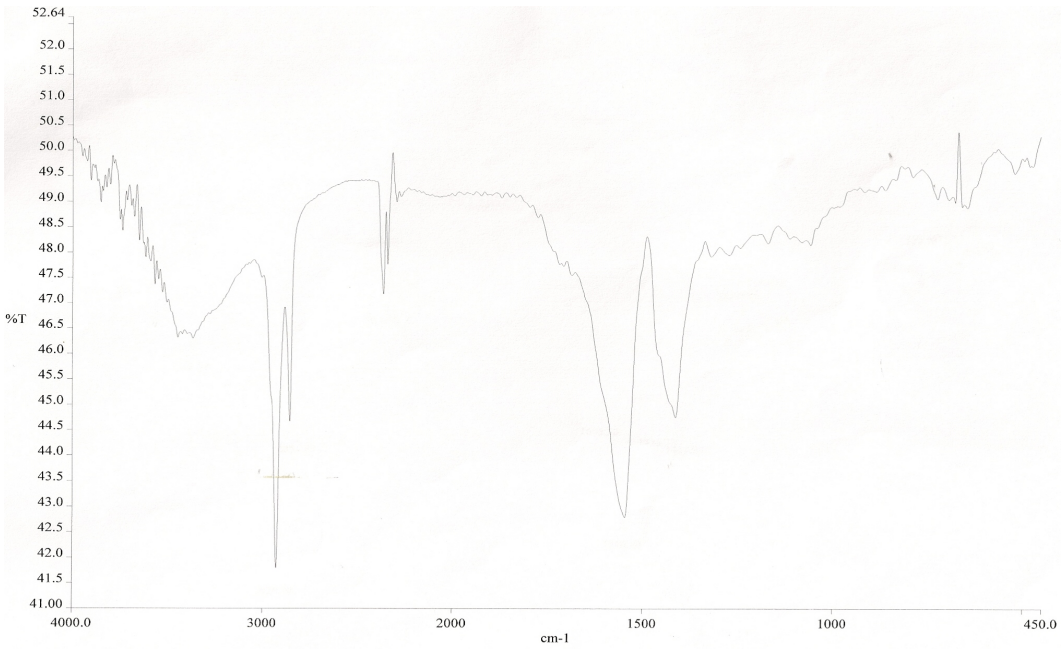

Figure 4.104 FTIR spectrum of Complex 17

Its **UV-vis** spectrum in methanol (in the presence of a few drops of acetic acid; **Figure 4.105**) shows a broad *d-d* band at 644 nm (ε_{max}= 8.76 x 10^2 $M^{-1}cm^{-1}$). This suggests a dimeric complex with square-pyramidal Cu(II) centres.

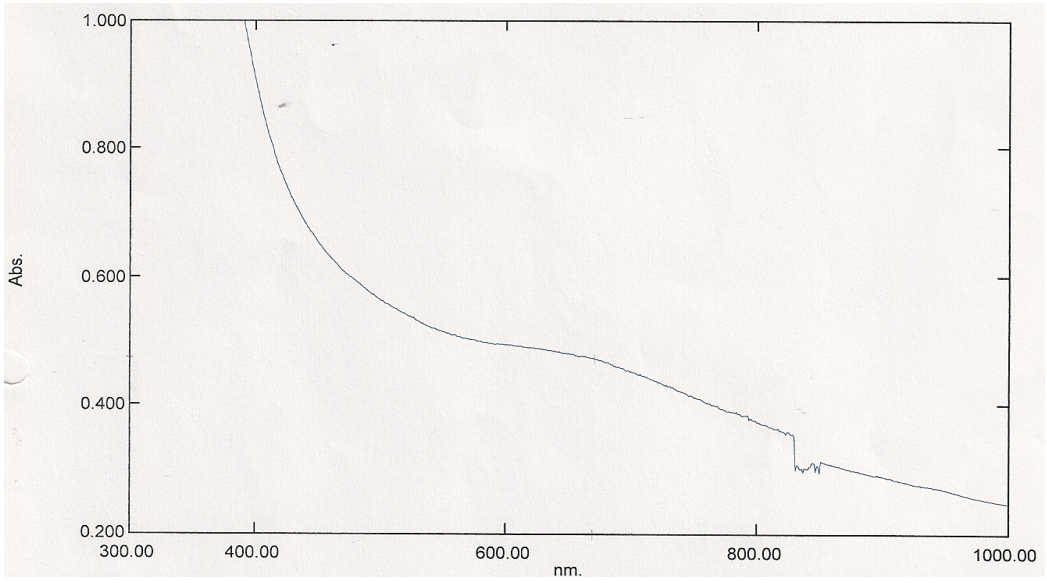

Figure 4.105 UV-vis spectrum of Complex 17 in methanol

Combining the above results, **Complex 17** is proposed to have the structural formula $[Cu_2(CH_3(CH_2)_7CH{=}CH(CH_2)_7COO)_2(OH)_2(H_2O)_2]$ (**Figure 4.106)**. The formula agrees with $Cu_2C_{36}H_{72}O_8$ from the elemental analyses, shows bridging carboxylates with *trans*-complex as inferred from FTIR, and square pyramidal Cu(II) from UV-vis. Thus, its yield was 16.9%, but it is **not** the intended ionic complex from the reaction.

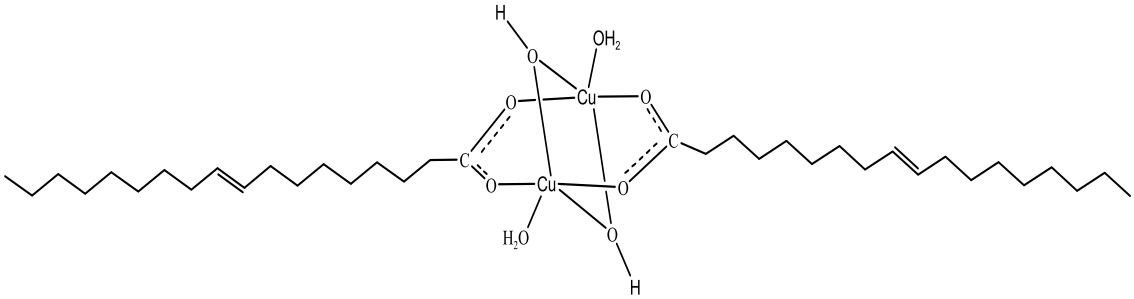

Figure 4.106 Proposed structural formula of **Complex 17**

The **TGA** thermogram (**Figure 4.107**) shows that the decomposition temperature for Complex 17 is 229°C. Thus, it is slightly more thermally stable than its "precursor" (**Complex 11;** $[Cu_2(p\text{-}HOC_6H_4COO)(CH_3(CH_2)_7CH{=}CH(CH_2)_7COO)_3]$; T_{dec} = 201°C).

The thermogram also shows an initial slow weight loss of 4.5% at 105°C is assigned the evaporation of weakly coordinated H_2O at the axial positions (expected, 4.7%). A second weight loss of 5.0% at 182°C is assigned to loss of two -OH ligands (expected, 4.5%). The total weight loss of 63.4% at 229°C is assigned to the decomposition of $CH_3(CH_2)_7CH{=}CH(CH_2)_7COO$ (expected, 74.1%). The lower than expected valuea may be due to incomplete decomposition of involatile polymer(s) formed during heating.

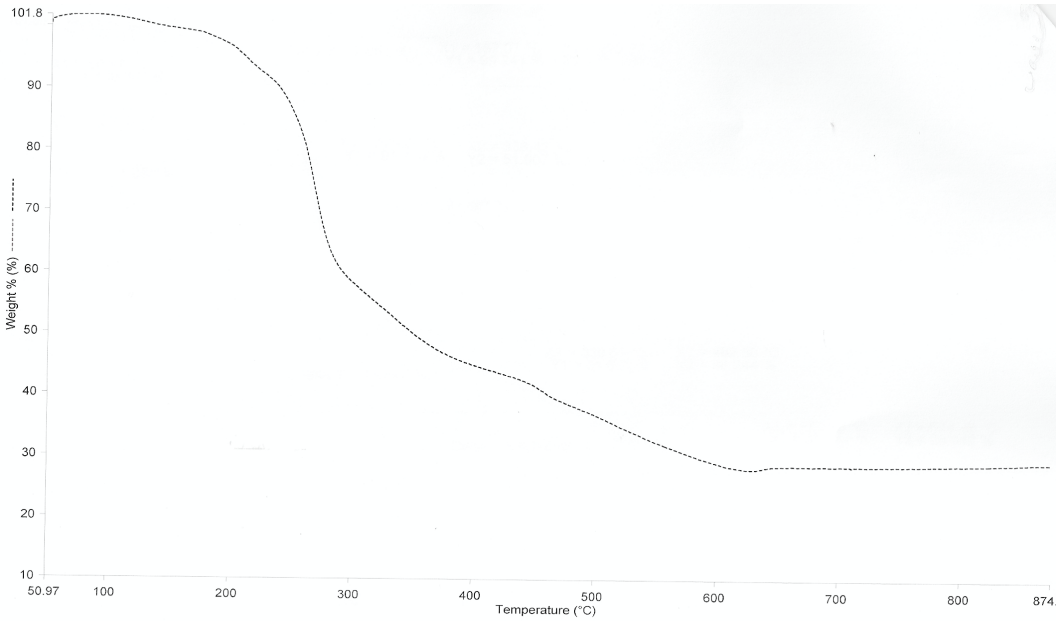

Figure 4.107 TGA of **Complex 17**

The **DSC** scan (**Figure 4.108**) shows a broad endotherm at 70°C (ΔH = +258.8 kJ mol^{-1}), assigned to the breaking of van der Waals bond between the alkyl chains, Cu-OH_{axial} bond, Cu-OOCR bond, and C=C bond (**Figure 4.106)**, and another broad endotherm at onset temperature of 222°C (ΔH = +45.2 kJ mol^{-1}) is probably due to the decomposition of the $CH_3(CH_2)_7CH=CH(CH_2)_7COO$ ligand (from TGA).

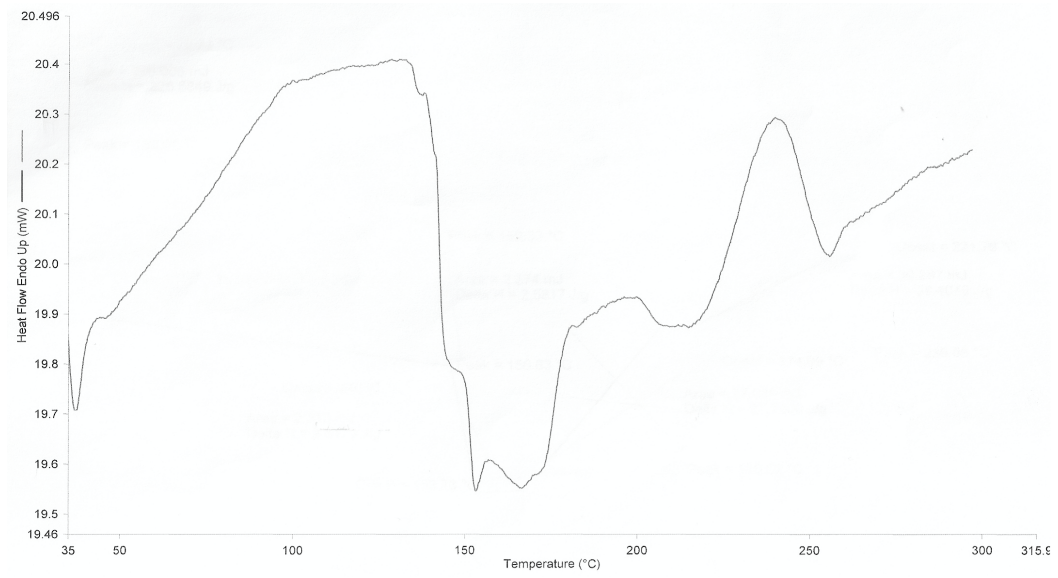

Figure 4.108 DSC of **Complex 17**

To summarise, **Complex 11** formed from the ligand-exchange reaction, was not successfully converted to the corresponding ionic complex.

4.5 Photoluminescence Spectroscopy

The photoluminesce spectra (PL) were recorded for all of the above complexes after excitation at 325 nm in the solid state, except for Complex 1, which was excited at 267 nm in solution. However, only the following complexes showed emission peak(s):

Complex 1 ($K[Cu(CH_3CH{=}CHCOO)(OH)_2(H_2O)].H_2O$)

Complex 2 ($K_2[Cu_2(p\text{-}OC_6H_4COO)_2(CH_3CH{=}CHCOO)_2(H_2O)_2]$)

Complex 3 ($K[Cu_2(p\text{-}OC_6H_4COO)(CH_3CH{=}CHCOO)_3(CH_3CH_2OH)_2]$)

Complex 4 ($K[Cu_2(p\text{-}OC_6H_4COO)(CH_3CH{=}CHCOO)_3].2H_2O$)

Complex 6 ($K[Cu_2(p\text{-}OC_6H_4COO)(CH_2{=}C(CH_3)COO)_3(CH_3CH_2OH)(CH_2{=}C(CH_3)COOH)]$)

Complex 7 ($K_3[Cu_2(p\text{-}OC_6H_4COO)_3(CH_2{=}C(CH_3)COO)(CH_3CH_2OH)_2].H_2O$)

Complex 8 ($[Cu_2(p\text{-}HOC_6H_4COO)_3(CH_3CH{=}CHCOO)(C_5H_5N)].C_5H_5N$)

Complex 15 ($[Cu_2(p\text{-}HOC_6H_4COO)(CH_3(CH_2)_7CH((CH_2)_5CH_3)COO)_3(H_2O)_2]$).

The PL spectra are shown in **Figure 4.109(a)-(h)**, and the corresponding data are shown in **Table 4.11**.

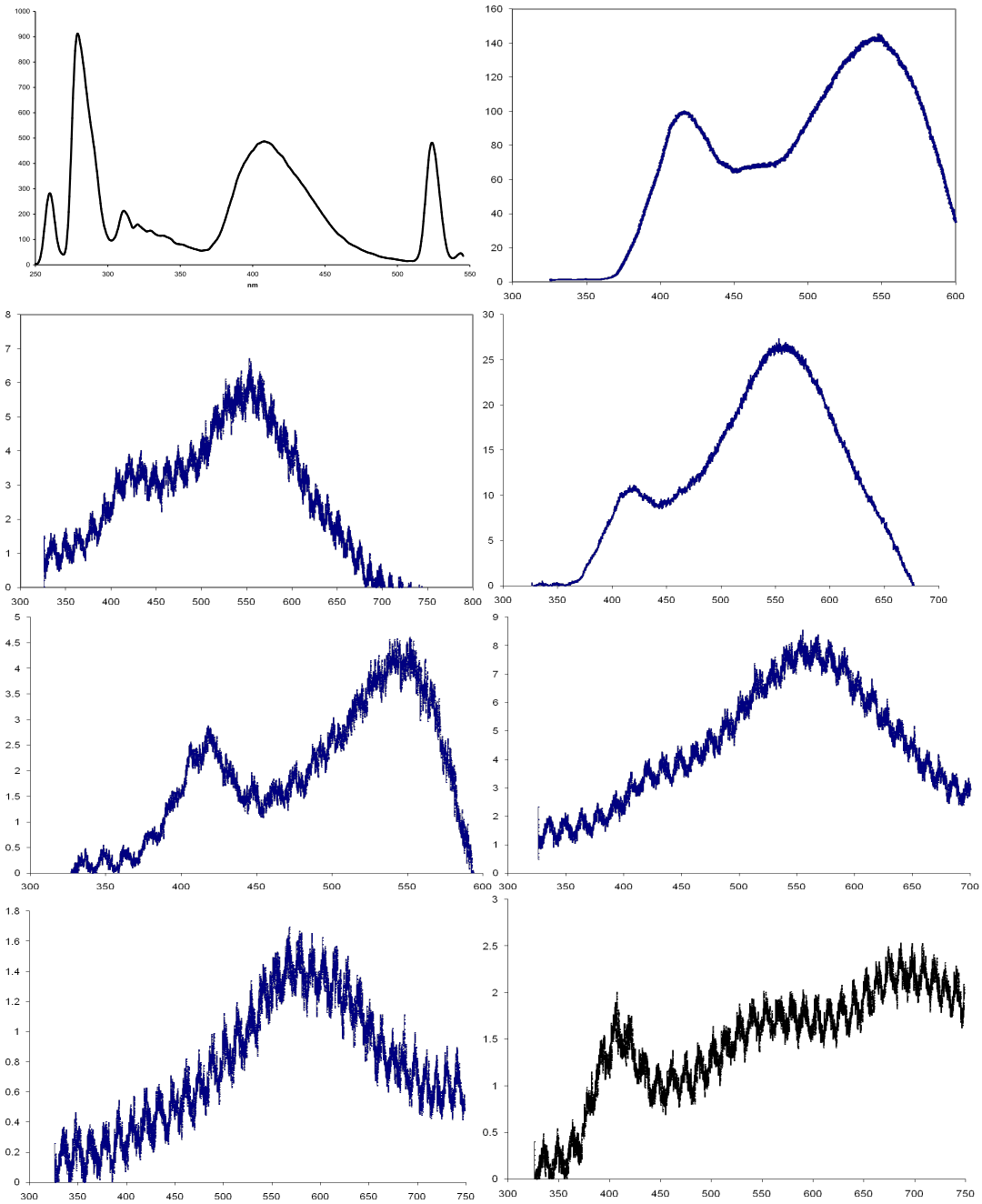

Figure 4.109 PL spectra of (a) **Complex 1**; (b) **Complex 2**; (c) **Complex 3**; (d) **Complex 4**; (e) **Complex 6**; (f) **Complex 7**; (g) **Complex 8**; and (h) **Complex 15**

Table 4.11 PL data

Complex	Chemical formula	Emission peak (nm)		
1	$K[Cu(RCOO)(OH)_2(H_2O)].H_2O$	279.0	408.0	524.0
2	$K_2[Cu_2(p\text{-}OC_6H_4COO)_2(RCOO)_2(H_2O)_2]$	415.6		551.3
3	$K[Cu_2(p\text{-}OC_6H_4COO)(RCOO)_3(CH_3CH_2OH)_2]$	423.5		546.4
4	$K[Cu_2(p\text{-}OC_6H_4COO)(RCOO)_3].2H_2O)$	414.1		552.3
6	$K[Cu_2(p\text{-}OC_6H_4COO)(R'COO)_3(CH_3CH_2OH)(R'COOH)]$	414.1		542.5
7	$K_3[Cu_2(p\text{-}OC_6H_4COO)_3(R'COO)(CH_3CH_2OH)_2].H_2O$	-		555.0
8	$[Cu_2(p\text{-}HOC_6H_4COO)_3(RCOO)(C_5H_5N)].C_5H_5N$	-		574.8
15*	$([Cu_2(p\text{-}HOC_6H_4COO)(R''COO)_3(H_2O)_2]$	401.1		552.8

R, $CH_3CH{=}CH$, R', $CH_2{=}C(CH_3)$, R", $CH_3(CH_2)_7CH((CH_2)_5CH_3)$; * a second order peak was observed at 690.9 nm

The excitation at 267 nm corresponds to intraligand $n \longrightarrow \pi^*$ electronic transition, while that at 325 nm corresponds to LMCT electronic transition.

All complexes have an emission peak at about 550 nm, which is normally associated with Cu(I) MLCT [29]. This suggests that the Cu(II) centre(s) in these complexes was/were photoreduced to Cu(I), and that the excited Cu(I) formed has sufficient time to trap the photonic energy.

All complexes, except for Complex & and Complex 8, have the expected emission peak at about 410 nm (and at 279 nm for Complex 1). Similar emission peak was noted for $[Cu_4(\mu_2\text{-dppm})_4(\mu_2\text{-}\mu_2\text{-}NS_2)(\mu_4\text{-}\mu_4\text{-}NS_2)]$ (410 nm) and $[Cu_5(\mu_2\text{-dppm})_4(\mu_3\text{-}\mu_3\text{-}NS_2)_2]PF_6$ (486 and 489 nm) after excitation at 380 nm [2].

However, it is uncertain why this peak is not observed from **Complex 7** and **Complex 8**. It may be due to the higher ratio of arylcarboxylate:alkylcarboxylate ligands (3:1) in these latter complexes compared to the other complexes. The results seem to suggest that the excited electron was effectively "trapped" by the aromatic ligand. As conclusion, these complexes are potential solar materials as they were able to capture and trap the photonic energy corresponding to MLCT transition.

References

[1] G. S. Attard, P. R. Cullum. *Liq. Cryst*., 8(3), (1990) 299

[2] H. Xu, and H. K. Yip, *Inorg. Chem.*, 42, (2003) 4492

[3] M. T. Miller, P. K. Gantzel, and T. B. Karpishin, *Inorg. Chem.*, 38, (1999) 3414

[4] N. Abdullah and Z. A. Kamarazaman, International Conference on Nanoscience and Nanotechnology (2008)

[5] F. Cariati, L. Erre, G. Micera, A. Panzanelli, G. Ciani and A. Sironi, *Inorganica Chimica Acta*, 80, (1983) 57

[6] G. B. Deacon, R. J. Philips, *Coord. Chem. Rev.*, 33, (1980) 227

[7] Y. Y. Wang, Q. Shi, Q. Z. Shi, Y. C. Gao, and X. Hou, *Polyhedron*, 19, (2000) 891

[8] M. I. Mohamadin and N. Abdullah, *Cent. Eur. J. Chem*. 8, (2010) 1090

[9] http://en.wikipedia.org/wiki/Cyclic_voltamettry (12 Feb 2010)

[10] B. K. Koo, *Bull. Korean Chem*. Soc. 22, (2001) 113

[11] F. P. W. Agterberg, H. A. J. P. Kluit, W. L. Drissen, H. Oevering, W. Buijis, M. T. Lankin, A. L. Spek and J. Reedijk, *Inorg. Chem.*, 36, (1997) 4321

[12] M. Pajtášová, D. Ondrušová, E. Jóna, S. C. Mojumdar, S. L'alíková, T. Bazyláková, and M. Gregor, *J. Therm. Anal. Calorim*. 100, (2010) 769

[13] E. Kokot, R.L. Martin, *Inorg. Chem*., 3, (1964) 1306

[14] C. Ratanatawanate, A. Bui, K. Vu, and K. J. Balkus, Jr, *J. Phys. Chem.*, 115, (2011) 6175

[15] http://en.wikipedia.org/wiki/Copper(II)_oxide (29 Dec 2010)

[16] Z. Jiang, F. Yang, N. Luo, B. T. T. Chu, P. Sun, H. Shi, T. Xiao, P. P. Edwards, *Chem. Commun*. (2008), 6732

[17] D. V. Bavykin, S. N. Gordeev, A. V. Muskalenko, A. A. Lapkin, F. C. Walsh, *J. Phys. Chem. B,* 109, (2005), 8565

[18] B. N. Figgis and R.L. Martin, *J. Chem. Soc.*, (1956) 3837

[19] B. Bleaney and K. Bowers, *Proc, R. Soc. London*, Ser. A, (1952) 451

[20] R. Cejudo, G. Alzuet, J. Borrás, M. Liu-González and F. Sanz-Ruiz, *polyhedron*, 21, (2002) 1057

[21] S. P. Perlepes, E. Libby, W. E. Streib, K. Folting and G. Christou, *Polyhedron*, 11, (1992) 923

[22] S. Konar, S. C. Manna, E. Zangrando, N. R. Chaudhuri, *Inorganica Chimica Acta*, doi:10.1016/j.ica.2003.12.003

[23] L. N. Ozair, N. Abdullah and K. M. Lo, *Acta Cryst.*, 67, (2010) 952

[24] I. Toledo, M. Arancibia, C. Andrade and I. Crivell, *Polyhedron*, 17, (1998) 173

[25] H. Dhillon, K. Sharma, R. Gehlot and S. Kumbhat, *Electrochem. Commun,* 11, (2009) 878

[26] L. N. Ozair, N. Abdullah, H. Khaledi and E. Tiekink, *Acta Cryst.,* 66, (2010) 589

[27] G. Blewett, C. Esterhuysen, M. W. Brendenkamp and K. R. Koch, *Acta Cryst.,* 62, (2006) 420

[28] P. Maldivi, L. Bonnet, A.-M. Giroud-Godquin, M. Ibn-Elhaj, D. Guillon and A. Skoulios, *Adv. Mater.*, 5, (1993) 909

[29] E. Badaruddin, Z. Aiyub and Z. Abdullah, *The Malaysian Journal of Analytical Sciences*, 12, (2008) 285